



Energy, Mines and
Resources Canada

Énergie, Mines et
Ressources Canada

CANMET

Canada Centre
for Mineral
and Energy
Technology

Centre canadien
de la technologie
des minéraux
et de l'énergie

HIGH TEMPERATURE TRIAXIAL TESTS ON ROCK SAMPLES FROM BOREHOLE URL-05, LAC DU BONNET, MANITOBA

J.S.O. Lau, R. Jackson and B. Gorski
Canadian Mine Technology Laboratory

August 1988

MINING RESEARCH LABORATORIES
DIVISION REPORT MRL 88-90(TR)

MRL 88-90 (TR)

1-7989548

HIGH TEMPERATURE TRIAXIAL TESTS ON ROCK SAMPLES FROM BOREHOLE URL-05, LAC DU BONNET, MANITOBA

by

J.S.O. Lau¹, R. Jackson² and B. Gorski³

ABSTRACT

Two series of high temperature triaxial tests, as well as ultrasonic tests, were conducted on granitic core samples obtained from Borehole URL-05 at the site of Atomic Energy of Canada Limited's Underground Research Laboratory (URL). The first series consisted of six sets of tests at three confining pressures (3.5, 17.0 and 35.0 MPa) and two temperatures (100° and 200° C). The second series consisted of nine sets of tests at three confining pressures (3.5, 17.0 and 35.0 MPa) and three temperatures (23°, 100° and 200° C). The purpose of these tests is to provide some strength and deformation data and interpretations for the study of the stability and deformability of the rock mass at the URL site under both the ambient and high temperature conditions. Pseudo Young's modulus was introduced to describe the slope of the stress-strain curve during each stress interval. The strength properties of the rock samples were expressed in terms of the Hoek and Brown failure criterion. Most of the changes in the elastic and strength properties of the rock samples were found to occur when the temperature was raised from 23° to 100° C.

¹Geotechnical Engineer, Atomic Energy of Canada Limited, on attachment to CANMET, Energy, Mines and Resources Canada, Ottawa, Ontario.

²Research Officer, Canadian Mine Technology Laboratory, Mining Research Laboratories, CANMET, Energy, Mines and Resources Canada, Ottawa, Ontario.

³Rock Mechanics and Development Technologist, Canadian Mine Technology Laboratory, Mining Research Laboratories, CANMET, Energy, Mines and Resources Canada, Ottawa, Ontario.

Keywords: thermal-mechanical, dynamic, elastic, strength, confining pressure, temperature, deviator stress, strain, Young's modulus

ESSAIS TRIAXIAUX MENÉS À UNE TEMPÉRATURE ÉLEVÉE SUR DES ÉCHANTILLONS PROVENANT DU SONDAGE URL-05, LAC DU BONNET, MANITOBA

par

J.S.O. Lau¹, R. Jackson² et B. Gorski³

RÉSUMÉ

Des échantillons granitiques carottés provenant du sondage URL-05 situé sur l'emplacement du Laboratoire de recherche souterrain (URL) de L'Énergie atomique du Canada Limitée ont été soumis à deux séries d'essais triaxiaux menés à une température élevée de même qu'à des essais ultrasoniques. La première série consistait en six ensembles d'essais menés à trois pressions de confinement (3.5, 17.0 et 35.0 MPa) et à deux températures (100° et 200° C). La deuxième série consistait en neuf ensembles d'essais conduits à trois pressions de confinement (3.5, 17.0 et 35.0 MPa) et à trois températures (23°, 100° et 200° C). Par ces essais, on cherchait à obtenir des données et des explications sur la résistance et la déformation des échantillons. Ces renseignements doivent servir aux fins de l'étude portant sur la stabilité et la déformabilité, tant à une température élevée qu'à l'air ambiant, de la masse rocheuse située sur l'emplacement de URL. Le pseudo-module de Young a été utilisé pour décrire la pente de la courbe de contrainte-déformation pendant chaque intervalle de contrainte. Les propriétés de résistance des échantillons de roche sont décrits d'après le critère de rupture de Hoek et Brown. La plupart des changements qui ont modifié les propriétés des échantillons de roche se sont produits quand on a augmenté la température de 23° à 100° C.

¹Ingénieur géotechnique de L'Énergie atomique de Canada Limitée, affecté à CANMET, Énergie, Mines et Ressources Canada, Ottawa, Ontario.

²Agent de recherche, Laboratoire canadien de technologie minière, Laboratoires de recherche minière, CANMET, Énergie, Mines et Ressources Canada, Ottawa, Ontario.

³Technicien, Développement et mécanique des roches, Laboratoire canadien de technologie minière, Laboratoires de recherche minière, CANMET, Énergie, Mines et Ressources Canada, Ottawa, Ontario.

Mots-clé: thermique-mécanique, dynamique, élastique, résistance, pression de confinement, température, déformation, module de Young.

CONTENTS

	<u>Page No.</u>
Abstract	i
Résumé	ii
1. Introduction	1
2. Sampling and specimen preparation	2
2.1 Core samples	2
2.2 Specimen preparation	2
3. Dynamic elastic properties	2
4. Test apparatus and procedure	4
4.1 Test apparatus	4
4.2 Assembling the test stack	5
4.3 Test procedure	6
5. Triaxial testing program	6
6. Results and discussion	7
6.1 Test results	7
6.2 Deviator stress and strain at failure	7
6.3 Effect of temperature on deviator stress and strain at failure	8
6.4 Tangent Young's modulus	9
6.5 Effect of temperature on tangent Young's modulus	10
6.6 Pseudo Young's modulus	10
6.7 Effect of temperature on pseudo Young's modulus	11
6.8 Strength properties	11
6.9 Effect of temperature on strength properties	14
7. Conclusions	15
8. Recommendations	16
Acknowledgements	17
References	17
Appendix A	49

1. Introduction

Atomic Energy of Canada Limited (AECL) and Canada Centre for Mineral and Energy Technology (CANMET) have undertaken a joint project to investigate the mechanical and thermal-mechanical properties of rock samples from the site of AECL's Underground Research Laboratory (URL). The site is located in the Lac du Bonnet Batholith which lies approximately 100 km northeast of Winnipeg, Manitoba. The investigation is an essential requirement of the geotechnical engineering component of the Canadian Nuclear Fuel Waste Management Program for the safe, long term disposal of high level nuclear wastes in a vault deep in plutonic rock. For the design and construction of such a vault, an understanding of the stability and deformability of the rock mass is required in terms of not only the in situ ambient conditions of stress and temperature, but also the estimated stress and temperature changes resulting from the construction of the vault and the emplacement of the wastes.

The effects of stress and temperature on the mechanical behaviour of some rock samples from the URL site and the Whiteshell research area in the Lac du Bonnet Batholith have been described previously by Annor et al. (1980), Jackson (1984) and Annor and Jackson (1985). They reported that the strength and the tangent modulus of elasticity (at 50% ultimate strength) of the rock increased with increasing confining pressure at room temperature. They also observed reductions in the average triaxial strength and the tangent Young's modulus of the rock with increasing temperature. They used a triaxial chamber for the high temperature tests and their specimens were heated to the predetermined temperatures before the confining pressures were applied.

This report presents the results of two series of high temperature triaxial tests on granitic core samples obtained from Borehole URL-05, between the depths of 260 and 269 metres, at the URL site. The apparatus used in this study was a MTS 815 Rock Mechanics Test System. The main difference between these tests and those conducted by Annor et al. (1980) and Jackson (1984) is that, in these tests, the confining pressures were applied to the specimens before they were heated to the predetermined test temperatures.

2. Sampling and specimen preparation

2.1 Core samples

Samples were prepared from NQ core obtained from Borehole URL-05 between the downhole lengths of 268.84 and 277.57 m (depth of 260.32 to 268.66 m) at the site of the Underground Research Laboratory.

Generally, the rock between those depths at Borehole URL-05 is a massive, grey to greenish-grey, medium to coarse grained granite, composed of approximately 30.4% of quartz, 26.3% of K-feldspar, 36.5% of plagioclase and 3.5% of biotite (Wong, 1984). The average grain sizes of the three major minerals in the grey granite are 1.6 x 2.5 mm in quartz, 2.1 x 3.1 mm in K-feldspar and 1.7 x 2.2 mm in plagioclase. The grey granite is relatively unaltered. The texture of the greenish-grey granite is similar to that of the grey granite, but the greenish-grey granite is characterized by numerous chlorite-filled microfractures (Kaminen et al., 1984).

2.2 Specimen preparation

The specimens used for these tests were prepared in accordance to the procedure described in the Pit Slope Manual Supplement 3-5 (Gyenge and Ladanyi, 1977) and the method suggested by the International Society for Rock Mechanics (Brown, 1981).

Cylindrical test specimens were cut slightly larger than their final dimensions from the core samples by means of a water-cooled diamond saw. Then, to ensure that the end surfaces of each specimen were parallel to each other and also perpendicular to the axis of the specimen, the end surfaces were ground flat to 0.025 mm, using a double lapper.

After the specimens had been prepared, they were oven dried, weighed and measured. The dimensions and bulk densities of the specimens are shown in Tables 1 and 2. The final dimensions of the specimens for these tests varied from 44.69 to 45.14 mm in diameter and 98.68 to 114.96 mm in length, with length to diameter ratios ranging from 2.2 to 2.5.

3. Dynamic elastic properties

Prior to the high temperature triaxial tests, the dynamic elastic constants of the rock were determined, using the measured compression and shear wave velocities and

the bulk density of each specimen. The ultrasonic testing apparatus, used to measure the wave velocities, consisted of pulsing and sensing heads, a pulse generator and an oscilloscope. For a detailed description of the apparatus and an outline of the test method, the reader is referred to the Instruction Manual - Sonic Velocity Equipment (Terrametric, 1980) and the Pit Slope Manual Supplement 3-2 (Gyenge and Herget, 1977).

The compression and shear wave velocities of each specimen were calculated by dividing the length of the specimen (pulse-travel distance) by the pulse-travel times of the compression wave and the shear wave respectively. The dynamic elastic constants were then determined by the use of the following equations.

Dynamic Young' modulus of elasticity:

$$E_u = \frac{\rho V_s^2 (3V_p^2 - 4V_s^2)}{V_p^2 - V_s^2} \quad (1)$$

where E_u = dynamic Young's modulus of elasticity

V_p = compression wave velocity

V_s = shear wave velocity

ρ = bulk density

Dynamic Shear modulus:

$$G_u = \rho V_s^2 \quad (2)$$

where G_u = dynamic shear modulus

Dynamic Poisson's ratio:

$$\nu_u = \frac{V_p^2 - 2V_s^2}{2(V_p^2 - V_s^2)} \quad (3)$$

where ν_u = dynamic Poisson's ratio

Tables 1 and 2 show the dynamic Young's modulus, dynamic shear modulus and dynamic Poisson's ratio determined for each of the specimens used in the high

temperature triaxial tests. The dynamic Young's moduli of the rock samples were found to vary from 31.08 to 47.93 GPa with a mean value of 38.85 GPa (standard deviation = 3.49 GPa). The dynamic shear moduli varied from 12.23 to 19.66 GPa with a mean value of 15.87 GPa (standard deviation = 1.69 GPa). The dynamic Poisson's ratios varied from 0.11 to 0.31 with a mean value of 0.22 (standard deviation = 0.05).

It should be noted that while some discrepancies exist between elastic constants determined dynamically and statically, ultrasonic velocity measurements offer a method of estimating various mechanical rock properties non-destructively prior to actual testing. Moreover, the ultrasonic measurements conducted here made it possible to estimate the Poisson's ratios of these core samples as the transverse normal strain could not be measured during the high temperature triaxial tests.

4. Test apparatus and procedure

4.1 Test apparatus

The triaxial apparatus used to carry out these tests was a MTS 815 Rock Mechanics Test System. The MTS system, previously described by Gorski (1987), is a servo-hydraulic system consisting of a load frame, hydraulic power supply, triaxial cell, confining pressure subsystem, test controller, data display, function generator, hydraulic controller, micro-console, test processor, temperature controller and DEC micro PDP 11/73 computer. For a detailed description of the MTS system and its operation, the reader is referred to the MTS Operation Manual (MTS Systems Corp., 1986).

The triaxial cell is rated up to 150 MPa and 200° C. The cell is equipped with a 2.22 MN rated load cell, heater, heat shroud, thermocouples and three linear variable differential transducers (LVDT) for the measurement of axial strain. Rock specimens with dimensions up to 200 mm in length and 100 mm in diameter can be tested in the triaxial cell.

The test controller regulates axial loading according to either a specified rate or one determined by axial or circumferential strain or axial displacement at the specimen during testing. The confining fluid pressure is generated by the confining pressure subsystem and controlled by the use of the micro-console. The confining fluid is heated by means of the internal heater element in the triaxial cell. The heater element has a temperature rating of 200° C. The control of the temperature is provided by the temperature controller.

The test processor contains the devices for the computer-controlled operation of the MTS test system. Built in software provides functions such as the command signal generation, data acquisition and handling, the monitoring and control of the operation of the test controller as well as other system components, and the initiation of computer interrupt routines upon the detection of certain programmed events.

4.2 Assembling the test stack

The test stack for the rock specimen (Fig. 1) was built using the following procedure.

First, the LVDT coils were assembled in the body mount bracket. The body mount bracket was fastened onto the load cell spacer and the LVDT cables were connected to the electrical feedthrough connectors. Then, the load cell spacer was placed on the load cell and a dowel pin was installed into the centre hole in the load cell spacer. After the lower heat dam had been placed on the load cell spacer, the lower specimen spacer was placed on the load cell spacer and dowel and a dowel pin was inserted in the centre hole on the lower specimen spacer. The heater assembly was then placed on the load cell spacer and the control thermocouple was connected.

To prepare the specimen for installation, O-rings were first placed in the groves in the specimen end caps. The core sample was then placed between the specimen end caps and a heat-shrink teflon jacket slid over the specimen end caps and core sample. The jacket was heat shrunk and wired on above and below both O-rings using black stove pipe wire. The installation of the specimen was completed by placing the jacketed specimen assembly on the lower specimen spacer and dowel pin.

Next, the LVDT cores, core extension rods, core connecting rods and core mounting bracket were assembled and the LVDT rod assemblies and mounting bracket were inserted over the upper specimen end cap through the lower heat dam into the appropriate LVDT coil. The core mounting jacket was secured to the upper specimen end cap using a setscrew. A dowel pin was inserted into the centre hole in the upper specimen end cap and the loading cap was placed on the upper specimen end cap and dowel. Thermocouples were installed to monitor the temperature near the core sample bottom, midpoint and top. Finally, the assembling of the test stack was completed by placing the shroud support ring on the loading cap and lowering the shroud over the stack assembly onto the lower heat dam.

4.3 Test procedure

In the high temperature triaxial tests, the confining fluid pressure and axial load were raised simultaneously to the predetermined test level and then the fluid was heated at a rate of 1°C per minute until the test temperature was reached. A soak time of one hour was utilized to ensure that the specimen also reached the test temperature.

All tests were stress controlled and conducted in a computer-controlled mode. The specimens were loaded through failure at a rate of 1 kN per second. Signals from the load cell and the three LVDTs were scanned by the computer every second. The signals were converted to engineering units and measurements from the LVDTs were corrected for end platen compression. The data were stored on hard disk in the micro PDP 11/73 computer for later transfer to the VAX computer. Real time plotting of load versus displacement (LVDT 1) was also obtained during the test using a HP7046B X-Y recorder wired to the MTS controller.

After each test had been completed, the confining fluid was cooled down, drained and the assembly dismantled. The specimen was removed from the stack. A note of the specimen failure characteristics was made and the angle between the failure plane and axis of the specimen was measured.

5. Triaxial testing program

The purpose of the high temperature triaxial testing program was to determine the behaviour of the URL rock samples under high temperature in order to compare it with the behaviour under ambient temperature. The program was divided into two parts. The first series of tests were carried out in February, 1988. Problems with the LVDTs were encountered during testing and therefore the accuracy of the axial strain obtained in those tests was doubtful. The problems were subsequently corrected and the second series of tests were conducted in May, 1988.

The first series of the program consisted of six sets of tests at three confining pressures (3.5, 17.0 and 35.0 MPa) and two temperatures (100° and 200°C). This part of the program which consisted of 21 tests (Sample Nos. A1T to A21T) is summarized in Table 3.

Nine sets of tests were conducted in the second series of the program at three confining pressures (3.5, 17.0 and 35.0 MPa) and three temperatures (23° , 100° and

200° C). Twenty-one tests (Sample Nos. A22T to A42T) were performed and the tests are summarized in Table 4.

6. Results and discussion

6.1 Test results

Tables 3 and 4 summarize the total axial strain, failure deviator stress, tangent Young's modulus and pseudo Young's modulus (see Section 6.6) at 50% failure deviator stress, failure angle and predominant failure characteristics of each specimen for the first and second test series respectively.

Deviator stress versus axial strain curves for all tests are illustrated in Appendix A. These curves were plotted by using the computer DATAPLOT fitting operation. The fit carried out was a cubic spline fit and the model used was a third degree equation:

$$\sigma = a_0 + a_1\varepsilon + a_2\varepsilon^2 + a_3\varepsilon^3 \quad (4)$$

where σ = stress

ε = strain

and a_0 , a_1 , a_2 and a_3 are coefficients

Note that the axial strain was computed by averaging the axial strain data obtained from the three LVDTs. However, due to the problems encountered with the LVDTs in the first part of the test program, for Samples A10T, A17T and A18T, the averages from two LVDTs were given; and for Samples A2T, A3T and A5T, the strain data from only one LVDT was used. No strain data was available from the tests for Samples A1T, A4T, A6T, A11T and A12T. Also, no stress data was available from the testing of Sample A11T.

6.2 Deviator stress and strain at failure

From Tables 3 and 4, it can be seen that the failure deviator stress increased as the confining pressure increased at all three test temperatures. At the temperature of 23° C, the failure deviator stress increased from 273 MPa at the confining pressure of 3.5 MPa to 426 MPa at the confining pressure of 17.0 MPa and to 513 MPa at the confining

pressure of 35.0 MPa. At 100° C, the failure deviator stress increased from 209 MPa to 373 MPa to 506 MPa as the confining pressure increased from 3.5 to 17.0 to 35.0 MPa. Results from Samples A13T and A27T were not used in this analysis because the presence of quartz inclusion and the microfractures associated with the quartz grains greatly reduced the strength of those two samples. At 200° C, the failure deviator stress increased from 201 MPa to 357 MPa to 484 MPa as the confining pressure increased from 3.5 to 17.0 to 35.0 MPa.

The total axial strain at failure also increased as the confining pressure increased. As the confining pressure increased from 3.5 to 17.0 to 35.0 MPa, the total axial strain increased from 0.485 to 0.715 to 0.853 at the temperature of 23° C; from 0.382 to 0.645 to 0.851 at 100° C; and from 0.423 to 0.627 to 0.814 at 200 ° C.

6.3 Effect of temperature on deviator stress and strain at failure

One of the main objectives of the high temperature triaxial tests is to study the effect of temperature on the strength of the rock. Results from the first series of tests (see Fig. 2 and Table 3) showed that at the confining pressure of 3.5 MPa, the failure deviator stress decreased from 218 MPa at the temperature of 100° C to 187 MPa at the temperature of 200° C. At the confining pressure of 17.0 MPa, the failure deviator stress decreased from 378 MPa to 336 MPa as the temperature increased from 100° to 200° C. At the confining pressure of 35.0 MPa, an increase of temperature from 100° to 200 ° C. reduced the failure deviator stress from 496 MPa to 466 MPa.

The second series of tests (see Fig. 3 and Table 4) showed that as the temperature increased from 23° to 100° C, the failure deviator stress decreased from 273 MPa to 190 MPa at the confining pressure of 3.5 MPa; and from 426 to 365 MPa at the confining pressure of 17.0 MPa. However, heating from 100° to 200° C at confining pressures of 3.5 and 17.0 MPa had a negligible effect. At the confining pressure of 35.0 MPa, the rock failed at deviator stresses of 514 MPa, 517 MPa and 503 MPa at temperatures of 23°, 100° and 200° C respectively, exhibiting little change with increasing temperature.

Results from the first series of tests indicated that the failure deviator stress of the rock decreased as the temperature increased at all three confining pressures. However, results from the second series of tests showed that a reduction in the failure deviator stress only occurred when the temperature was increased from 23° to 100° C and only at the confining pressures of 3.5 and 17.0 MPa. No reduction was observed at the confining pressure of 35.0 MPa. No reduction in the failure deviator stress was observed when the temperature was increased from 100° to 200° C at any of the confining pressures.

More tests, then, are recommended to study the effect of the temperature on the failure deviator stress of the rock.

Results from both series of tests showed a slight decrease in the axial strain at failure as the temperature increased from 23° to 100° to 200° C at all three confining pressures.

6.4 Tangent Young's modulus

Due to the inaccuracy of the strain data obtained in the first series of tests, only the data obtained in the second series were used to study the elastic properties of the rock. Table 5 presents the tangent Young's moduli of the rock samples at stress levels corresponding to 10%, 20%, 30%, 40%, 50%, 75% and 100% of the failure deviator stress, $(\sigma_1 - \sigma_3)_f$, on the stress-strain curves. For each sample, the tangent modulus at each stress level was computed by solving the third degree equation (Equation 4) representing the stress-strain curve and substituting the strain value into the derivative of the equation.

The variation of the tangent modulus of elasticity with confining pressure for the temperatures of 23°, 100° and 200° C are illustrated in Figures 4, 5 and 6 respectively. Note that the deviator stresses here have been normalized by dividing them by the failure deviator stress. These figures as well as results from Table 5 indicate that, for all temperatures, at the confining pressure of 3.5 MPa, the tangent modulus increased until approximately $0.5(\sigma_1 - \sigma_3)_f$ and subsequently decreased until failure. At 17.0 MPa, the tangent modulus increased slowly until approximately $0.25(\sigma_1 - \sigma_3)_f$ was reached and then decreased slowly with increasing stress. At the high confining pressure of 35.0 MPa, the tangent modulus decreased with increasing stress. At all temperatures and confining pressures, the tangent modulus started to decrease more rapidly at approximately $0.5(\sigma_1 - \sigma_3)_f$. It is interesting to point out that all these plots join at approximately $0.75(\sigma_1 - \sigma_3)_f$, indicating that the confining pressure had no effect on the tangent modulus at stress levels above that. Below $0.75(\sigma_1 - \sigma_3)_f$, an increase in confining pressure resulted in an increase in the modulus value, especially at low stress levels. The increase was particularly pronounced when the confining pressure was raised from 3.5 MPa to 17.0 MPa. This would seem to indicate that some stress relaxation had occurred and consequently the increase in crack porosity had resulted in larger deformations and lower modulus values at the lowest confining pressure (3.5 MPa).

6.5 Effect of temperature on tangent Young's modulus

The variation of the tangent modulus with temperature for confining pressures of 3.5, 17.0 and 35.0 MPa are shown in Figures 7, 8 and 9 respectively. At the low confining pressure of 3.5 MPa, there were a significant decrease in the tangent modulus when the temperature was increased from 23° to 100° C, especially at low stress level, and a slight decrease when the temperature was increased from 100° to 200° C. The effect of temperature decreased as the normalized deviator stress increased and became minimal at approximately $0.75(\sigma_1 - \sigma_3)_f$. At the confining pressures of 17.0 MPa and 35.0 MPa, no significant change in the tangent modulus was observed at any stress level as the temperature increased from 23° to 100° to 200° C.

6.6 Pseudo Young's modulus

From the deviator stress-strain curves, it can be seen that the rock samples tested did not behave perfectly elastically and the stress-strain curves are not linear. The slope of the deviator stress-strain curve can be described more properly by treating the nonlinear curve as a series of straight lines. These straight lines join the stress-strain curve at stress points of 0.0, 0.1, 0.2, 0.3, 0.4, 0.5, 0.75 and 1.0 failure deviator stress. In other words, over each stress interval, the stress-strain curve is considered to be linear. The slope of the stress-strain curve during each stress interval is defined as the pseudo Young's modulus. The pseudo Young's modulus is so defined that it can be used to describe the stress-strain curve for use in the finite element program. The pseudo Young's moduli of the rock samples are given in Table 6. In general, the pseudo modulus of the rock tested was lower than the tangent modulus at stress levels below $0.5(\sigma_1 - \sigma_3)_f$. At the stress level of $0.5(\sigma_1 - \sigma_3)_f$, the pseudo modulus was equal to the tangent modulus. The pseudo modulus was higher than the tangent modulus at stress levels above $0.5(\sigma_1 - \sigma_3)_f$. It is interesting to point out that at the ambient room temperature of 23° C and at the low confining pressure of 3.5 MPa, the pseudo Young's modulus at $0.1(\sigma_1 - \sigma_3)_f$ appeared to be similar to the dynamic Young's modulus of the rock.

Figures 10, 11 and 12 show the plots of the pseudo Young's modulus versus the normalized deviator stress of the rock samples tested under the same temperature condition but different confining pressure condition. They display the same patterns as those of the tangent Young's modulus (see Figs. 4, 5 and 6) do. These plots also join at approximately $0.75(\sigma_1 - \sigma_3)_f$, indicating that the confining pressure also had no effect on the pseudo Young's modulus at stress levels above $0.75(\sigma_1 - \sigma_3)_f$.

6.7 Effect of temperature on pseudo Young's modulus

The pseudo Young's moduli of the rock samples tested under the same confining pressure condition, but at different temperatures, were also plotted against the normalized deviator stress, as illustrated in Figures 13, 14 and 15, in order to study the effect of temperature on the pseudo Young's modulus. They show the same patterns as those of the tangent Young's modulus (see Figs. 7, 8 and 9) do. There was a significant decrease in the pseudo modulus when the temperature increased from 23° to 100° C at the low confining pressure of 3.5 MPa. However, no change in the pseudo modulus was observed when the temperature increased from 100° to 200° C. At the confining pressures of 17.0 and 35.0 MPa, an increase of temperature from 23° to 100° to 200° C resulted in no change in the pseudo modulus.

6.8 Strength properties

The strength properties of the intact rock material can be expressed in terms of two commonly employed empirical criteria: the Mohr-Coulomb failure criterion (Goodman, 1980) and the Hoek and Brown failure criterion (Hoek and Brown, 1980).

Using the Mohr-Coulomb failure criterion, the major principal stress at failure can be expressed as follows:

$$\sigma_1 = \sigma_c + \sigma_3 \tan^2(45^\circ + \phi/2) \quad (5)$$

where σ_1 = major principal stress at failure

σ_c = uniaxial compressive strength

σ_3 = minor principal stress (confining pressure)

ϕ = angle of internal friction

This criterion yields a curved failure envelope.

The relationship between the principal stresses associated with the failure of rock drawn by Hoek and Brown is as follows:

$$\sigma_1 = \sigma_3 + \sqrt{m\sigma_c\sigma_3 + s\sigma_c^2} \quad (6)$$

where σ_1 = major principal stress at failure

σ_3 = minor principal stress applied to the rock sample

σ_c = uniaxial compressive strength of the intact rock material
in the specimen

m and s are constants

The values of m and s depend on the properties of the rock and the extent to which the rock has been broken before being subjected to the stresses σ_1 and σ_3 . For intact rock, $s = 1$, and the uniaxial compressive strength σ_c and the material constant m can be computed as follows:

$$\sigma_c^2 = \frac{\sum y_i}{n} - \left[\frac{\sum x_i y_i - \frac{\sum x_i \sum y_i}{n}}{\sum x_i^2 - \frac{(\sum x_i)^2}{n}} \right] \frac{\sum x_i}{n} \quad (7)$$

$$m = \frac{1}{\sigma_c} \left[\frac{\sum x_i y_i - \frac{\sum x_i \sum y_i}{n}}{\sum x_i^2 - \frac{(\sum x_i)^2}{n}} \right] \quad (8)$$

where $x = \sigma_3$

$y = (\sigma_1 - \sigma_3)^2$

n = total number of data pairs x_i and y_i

The coefficient of determination r^2 is given by:

$$r^2 = \frac{\left[\sum x_i y_i - \frac{\sum x_i \sum y_i}{n} \right]^2}{\left[\sum x_i^2 - \frac{(\sum x_i)^2}{n} \right] \left[\sum y_i^2 - \frac{(\sum y_i)^2}{n} \right]} \quad (9)$$

The closer the value of r^2 is to 1.00, the better the fit of Equation 6 to the triaxial test data is.

Hoek and Brown also suggest that the relationship between the shear and normal stresses (τ and σ) and the principal stresses can be expressed as:

$$\sigma = \sigma_3 + \frac{\tau_m^2}{\tau_m + m\sigma_c/8} \quad (10)$$

$$\tau = (\sigma - \sigma_3)\sqrt{1 + m\sigma_c/4\tau_m} \quad (11)$$

where $\tau_m = \frac{1}{2}(\sigma_1 - \sigma_3)$

These two equations were used to develop the failure envelopes for the specimens. Since no uniaxial compressive strength σ_c of the rock at 100° and 200° C was available, the values of σ_c and m for samples tested at 100° and 200° C were computed, using Equations 7 and 8, and then substituted into Equations 10 and 11 to obtain the values of σ and τ to develop the failure envelopes. The computed values of σ_c , m and r^2 are shown in Table 7. The values of r^2 ranged from 0.9696 to 0.9930, indicating that the fit of the triaxial data to Equation 6 was good. The Mohr circles for these specimens and the failure envelopes developed were plotted in Figures 16 to 20. The failure envelopes developed by using Equations 10 and 11 fit very well with the Mohr circles. Note that only the average Mohr circle was plotted for each set of tests carried out under the same conditions of confining pressure and temperature.

The mean uniaxial compressive strength of two rock samples obtained from Borehole URL-05, between the downhole lengths of 274.51 - 277.59 m, reported by Jackson (1984), is 186 MPa. This value was used to compute the value of m for the tests carried out at the ambient room temperature of 23° C, and the value of m obtained is 31.9. The mean value of m for unheated Lac du Bonnet granitic samples established by Annor and Jackson (1985) is 29.9 and the m values for granitic rocks reported by Hoek and Brown (1980) range from 20.8 to 32.8. There is a good agreement between the m value for the unheated samples derived from these tests and the m values reported in published literature for granitic rocks.

The values of the angle of internal friction were determined by drawing the tangent to the Mohr circle for each confining pressure at the point of contact with the envelope, and the corresponding cohesion intercepts measured. Table 8 shows the resulting angles of internal friction and the cohesion of the rock samples.

At all temperatures, the angle of internal friction decreased with increasing confining pressure. As the confining pressure increased from 3.5 to 17.0 to 35.0 MPa, the

angle of internal friction decreased from 65° to 53° to 44° respectively at the temperature of 23° C; from 63° to 56° to 49° at 100° C; and from 61° to 54° to 48° at 200° C.

The cohesive strength of the rock samples increased as the confining pressure increased at all temperatures. As the confining pressure increased from 3.5 to 17.0 to 35.0 MPa, the cohesion increased from 24 to 48 to 78 MPa respectively at the temperature of 23° C; from 19 to 33 to 56 MPa at 100° C; and from 17 to 35 to 57 MPa at 200° C.

6.9 Effect of temperature on strength properties

To study the effect of temperature on the strength of the rock, the failure envelopes at the three test temperatures were plotted in Figures 21 and 22. Results from the first series of tests show that there was a slight decrease in the strength of the rock when the temperature was raised from 100° to 200° C. However, results from the second series of tests show no such a decrease when the temperature increased from 23° to 200° C. More tests are required to study the effect of temperature on the strength of the rock.

For the tests carried out at 100° and 200° C, the values of m obtained were higher than those for unheated samples and also higher than those reported by Annor and Jackson (1985) for heated Lac du Bonnet rock samples. The reason is that the estimated values of σ_c (see Table 7) used in the computation of m are low. However, due to the absence of uniaxial compressive strength test data of heated samples, only the computed values of σ_c could be used in this analysis. In order to obtain more meaningful values of m for the heated Lac du Bonnet granite, uniaxial compression tests should also be performed on heated samples.

Tests conducted at 3.5 MPa confining pressure exhibited a slight decrease in the angle of internal friction with increasing temperature. Results obtained at the higher confining pressures of 17.0 and 35.0 MPa, however, showed no significant changes with heating.

The cohesion of the rock samples decreased when the temperature increased from 23° to 100° C (see Table 8). But, when the temperature was raised from 100° to 200° C, the cohesion appeared to be relatively insensitive to the increase in temperature.

7. Conclusions

The results of these two series of high temperature triaxial tests and the results of ultrasonic tests on the rock samples from Borehole URL-05 have provided some strength and deformation data and interpretations for the study of the stability and deformability of the rock mass at the site of the AECL Underground Research Laboratory, under both the ambient and high temperature conditions. The data could also be used for the vault design study, URL in situ test planning and geosphere modelling activities being carried out by AECL. From the results, the following conclusions can be made:

At the ambient room temperature, the mean values of the dynamic Young's modulus, dynamic shear modulus and Poisson's ratio of the rock samples were found to be 38.85 GPa, 15.87 GPa and 0.22 respectively.

The failure deviator stress and the total strain at failure increased as the confining pressure increased at all three test temperatures of 23°, 100° and 200° C.

The failure deviator stress decreased when the temperature increased from 23° to 100° C at the confining pressures of 3.5 and 17.0 MPa, but no reduction in the triaxial strength was observed at the confining pressure of 35.0 MPa. Results from the tests conducted at 200° C were inconclusive. In the first series of tests, a decrease in the failure deviator stress was observed when the temperature was raised from 100° to 200° C at all three confining pressures. However, in the second series of tests, no such a reduction was observed.

The pseudo Young's modulus was introduced to describe the slope of the stress-strain curve during each stress interval. In general, at the stress level of $0.5(\sigma_1 - \sigma_3)_f$, the pseudo Young's modulus was equal to the tangent Young's modulus. Below that level, the pseudo modulus was lower than the tangent modulus, and above that level, the pseudo modulus was higher than the tangent modulus. At the ambient temperature of 23° C and at the low confining pressure of 3.5 MPa, the pseudo Young's modulus at $0.1(\sigma_1 - \sigma_3)_f$ appeared to be similar to the dynamic Young's modulus.

The stress-strain curves showed that at a confining pressure of 3.5 MPa, the tangent and pseudo Young's moduli increased with increasing deviator stress until approximately $0.5(\sigma_1 - \sigma_3)_f$ was reached and then decreased. At 17.0 MPa, the moduli increased slowly, but at approximately $0.25(\sigma_1 - \sigma_3)_f$, started to decrease with increasing stress. At a confining pressure of 35.0 MPa, the moduli decreased with increasing stress.

Both the tangent and pseudo Young's moduli increased with increasing confining pressure at stress levels below approximately $0.75(\sigma_1 - \sigma_3)_f$. The increase was particularly pronounced at low stress level. Above $0.75(\sigma_1 - \sigma_3)_f$, the confining pressure seemed to have no effect on the moduli.

Temperature has a significant effect on the tangent and pseudo Young's moduli at low confining pressure and particularly at low stress level. At a confining pressure of 3.5 MPa, the moduli decreased as the temperature increased. However, at approximately $0.75(\sigma_1 - \sigma_3)_f$, the temperature effect became minimal. The temperature had no effect on the moduli at the confining pressures of 17.0 and 35.0 MPa.

In this report, the strength properties of the rock samples were expressed in terms of the Hoek and Brown failure criterion. The value of the material constant m for the unheated samples was found to be 31.9. There is a good agreement between this value and the m values reported in published literature for Lac du Bonnet granite and other granitic rocks. The values of m for the heated samples obtained from these tests were higher than those for the unheated samples and also higher than those previously reported for heated Lac du Bonnet rock samples.

There was apparently very little change in the failure envelope when the temperature was increased from 23° to 200° C.

The angle of internal friction decreased with increasing confining pressure at all three test temperatures. There was no significant change in the angle of internal friction with increasing temperature. Only at the low confining pressure of 3.5 MPa, the angle of internal friction appeared to decrease with increasing temperature.

The cohesive strength increased with increasing confining pressure at all three test temperatures. The cohesion decreased when the temperature was raised from 23° to 100° C, but no significant change in cohesion was observed when the temperature increased from 100° to 200° C.

8. Recommendations

From the results of these tests, it can be seen that most of the changes in the elastic and strength properties of the rock samples occurred when the temperature was raised from 23° to 100° C. It is therefore recommended that further testing be carried out in this temperature range to better define the effects of high temperature on the properties of the Lac du Bonnet granite. This temperature range also conforms with the maximum design container-surface temperature of 100° C (Baumgartner, 1986).

Uniaxial compression tests and triaxial compression tests conducted at very low confining pressures (less than 3.5 MPa) and at very high confining pressures (greater than 35.0 MPa) should be performed on heated rock samples to obtain data to better develop the failure envelope for heated samples in this region.

Results of the tests conducted at a temperature of 200° C are inconclusive. More tests should be carried out to understand the behaviour of the rock at this temperature.

At present, all the URL rock samples used in the high temperature triaxial tests are samples obtained from the upper 270 m of the rock mass. Further testing should be performed on samples obtained at greater depth, e.g. 500 m, to better understand the effects of high temperature on rock at great depth and also the effects of stress relaxation.

Acknowledgements

The authors wish to express their thanks to S.M. Grinnell and G.B. Murray for carrying out the second series of ultrasonic tests.

References

Annor, A., Miles, P., Kapeller, F. and Larocque, G. (1980), "High temperature and pressure triaxial compression tests on rock samples from Pinawa and the Creighton Mine", Atomic Energy of Canada Limited Technical, Record TR-158, 51 p.

Annor, A. and Jackson, R. (1985), "Mechanical properties of rock samples from the Lac du Bonnet Batholith, Manitoba", Division Report M&ET/MRL 85-41(TR), CANMET, Energy, Mines and Resources Canada, 101 p.

Baumgartner, P. (1986), "The used fuel disposal centre study: study plan and technical specifications", in Proceedings of the 2nd International Conference on Radioactive Waste Management, Winnipeg, Manitoba, Canada, September 7-11, 1986, p. 427-431.

Brown, E.T. (1981), "Rock characterization testing and monitoring, ISRM suggested methods", International Society for Rock Mechanics, the Commission on Testing Methods, Pergamon, 211 p.

Goodman, R.E. (1980), "Introduction to Rock Mechanics", John Wiley and Sons, Inc., New York, 478 p.

Gorski, B. (1987), "Post-failure uniaxial strength determinations using a servo-hydraulic test system", Division Report MRL 87-33(INT), CANMET, Energy, Mines and Resources Canada, 77 p.

Gyenge, M. and Herget, G. (1977), "Pit slop manual supplement 3-2 - laboratory tests for design parameters", CANMET, CANMET Report 77-26, 74 p.

Gyenge, M. and Ladanyi, B. (1977), "Pit slope manual supplement 3-5 - sampling and specimen preparation", CANMET, CANMET Report 77-29, 30 p.

Hoek, E. and Brown, E.T. (1980), "Underground excavations in rock", The institution of Mining and Metallurgy, London, 527 p.

Jackson, R. (1984), "Summary of mechanical properties of Lac du Bonnet and Eye-Dashwa specimens", Division Report MRP/MRL 84-85(TR), CANMET, Energy, Mines and Resources Canada, 48 p.

Kamineni, D.C., Dugal, J.J.B. and Ejeckam, R.B. (1984), "Geochemical investigations of granitic core samples from boreholes at the Underground Research Laboratory site near Lac du Bonnet, Manitoba", Atomic Energy of Canada Limited Technical Record, TR-221, 61 p.

MTS Systems Corporation (1986), "Operation manual for 815 rock mechanics test systems", MTS Systems Corp., Minneapolis, Minnesota, U.S.A.

Terrametrics (1980), "Instruction manual - sonic velocity equipment", Terrametrics, Inc., Golden, Colorado, U.S.A., 17 p.

Wong, A.S. (1984), "Modal analyses of URL-01, URL-02, URL-05 and URL-06 extended engineering core samples from the Underground Research Laboratory site near Lac du Bonnet, Manitoba", Division Report ERP/MRL 84-27(TR), CANMET, Energy, Mines and Resources Canada, 21 p.

Table 1. Dimensions, densities and dynamic elastic properties of rock samples (first series)

Specimen identification	Length (mm)	Diameter (mm)	Bulk density (g/cc)	P-wave velocity (km/s)	S-wave velocity (km/s)	Dynamic Young's modulus (GPa)	Dynamic shear modulus (GPa)	Dynamic Poisson's ratio
URL-5-273.18	101.74	45.13	2.620	4.037	2.626	40.950	18.067	0.13
URL-5-273.40	100.70	45.13	2.634	4.077	2.603	41.260	17.847	0.16
URL-5-273.60	98.68	45.12	2.641	4.253	2.598	42.866	17.826	0.20
URL-5-273.70	100.00	45.14	2.636	4.255	2.571	42.253	17.424	0.21
URL-5-273.91	100.50	45.14	2.633	3.926	2.510	38.297	16.588	0.15
URL-5-274.01	100.48	45.12	2.637	3.979	2.513	38.909	16.653	0.17
URL-5-274.12	99.98	45.14	2.634	4.040	2.541	38.890	17.007	0.17
URL-5-274.30	100.08	45.12	2.635	4.127	2.518	40.213	16.707	0.20
URL-5-274.40	100.51	45.13	2.637	4.028	2.504	39.188	16.534	0.19
URL-5-274.97	100.79	45.11	2.628	4.122	2.527	40.241	16.782	0.20
URL-5-275.07	101.60	44.92	2.632	4.536	2.725	47.596	19.544	0.22
URL-5-275.18	100.40	44.69	2.632	4.512	2.733	47.585	19.659	0.21
URL-5-275.96	102.25	44.89	2.631	3.851	2.547	47.933	17.068	0.11
URL-5-276.23	100.54	44.90	2.628	3.943	2.468	37.711	16.007	0.18
URL-5-276.33	100.72	44.89	2.624	3.934	2.560	38.959	17.197	0.13
URL-5-276.44	101.64	44.90	2.641	3.978	2.535	39.310	16.972	0.16
URL-5-276.57	100.00	44.90	2.637	4.024	2.476	38.649	16.166	0.20
URL-5-276.67	101.01	44.91	2.641	4.048	2.501	39.359	16.519	0.19
URL-5-276.86	99.84	44.92	2.640	4.117	2.506	39.980	16.579	0.21
URL-5-276.96	101.40	44.91	2.642	3.976	2.542	39.414	17.072	0.15
URL-5-277.07	101.00	44.92	2.638	3.984	2.507	38.870	16.580	0.17

Table 2. Dimensions, densities and dynamic elastic properties of rock samples (second series)

Specimen identification	Length (mm)	Diameter (mm)	Bulk density (g/cc)	P-wave velocity (km/s)	S-wave velocity (km/s)	Dynamic Young's modulus (GPa)	Dynamic shear modulus (GPa)	Dynamic Poisson's ratio
URL-5-269.98	111.62	45.10	2.639	3.810	2.250	32.931	13.365	0.23
URL-5-270.10	112.03	45.08	2.674	4.411	2.435	40.624	15.860	0.28
URL-5-270.26	110.80	45.10	2.642	3.895	2.393	36.213	15.130	0.20
URL-5-270.38	111.85	45.09	2.635	4.075	2.233	33.766	13.133	0.29
URL-5-270.50	110.86	45.10	2.635	4.176	2.267	34.967	13.543	0.29
URL-5-270.67	110.90	45.10	2.636	3.844	2.153	31.080	12.225	0.27
URL-5-270.78	109.86	45.10	2.636	4.061	2.358	36.507	14.651	0.25
URL-5-270.90	111.10	45.08	2.635	4.107	2.405	37.766	15.238	0.24
URL-5-271.01	112.46	45.10	2.631	4.436	2.408	39.399	15.258	0.29
URL-5-271.22	114.02	45.10	2.630	4.286	2.473	40.236	16.089	0.25
URL-5-271.35	108.98	45.08	2.630	4.350	2.294	36.198	13.844	0.31
URL-5-271.46	110.32	45.08	2.631	4.284	2.602	43.026	17.811	0.21
URL-5-271.58	112.01	45.09	2.621	4.235	2.473	39.785	16.025	0.24
URL-5-271.75	110.51	45.10	2.620	4.178	2.298	35.495	13.830	0.28
URL-5-271.87	113.01	45.09	2.629	4.248	2.330	36.681	14.274	0.29
URL-5-271.99	109.36	45.08	2.638	4.247	2.352	37.320	14.591	0.28
URL-5-272.11	113.72	45.12	2.627	4.173	2.345	36.666	14.443	0.27
URL-5-272.23	109.00	45.11	2.630	4.233	2.276	35.321	13.619	0.30
URL-5-272.34	114.46	45.10	2.626	4.066	2.467	38.632	15.980	0.21
URL-5-272.61	114.96	45.11	2.635	4.188	2.478	39.815	16.175	0.23
URL-5-272.73	110.28	45.11	2.630	4.201	2.302	35.838	13.941	0.29
URL-5-272.84	112.58	45.10	2.627	4.131	2.380	37.253	14.882	0.25
URL-5-272.97	111.86	45.10	2.625	4.237	2.274	35.221	13.569	0.30

Table 3. Results of high temperature triaxial tests (first series)

Specimen	Sample Number	Length (mm)	Diameter (mm)	Confining Pressure (MPa)	Temp. (deg C.)	Total Axial Strain (%)	Failure Deviator Stress (MPa)	Tangent Young's Modulus (GPa)	Pseudo Young's Modulus (GPa)	θ (deg)	Failure characteristics
URL05-273.18	A 1T	101.74	45.13	3.5	100		220			70	2 fragments, single shear plane
URL05-273.40	A 2T	100.70	45.13	3.5	100	0.376	220	66.83	67.56	75	2 fragments, single shear plane
URL05-273.60	A 3T	98.68	45.12	3.5	100	0.407	217	60.49	58.85	72	3 fragments, shear plane, bottom wedge
URL05-273.91	A19T	100.50	45.14	3.5	100	0.390	216	64.70	65.26	72	2 fragments, single shear plane
URL05-273.70	A 4T	100.00	45.14	3.5	200		184			70	2 fragments, single shear plane
URL05-274.01	A 5T	100.48	45.12	3.5	200	0.402	194	66.36	65.46	70	2 fragments, single curved plane
URL05-274.12	A 6T	99.98	45.14	3.5	200		167			69	2 fragments, curved plane, cracks
URL05-275.96	A20T	102.25	44.89	3.5	200	0.386	202	62.88	62.95	72	2 fragments, single shear plane
URL05-274.30	A 7T	100.08	45.12	17.0	100	0.689	376	62.08	63.86	75	2 fragments, single curved plane
URL05-274.40	A 8T	100.51	45.13	17.0	100	0.633	367	62.37	64.35	70	2 fragments, single shear plane
URL05-274.97	A 9T	100.79	45.11	17.0	100	0.649	385	64.92	67.29	69	2 fragments, single shear plane
URL05-276.23	A21T	100.54	44.90	17.0	100	0.708	384	62.76	64.95	73	2 fragments, single shear plane
URL05-275.07	A10T	101.60	44.92	17.0	200	0.629	331	59.90	60.51	71	2 fragments, single shear plane
URL05-275.18	A11T	100.40	44.69	17.0	200					67	3 fragments, shear plane, top wedge
URL05-276.33	A12T	100.72	44.89	17.0	200		323			70	2 fragments, curved plane, cracks
URL05-277.07	A18T	101.00	44.92	17.0	200	0.623	353	63.65	65.96	72	2 fragments, single shear plane
URL05-276.44	A13T	101.64	44.90	35.0	100	0.881	402	63.00	64.38		bottom wedge
URL05-276.57	A14T	100.00	44.90	35.0	100	0.885	496	62.15	64.41	67	2 fragments, curved plane, cracks
URL05-276.67	A15T	101.01	44.91	35.0	100	0.886	495	61.89	64.20	70	3 fragments, curved plane, top wedge
URL05-276.86	A16T	99.84	44.92	35.0	200	0.826	464	61.93	64.28	69	2 fragments, single curved plane
URL05-276.96	A17T	101.40	44.91	35.0	200	0.826	467	63.96	66.62	70	2 fragments, single curved plane

Table 4. Results of high temperature triaxial tests (second series)

Specimen	Sample Number	Length (mm)	Diameter (mm)	Confining Pressure (MPa)	Temp. (deg C.)	Total Axial Strain (%)	Failure Deviator Stress (MPa)	Tangent Young's Modulus (GPa)	Pseudo Young's Modulus (GPa)	θ (deg)	Failure characteristics
URL05-271.87	A36T	113.01	45.09	3.5	23	0.477	272	69.20	69.37		multiple cracks parallel to core axis
URL05-271.99	A37T	109.36	45.08	3.5	23	0.492	274	68.51	68.82	69	2 fragments, single shear plane
URL05-269.98	A22T	111.62	45.10	3.5	100	0.391	204	64.67	64.34	70	3 fragments, shear plane, conical top end
URL05-270.10	A23T	112.03	45.08	3.5	100	0.344	176	65.55	65.27	57	2 fragments, curved plane, cracks
URL05-270.90	A29T	111.10	45.08	3.5	200	0.463	229	62.79	62.43	75	3 fragments, shear plane, top wedge
URL05-271.01	A30T	112.46	45.10	3.5	200	0.440	228	64.85	64.42	68	2 fragments, shear plane, cracks
URL05-272.11	A38T	113.72	45.12	17.0	23	0.717	434	70.07	71.40	72	2 fragments, curved plane, cracks
URL05-272.23	A39T	109.00	45.11	17.0	23	0.712	418	68.97	70.32	70	2 fragments, single shear plane
URL05-270.26	A24T	110.80	45.10	17.0	100	0.614	368	68.79	69.80	70	2 fragments, single shear plane
URL05-270.38	A25T	111.85	45.09	17.0	100	0.646	378	68.35	69.46	72	2 fragments, curved plane
URL05-270.50	A26T	110.86	45.10	17.0	100	0.579	350	70.92	71.85	68	2 fragments, curved plane
URL05-271.22	A31T	114.02	45.10	17.0	200	0.616	372	69.67	70.65	70	2 fragments, single shear plane
URL05-271.35	A32T	108.98	45.08	17.0	200	0.666	385	67.26	68.13	73	3 fragments, shear plane, bottom wedge
URL05-271.46	A33T	110.32	45.08	17.0	200	0.601	376	68.59	69.40	71	3 fragments, shear plane, top wedge
URL05-272.34	A40T	114.46	45.10	35.0	23	0.876	506	54.25	55.67	70	2 fragments, single shear plane
URL05-272.61	A41T	114.96	45.11	35.0	23	0.829	521	70.05	71.80	60	2 fragments, curved plane
URL05-270.67	A27T	110.90	45.10	35.0	100	0.760	449	68.01	68.01	65	2 fragments, single shear plane
URL05-270.78	A28T	109.86	45.10	35.0	100	0.824	508	70.07	71.68	65	2 fragments, curved plane, bottom wedge
URL05-272.73	A42T	110.28	45.11	35.0	100	0.808	525	71.43	73.02	67	2 fragments, curved plane
URL05-271.58	A34T	112.01	45.09	35.0	200	0.804	518	69.19	70.40	70	2 fragments, curved plane
URL05-271.75	A35T	110.51	45.10	35.0	200	0.798	487	69.10	70.35	70	2 fragments, single shear plane

Table 5. Tangent Young's moduli of the rock samples (second series)

Specimen Identification	Sample Number	Pressure (MPa)	Temp. (deg C.)	Tangent Young's Modulus (GPa)						
				0.10	0.20	0.30	0.40	0.50	0.75	1.00
URL05-271.87	A36T	3.5	23	57.04	64.56	67.79	69.29	69.20	61.58	19.43
URL05-271.99	A37T	3.5	23	57.90	65.63	67.98	68.91	68.51	61.08	13.76
URL05-269.98	A22T	3.5	100	47.59	56.27	61.05	63.74	64.67	59.52	19.36
URL05-270.10	A23T	3.5	100	47.29	56.99	61.96	64.69	65.55	59.64	12.87
URL05-270.90	A29T	3.5	200	44.71	53.38	58.77	61.76	62.79	57.05	7.35
URL05-271.01	A30T	3.5	200	45.85	55.11	60.59	63.69	64.85	59.63	21.33
URL05-272.11	A38T	17.0	23	74.08	75.50	74.40	72.62	70.07	59.40	20.79
URL05-272.23	A39T	17.0	23	72.85	74.43	73.34	71.55	68.97	58.14	14.45
URL05-270.26	A24T	17.0	100	70.07	71.37	71.49	70.64	68.79	58.68	21.47
URL05-270.38	A25T	17.0	100	70.93	71.88	71.58	70.42	68.35	58.13	13.71
URL05-270.50	A26T	17.0	100	71.62	73.11	73.33	72.62	70.92	61.55	1.40
URL05-271.22	A31T	17.0	200	70.71	71.92	72.18	71.45	69.67	59.63	17.83
URL05-271.35	A32T	17.0	200	71.28	70.92	70.14	68.93	67.26	60.57	14.37
URL05-271.46	A33T	17.0	200	69.86	70.62	70.75	70.08	68.59	60.55	27.74
URL05-272.34	A40T	35.0	23	77.93	72.35	64.07	57.70	54.25	61.50	9.07
URL05-272.61	A41T	35.0	23	80.21	79.04	76.46	73.49	70.05	58.74	25.88
URL05-270.67	A27T	35.0	100	73.48	73.19	72.22	70.52	68.01	57.14	15.40
URL05-270.78	A28T	35.0	100	79.41	77.77	75.75	73.20	70.07	58.82	18.08
URL05-272.73	A42T	35.0	100	80.94	79.20	77.11	74.54	71.43	60.56	26.11
URL05-271.58	A34T	35.0	200	79.76	74.73	73.37	71.54	69.19	60.48	26.88
URL05-271.75	A35T	35.0	200	73.35	74.36	73.23	71.50	69.10	59.44	20.60

Table 6. Pseudo Young's moduli of the rock samples (second series)

Specimen Identification	Sample Number	Pressure (MPa)	Temp. (deg C.)	Pseudo Young's Modulus (GPa)						
				0.10	0.20	0.30	0.40	0.50	0.75	1.00
URL05-271.87	A36T	3.5	23	46.11	61.55	66.32	68.67	69.37	66.28	45.31
URL05-271.99	A37T	3.5	23	39.77	62.89	66.92	68.56	68.82	65.56	43.83
URL05-269.98	A22T	3.5	100	35.30	52.45	58.83	62.54	64.34	63.00	45.19
URL05-270.10	A23T	3.5	100	35.04	52.75	59.65	63.48	65.27	63.57	42.23
URL05-270.90	A29T	3.5	200	39.69	49.18	56.26	60.43	62.43	60.92	39.30
URL05-271.01	A30T	3.5	200	34.97	50.83	58.04	62.30	64.42	63.22	45.74
URL05-272.11	A38T	17.0	23	62.23	75.54	75.01	73.57	71.40	65.18	44.83
URL05-272.23	A39T	17.0	23	62.47	74.40	73.94	72.50	70.32	64.02	41.88
URL05-270.26	A24T	17.0	100	66.98	70.88	71.51	71.15	69.80	64.35	44.19
URL05-270.38	A25T	17.0	100	64.80	71.65	71.80	71.08	69.46	63.80	42.09
URL05-270.50	A26T	17.0	100	68.10	72.57	73.30	73.05	71.85	66.82	42.45
URL05-271.22	A31T	17.0	200	70.52	71.37	72.13	71.90	70.65	65.29	44.00
URL05-271.35	A32T	17.0	200	71.30	71.13	70.56	69.57	68.13	64.23	40.60
URL05-271.46	A33T	17.0	200	71.04	70.22	70.75	70.48	69.40	65.06	49.15
URL05-272.34	A40T	35.0	23	69.57	76.27	68.00	60.63	55.67	56.00	47.90
URL05-272.61	A41T	35.0	23	76.76	80.02	77.77	75.00	71.80	64.61	46.28
URL05-270.67	A27T	35.0	100	73.49	73.38	72.76	71.43	69.33	63.06	41.37
URL05-270.78	A28T	35.0	100	80.25	78.60	76.79	74.51	71.68	64.76	43.74
URL05-272.73	A42T	35.0	100	81.86	80.08	78.19	75.86	73.02	66.28	47.78
URL05-271.58	A34T	35.0	200	90.74	75.85	74.08	72.49	70.40	65.12	48.85
URL05-271.75	A35T	35.0	200	68.42	74.40	73.84	72.41	70.35	64.65	45.27

Table 7. Values of σ_c , m , s and r^2 computed by using Hoek and Brown failure criterion

Test Series	Test Temperature (°C.)	Number of Samples n	Uniaxial Compressive Strength σ_c (MPa)	Estimated Uniaxial Compressive Strength σ_c (MPa)	m	s	r^2
First	100	10		170	37.22	1.00	0.9930
First	200	9		122	47.32	1.00	0.9929
Second	23	6	186		31.88	1.84	0.9696
Second	100	7		100	73.50	1.00	0.9921
Second	200	7		179	35.39	1.00	0.9860

Table 8. Strength properties of rock samples.

Test Series	Test Temperature (°C)	Confining Pressure (MPa)	Angle of Internal Friction (degree)	Cohesion (MPa)
First	100	3.5	62	22
First	100	17.0	55	36
First	100	35.0	47	62
First	200	3.5	61	18
First	200	17.0	54	32
First	200	35.0	46	60
Second	23	3.5	65	24
Second	23	17.0	53	48
Second	23	35.0	44	78
Second	100	3.5	63	16
Second	100	17.0	57	30
Second	100	35.0	51	49
Second	200	3.5	60	16
Second	200	17.0	54	37
Second	200	35.0	49	53

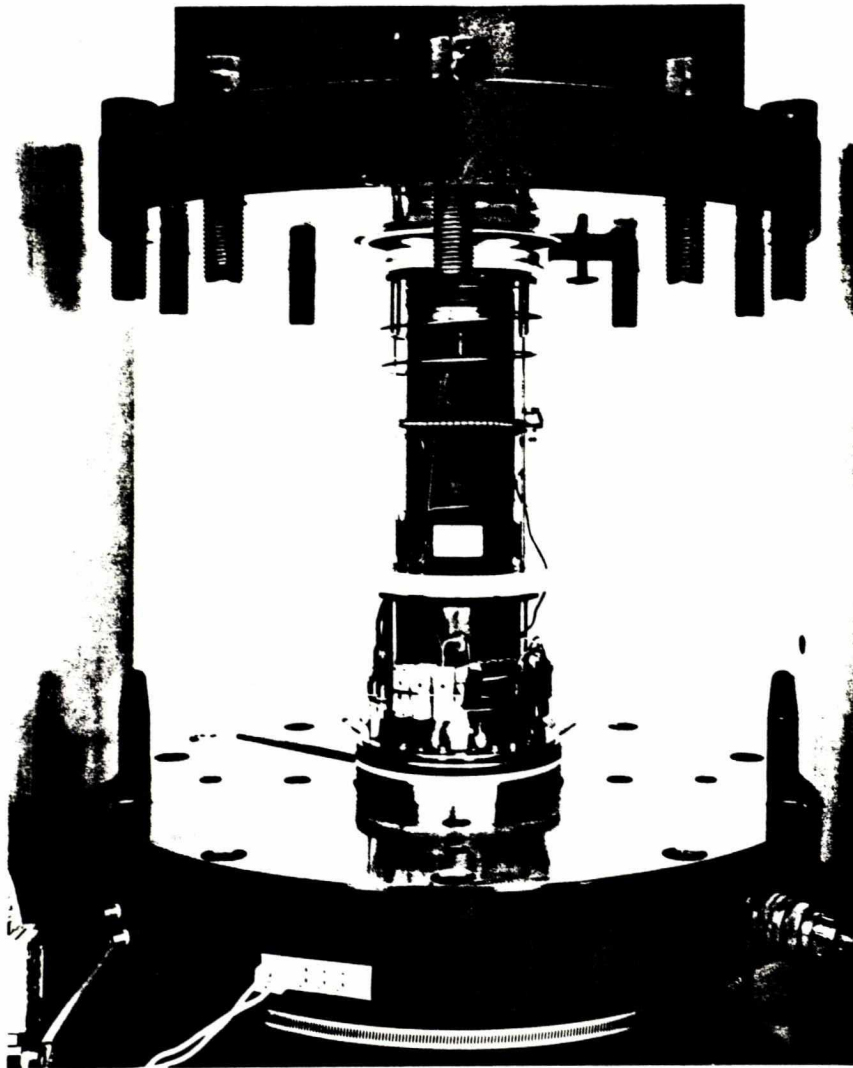


Figure 1. The test stack for the rock specimen

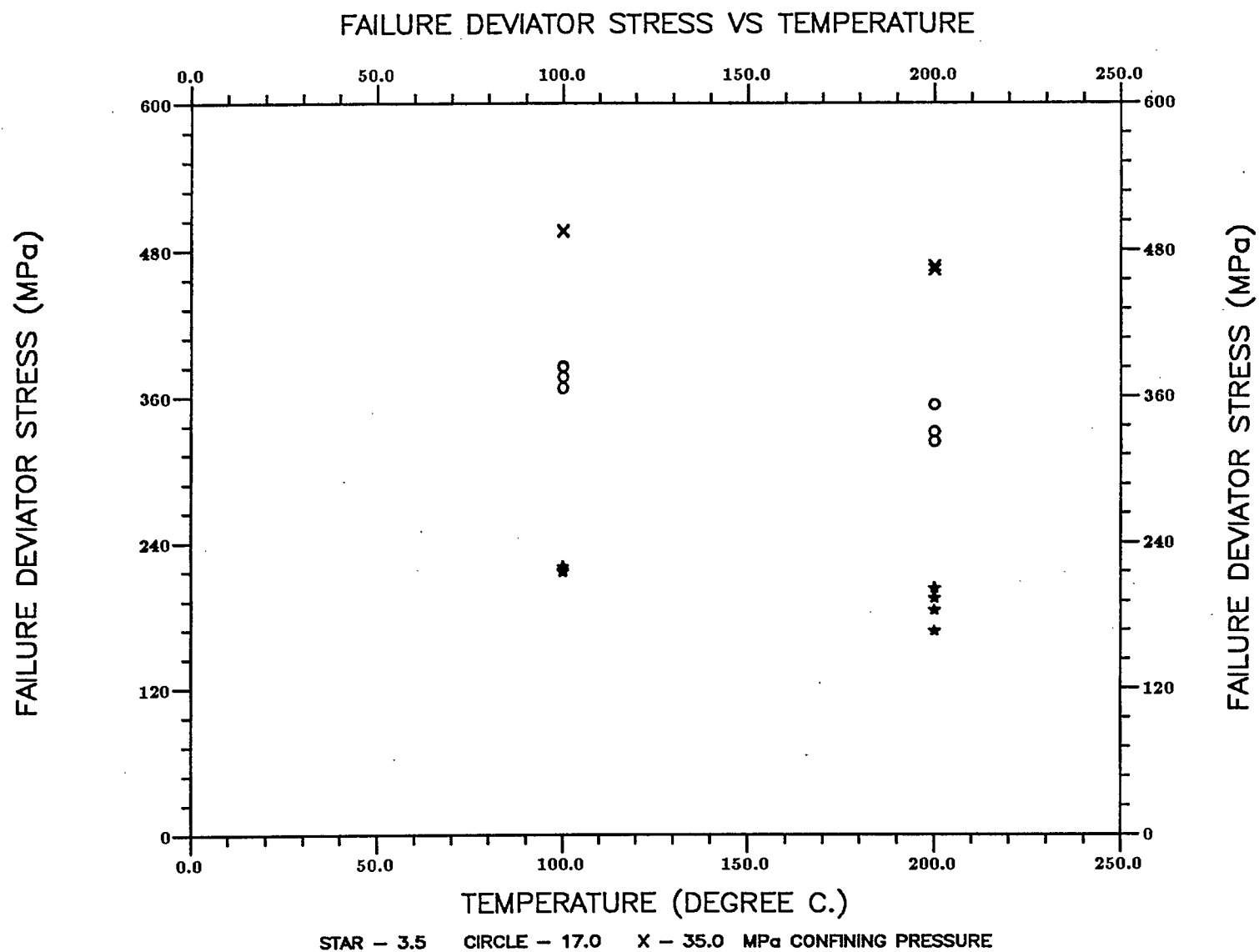


Figure 2. Plots of failure deviator stresses versus temperature for the first series of tests conducted at the confining pressures of 3.5, 17.0 and 35.0 MPa.

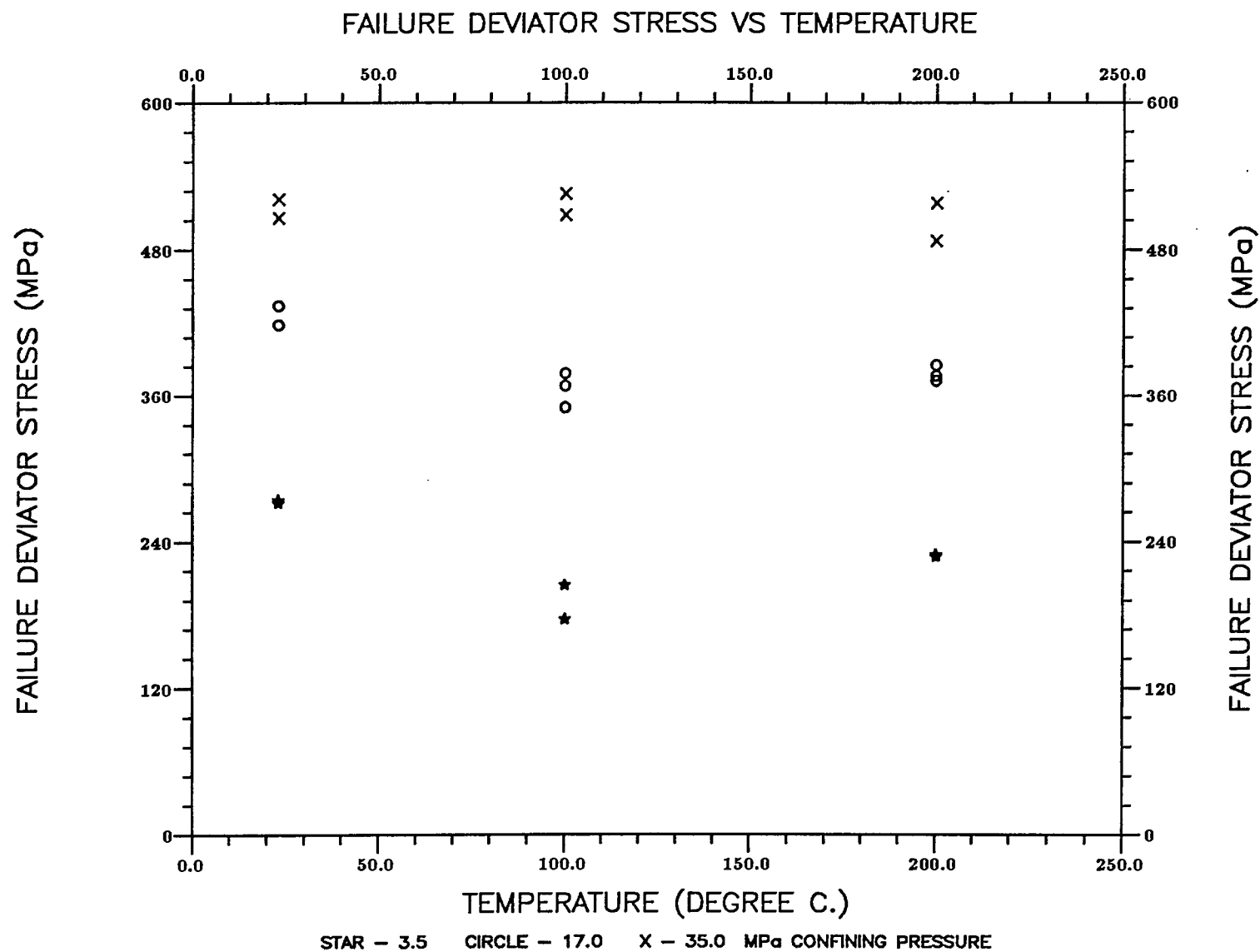


Figure 3. Plots of failure deviator stresses versus temperature for the second series of tests conducted at the confining pressures of 3.5, 17.0 and 35.0 MPa.

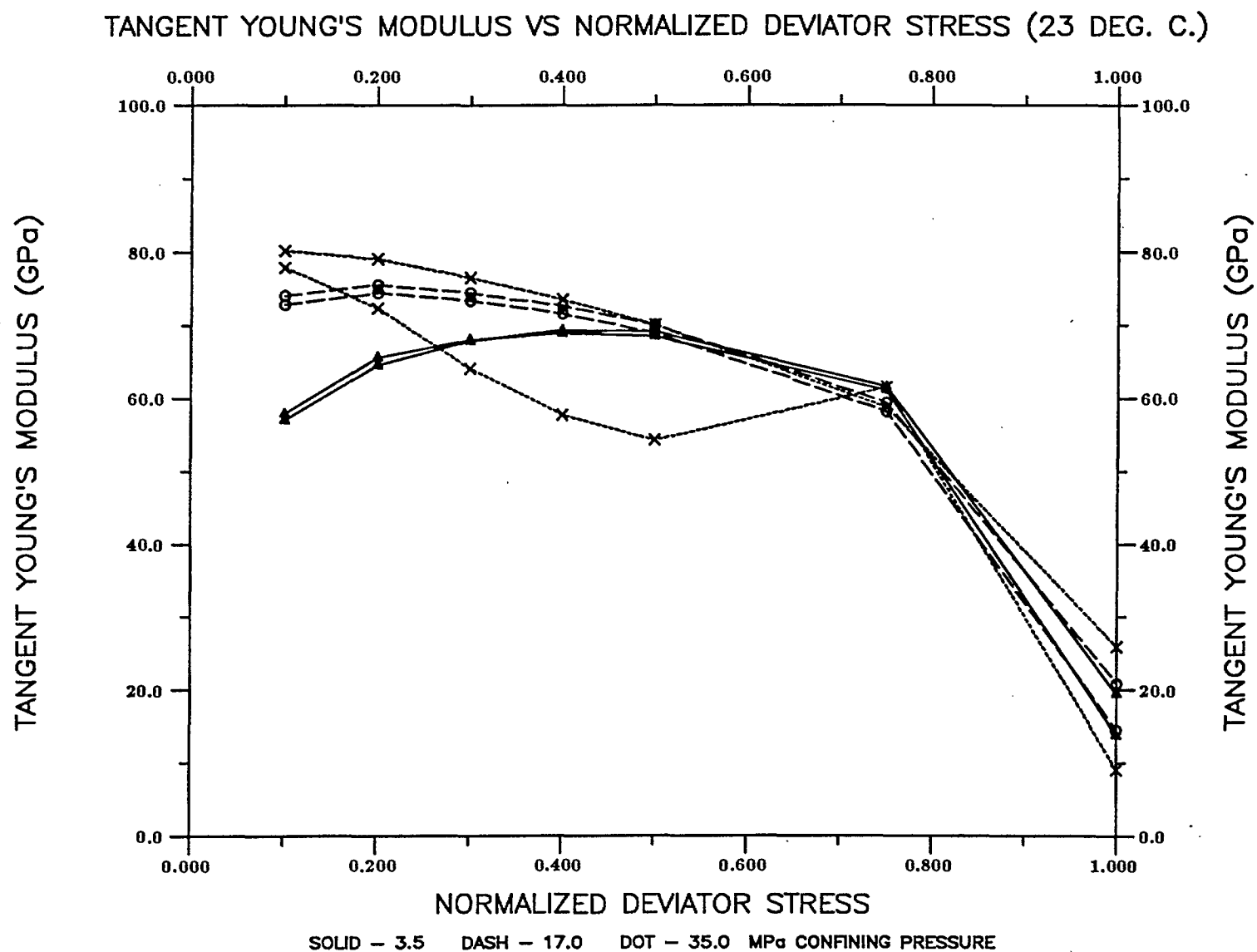


Figure 4. Plots of tangent Young's modulus versus normalized deviator stress for the second series of tests conducted at the temperature of 23° C.

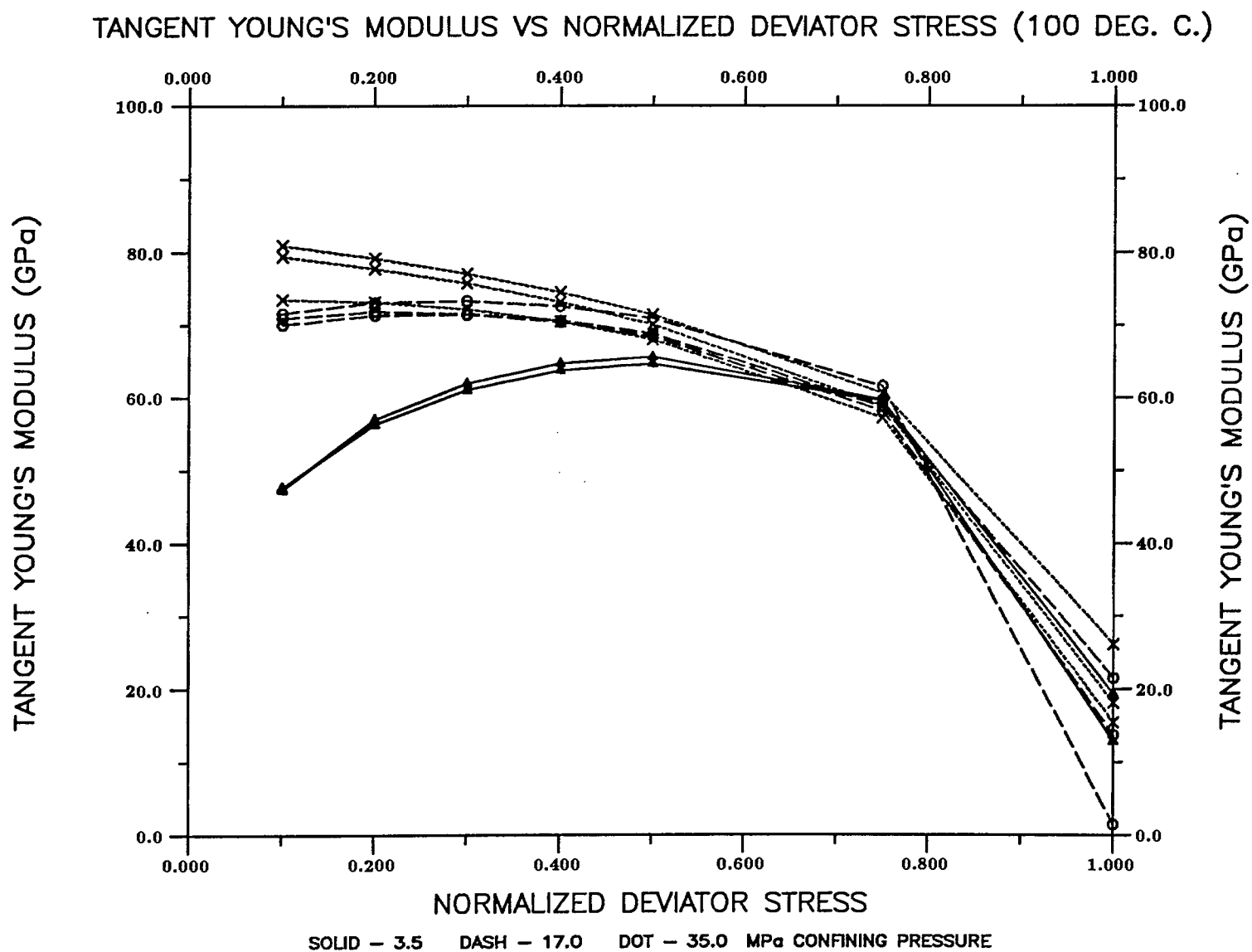


Figure 5. Plots of tangent Young's modulus versus normalized deviator stress for the second series of tests conducted at the temperature of 100° C.

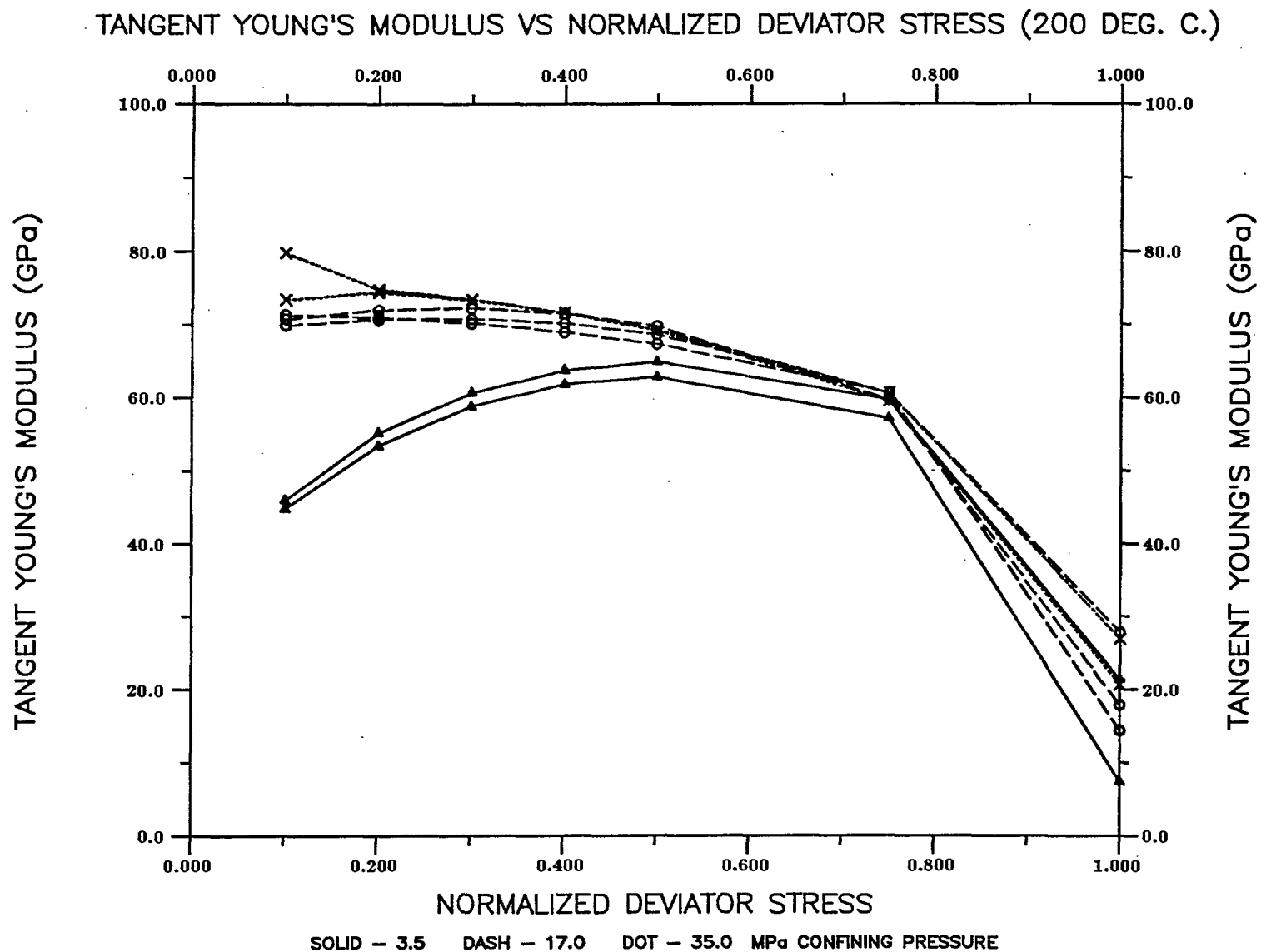


Figure 6. Plots of tangent Young's modulus versus normalized deviator stress for the second series of tests conducted at the temperature of 200° C.

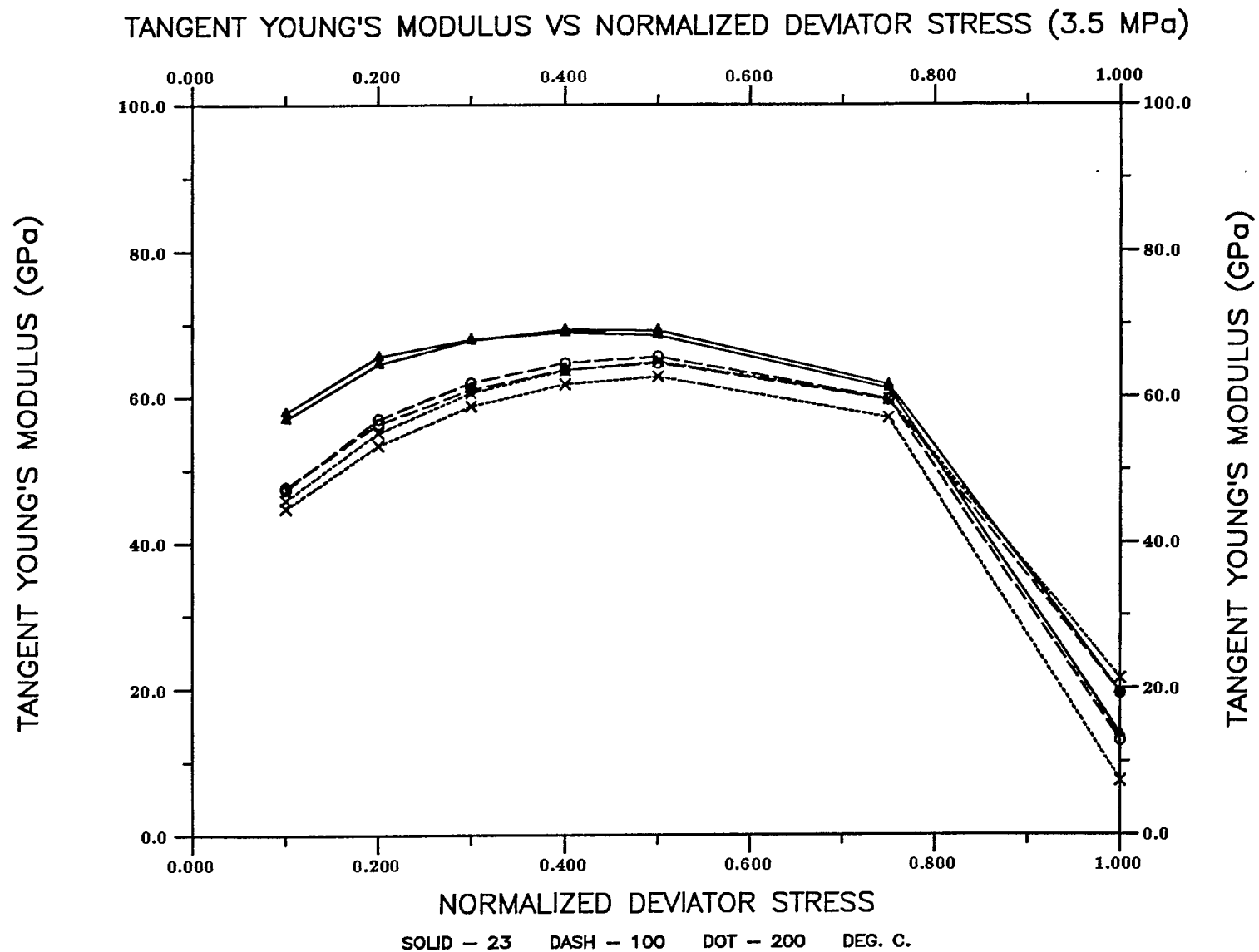


Figure 7. Plots of tangent Young's modulus versus normalized deviator stress for the second series of tests conducted at the confining pressure of 3.5 MPa.

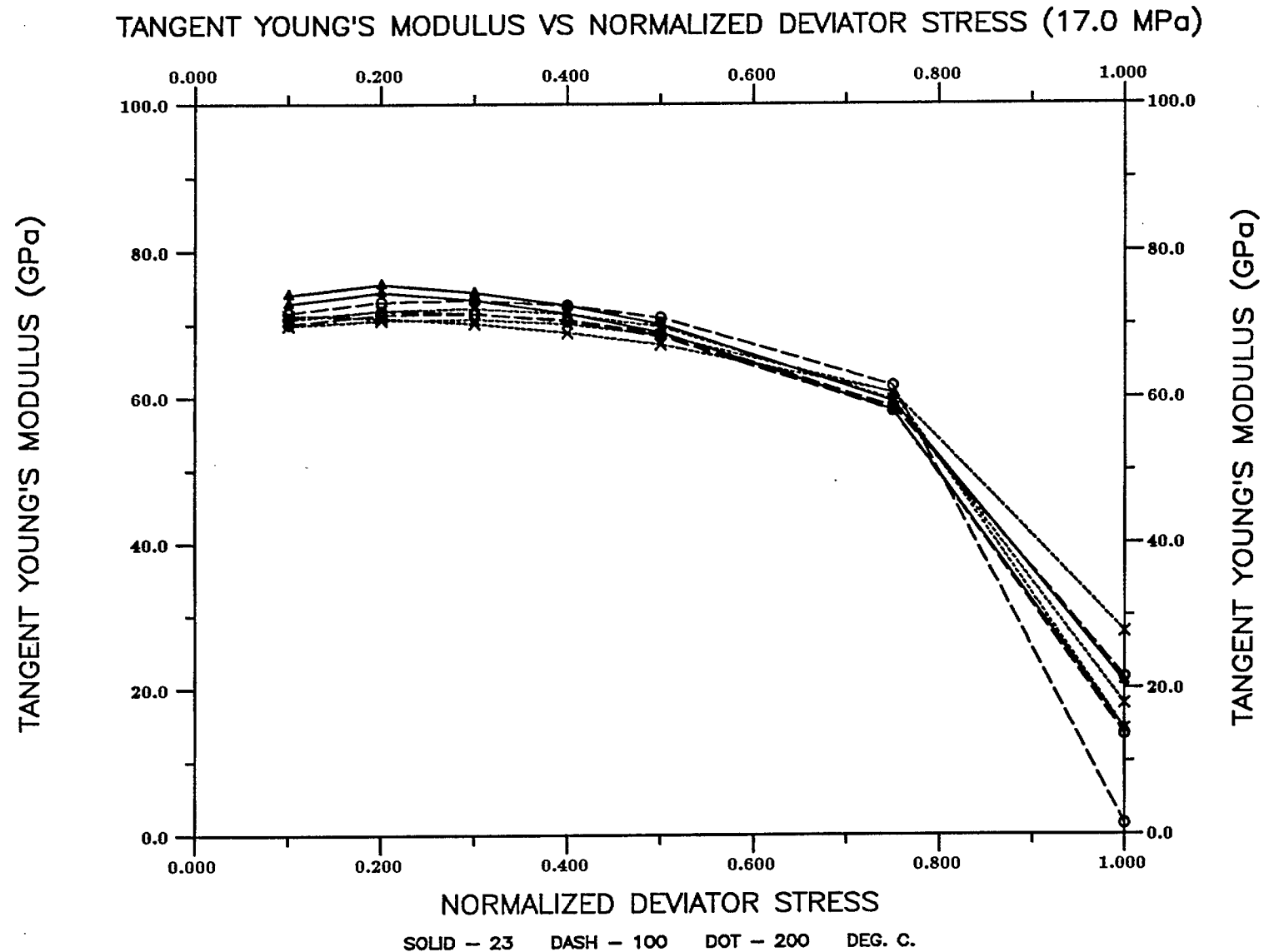


Figure 8. Plots of tangent Young's modulus versus normalized deviator stress for the second series of tests conducted at the confining pressure of 17.0 MPa.

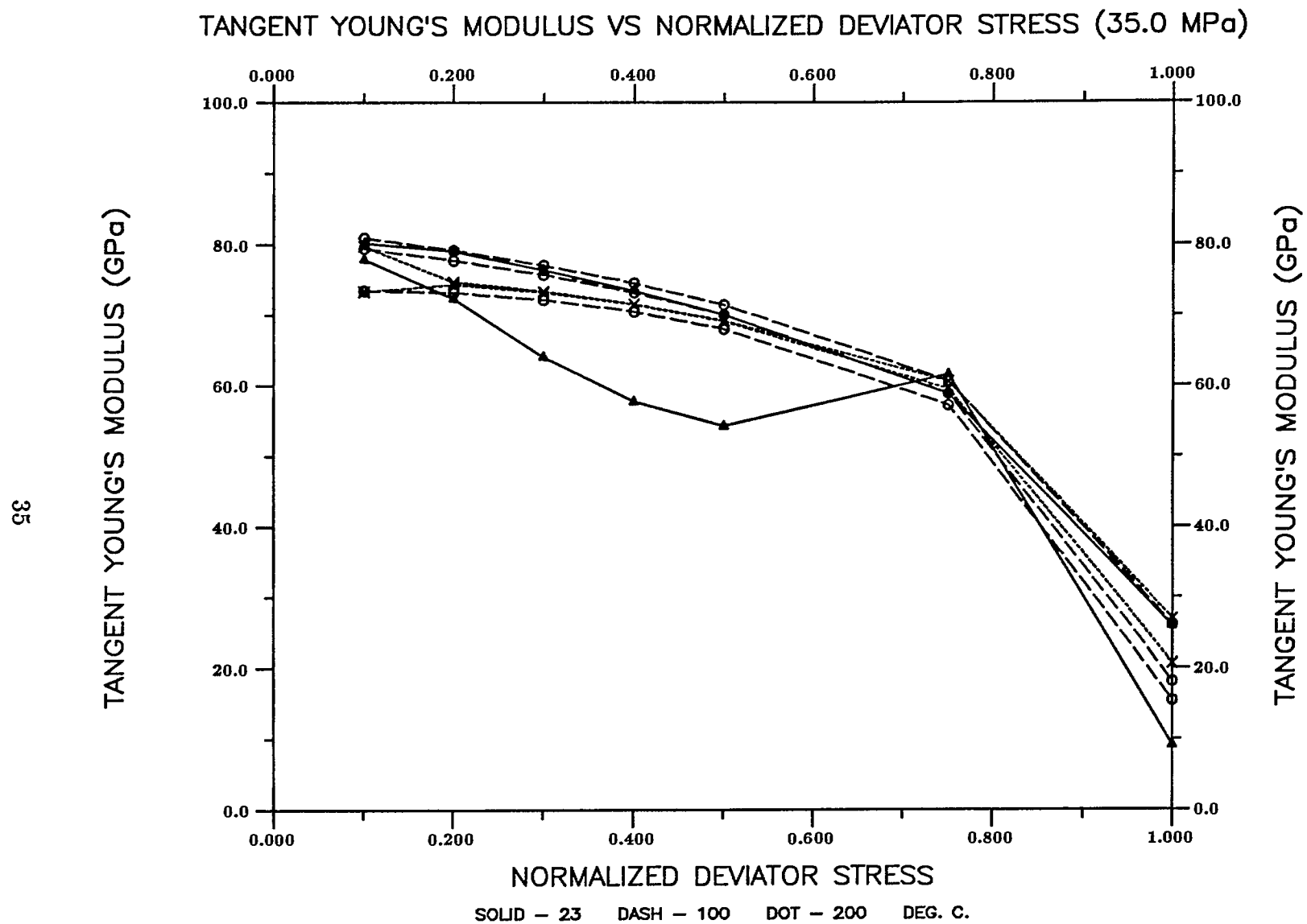


Figure 9. Plots of tangent Young's modulus versus normalized deviator stress for the second series of tests conducted at the confining pressure of 35.0 MPa.

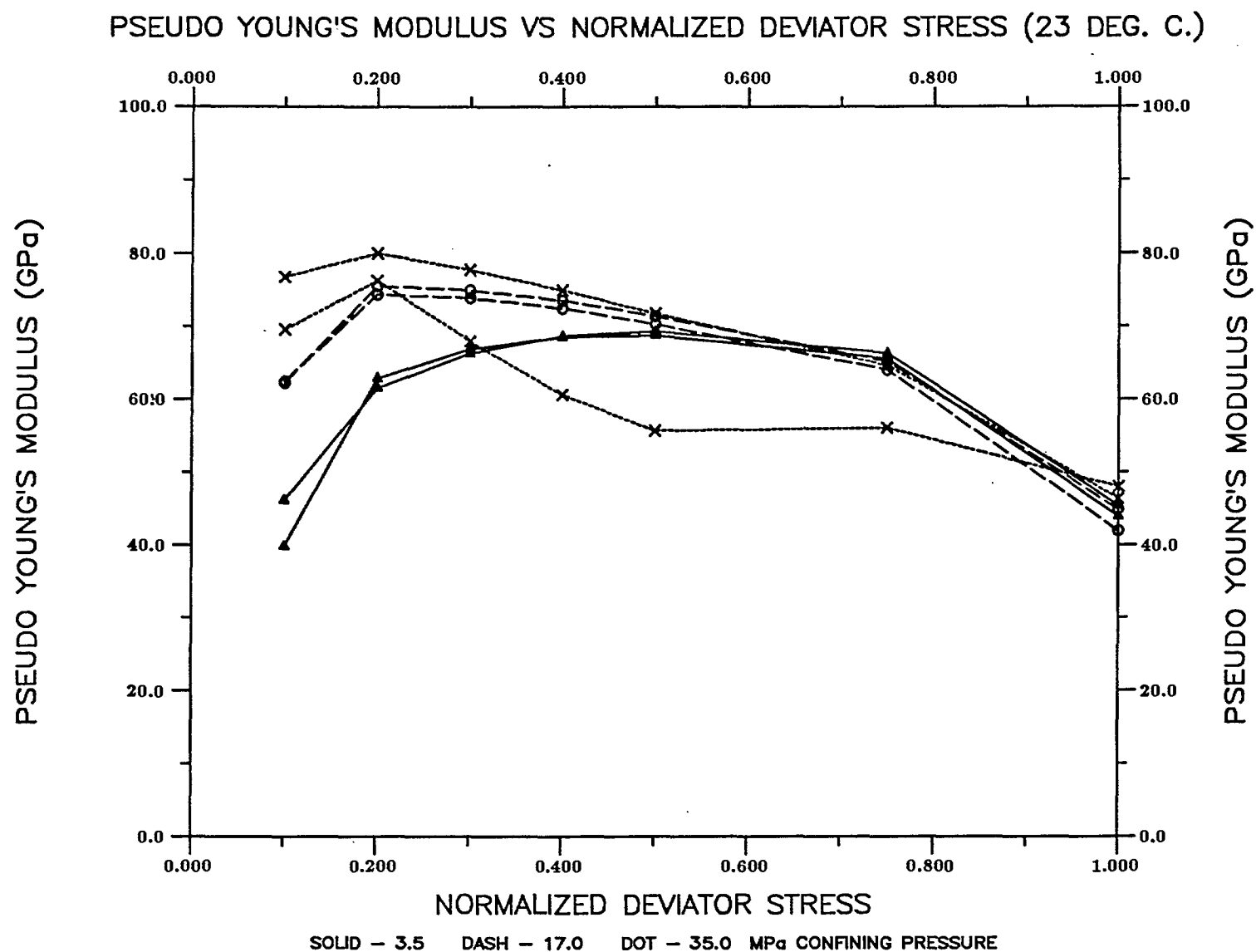


Figure 10. Plots of pseudo Young's modulus versus normalized deviator stress for the second series of tests conducted at the temperature of 23° C.

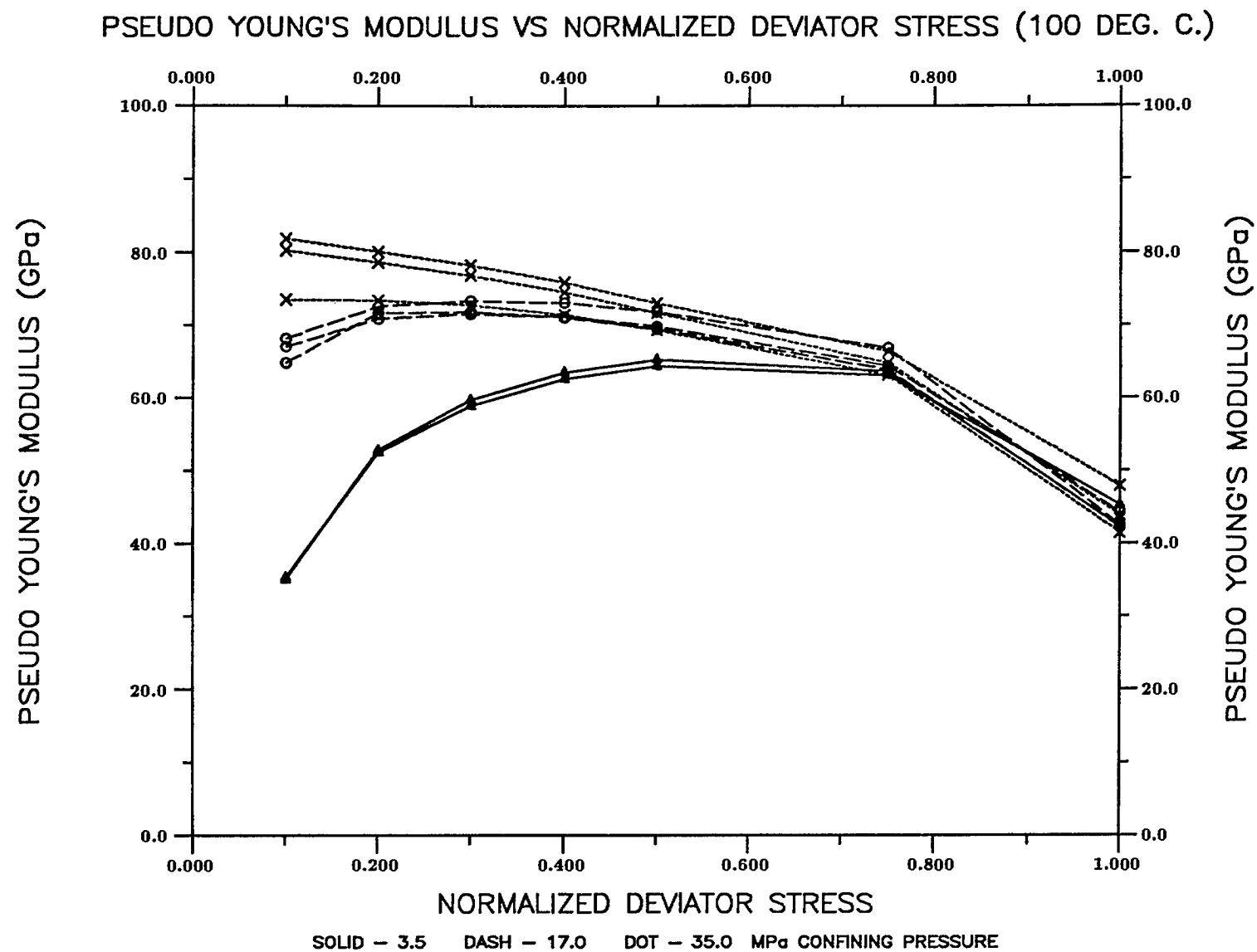


Figure 11. Plots of pseudo Young's modulus versus normalized deviator stress for the second series of tests conducted at the temperature of 100° C.

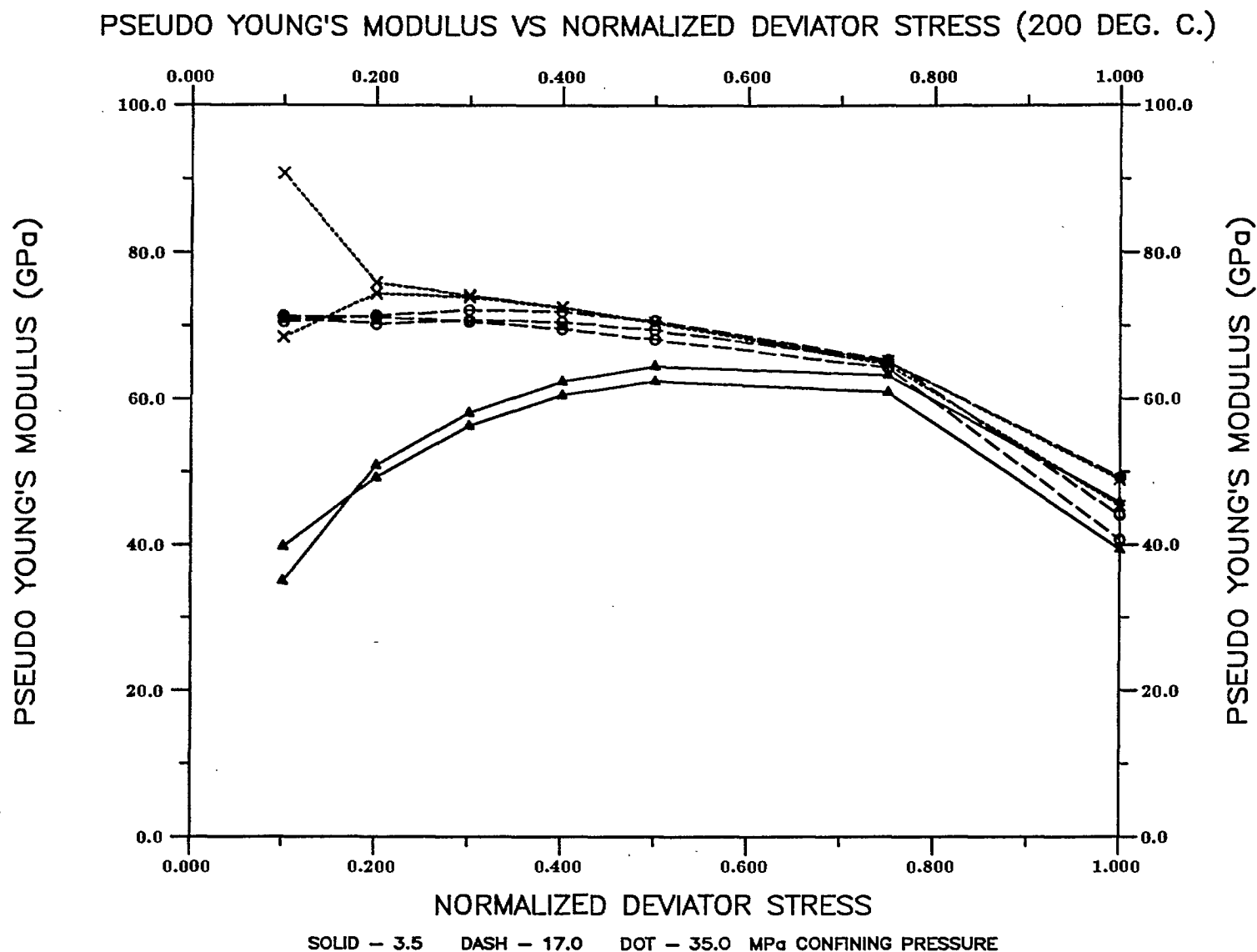


Figure 12. Plots of pseudo Young's modulus versus normalized deviator stress for the second series of tests conducted at the temperature of 200° C.

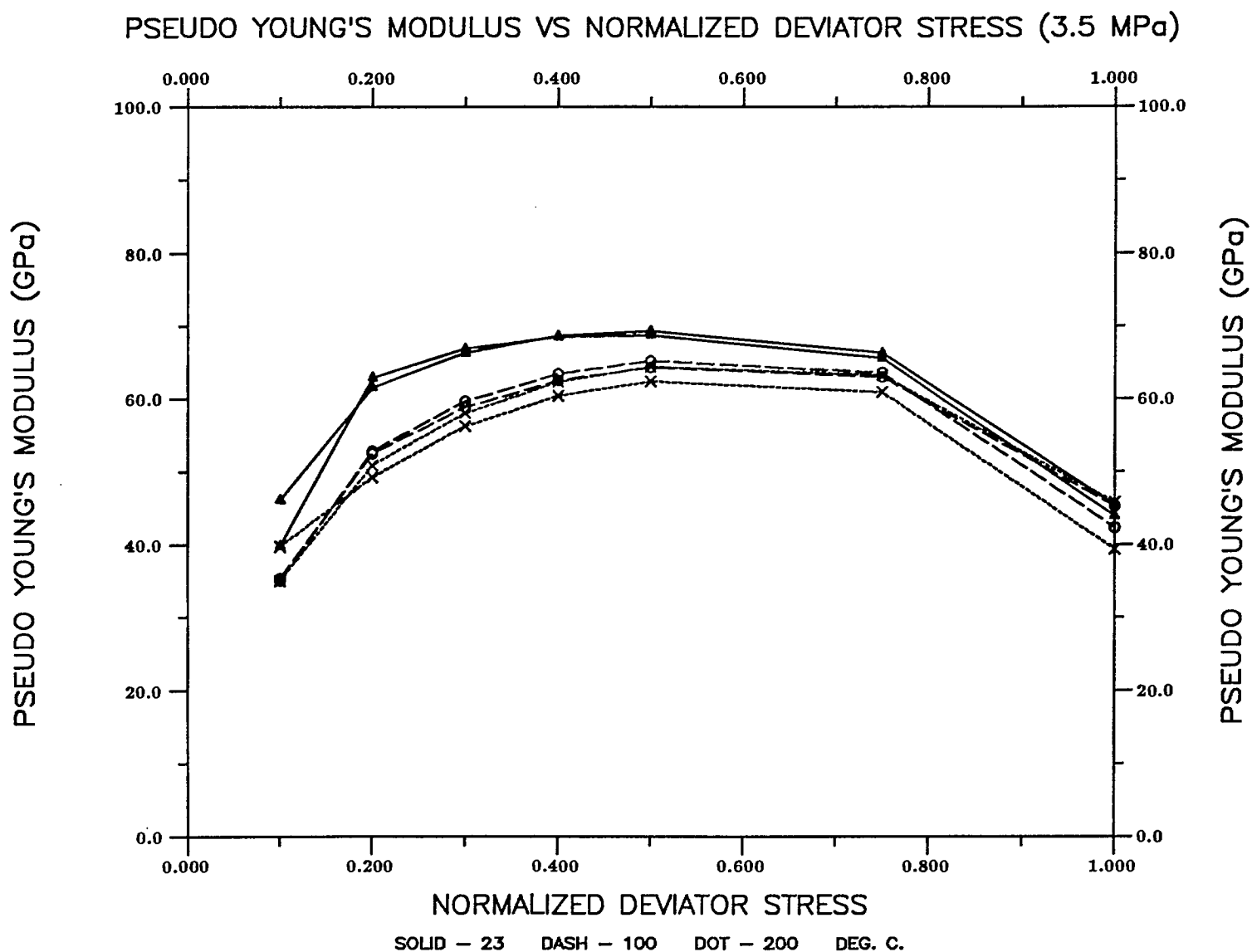


Figure 13. Plots of pseudo Young's modulus versus normalized deviator stress for the second series of tests conducted at the confining pressure of 3.5 MPa.

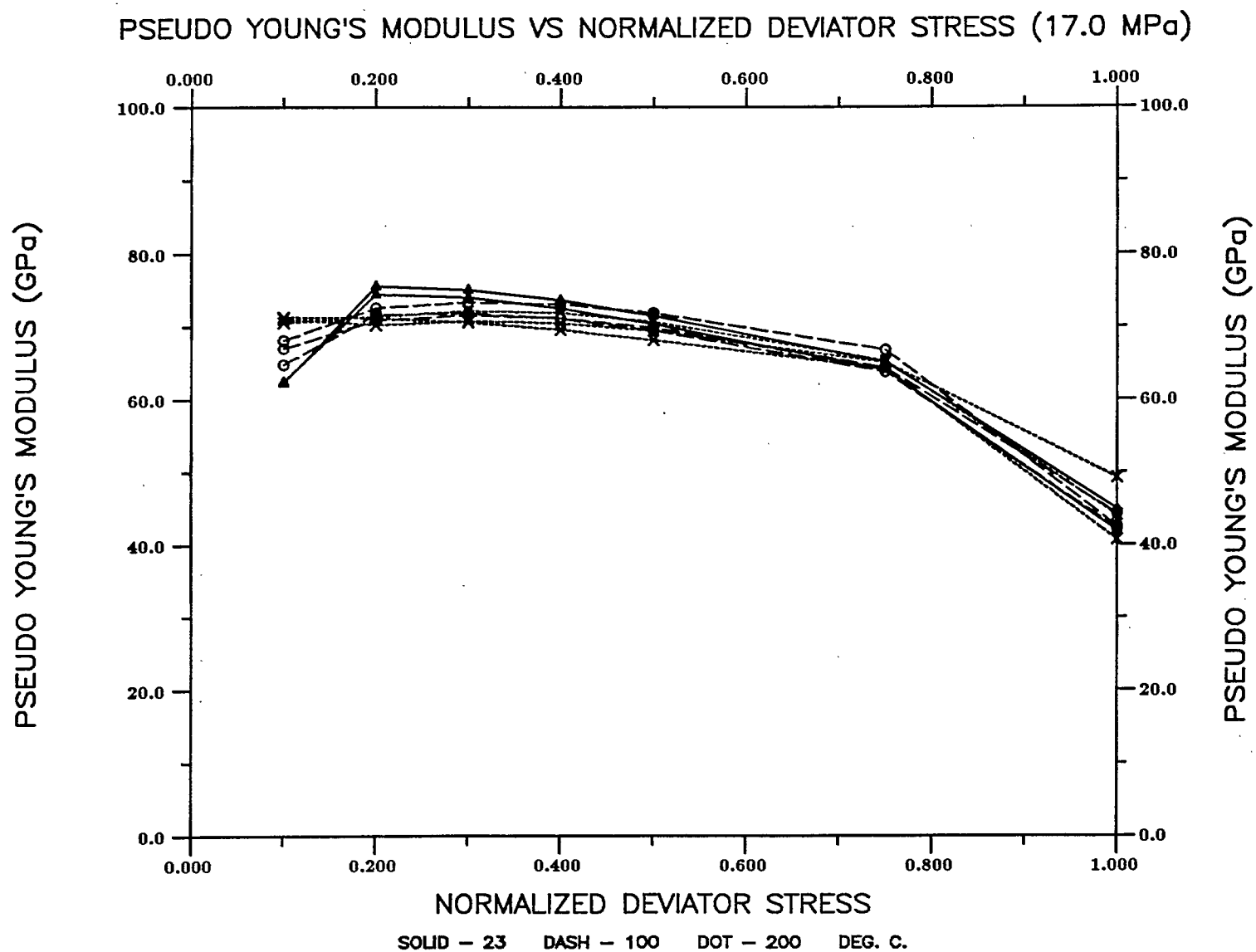


Figure 14. Plots of pseudo Young's modulus versus normalized deviator stress for the second series of tests conducted at the confining pressure of 17.0 MPa.

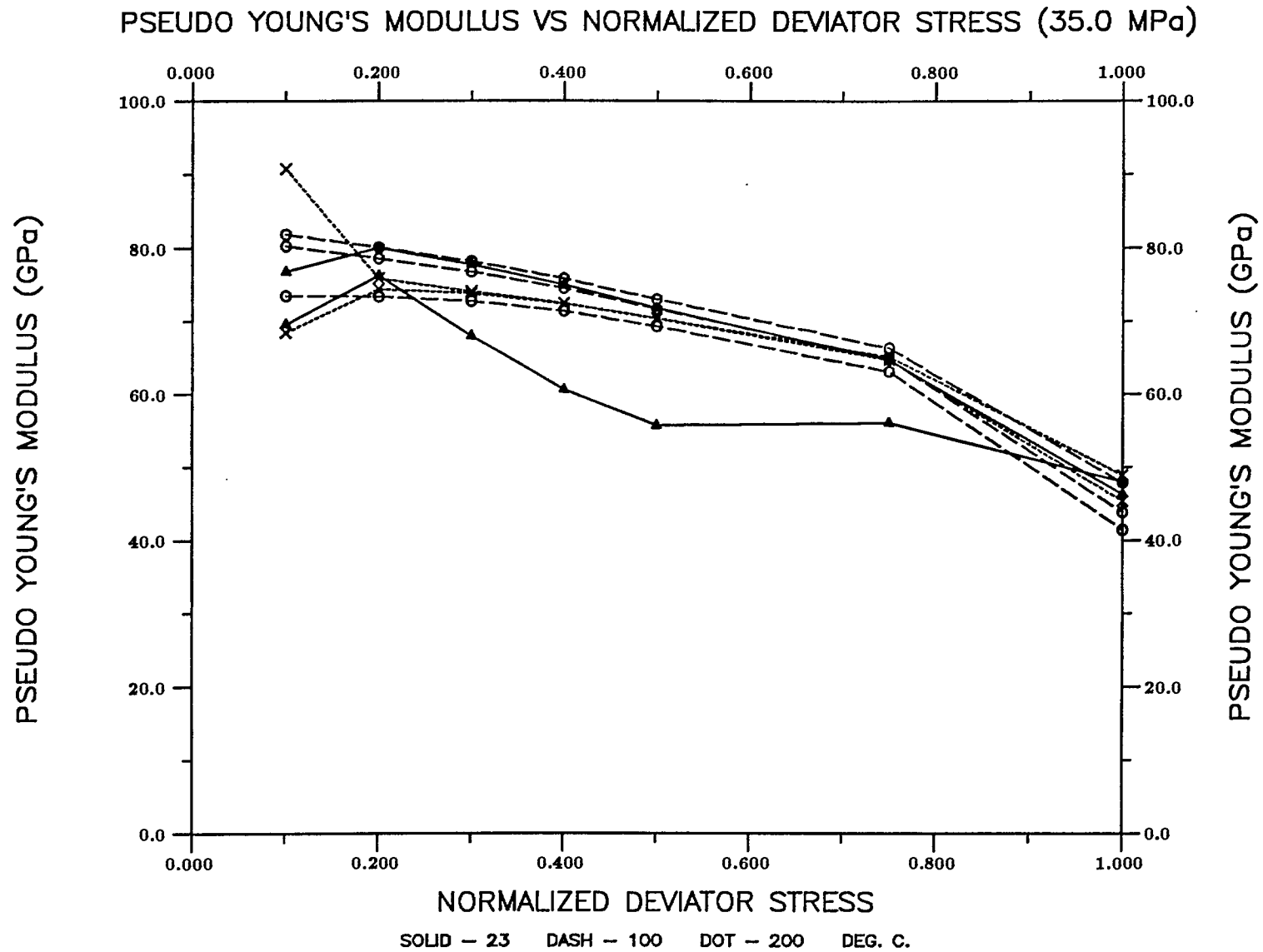


Figure 15. Plots of pseudo Young's modulus versus normalized deviator stress for the second series of tests conducted at the confining pressure of 35.0 MPa.

MOHR CIRCLES AND FAILURE ENVELOPE (FIRST SERIES, 100 DEG C.)

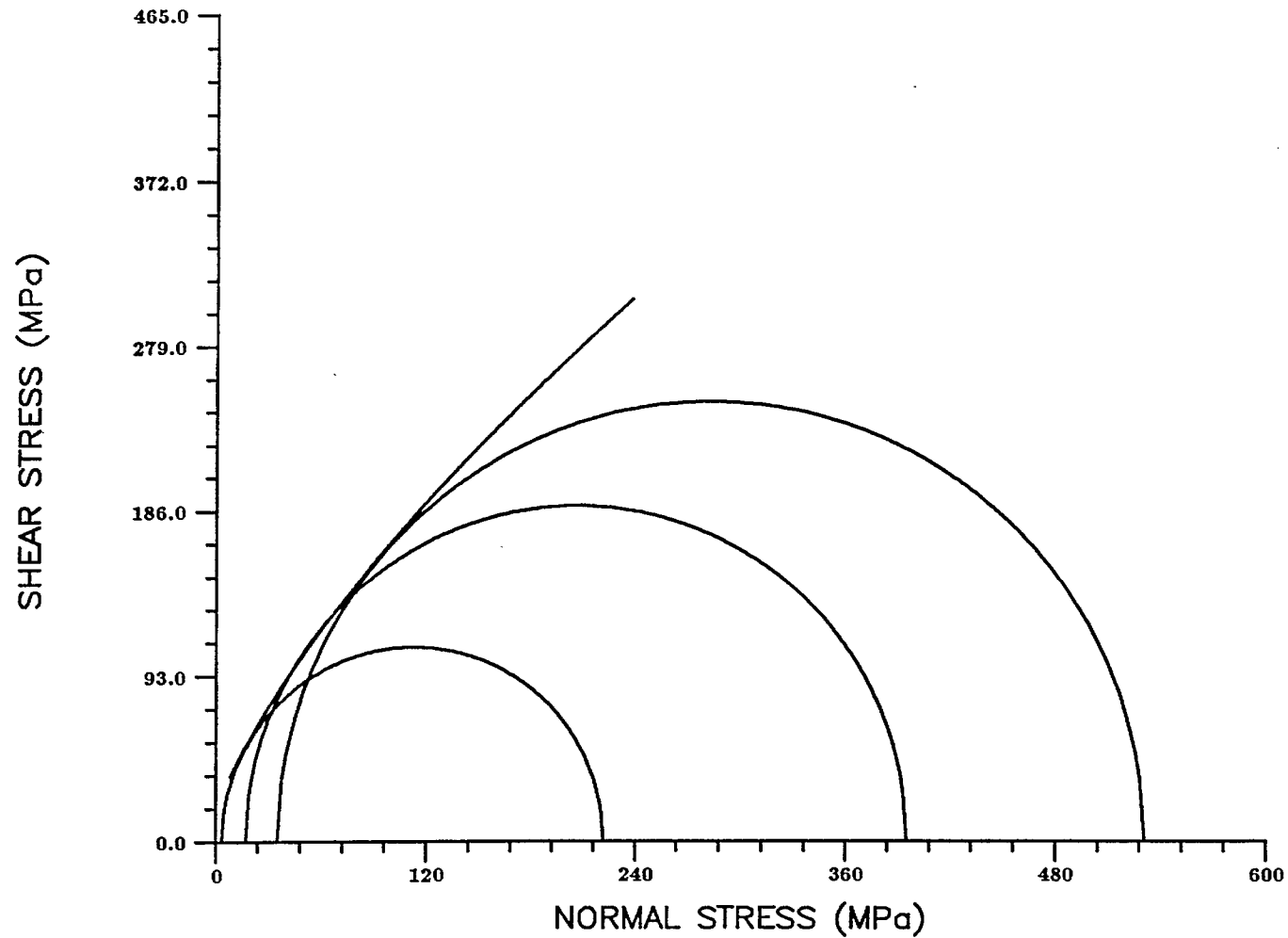


Figure 16. Mohr circles and failure envelope for the first series of tests carried out at the temperature of 100° C.

MOHR CIRCLES AND FAILURE ENVELOPE (FIRST SERIES, 200 DEG C.)

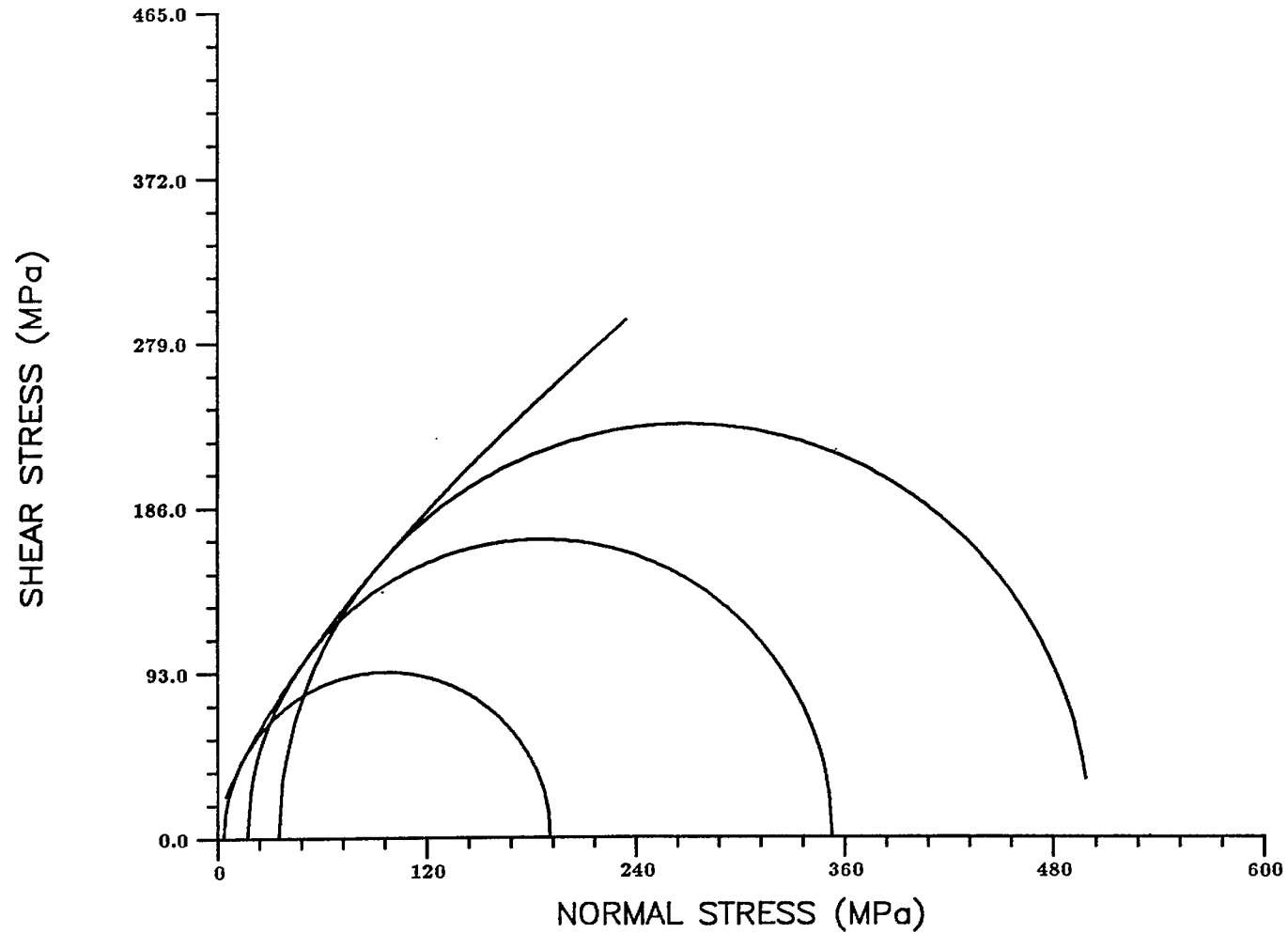


Figure 17. Mohr circles and failure envelope for the first series of tests carried out at the temperature of 200° C.

MOHR CIRCLES AND FAILURE ENVELOPE (SECOND SERIES, 23 DEG C.)

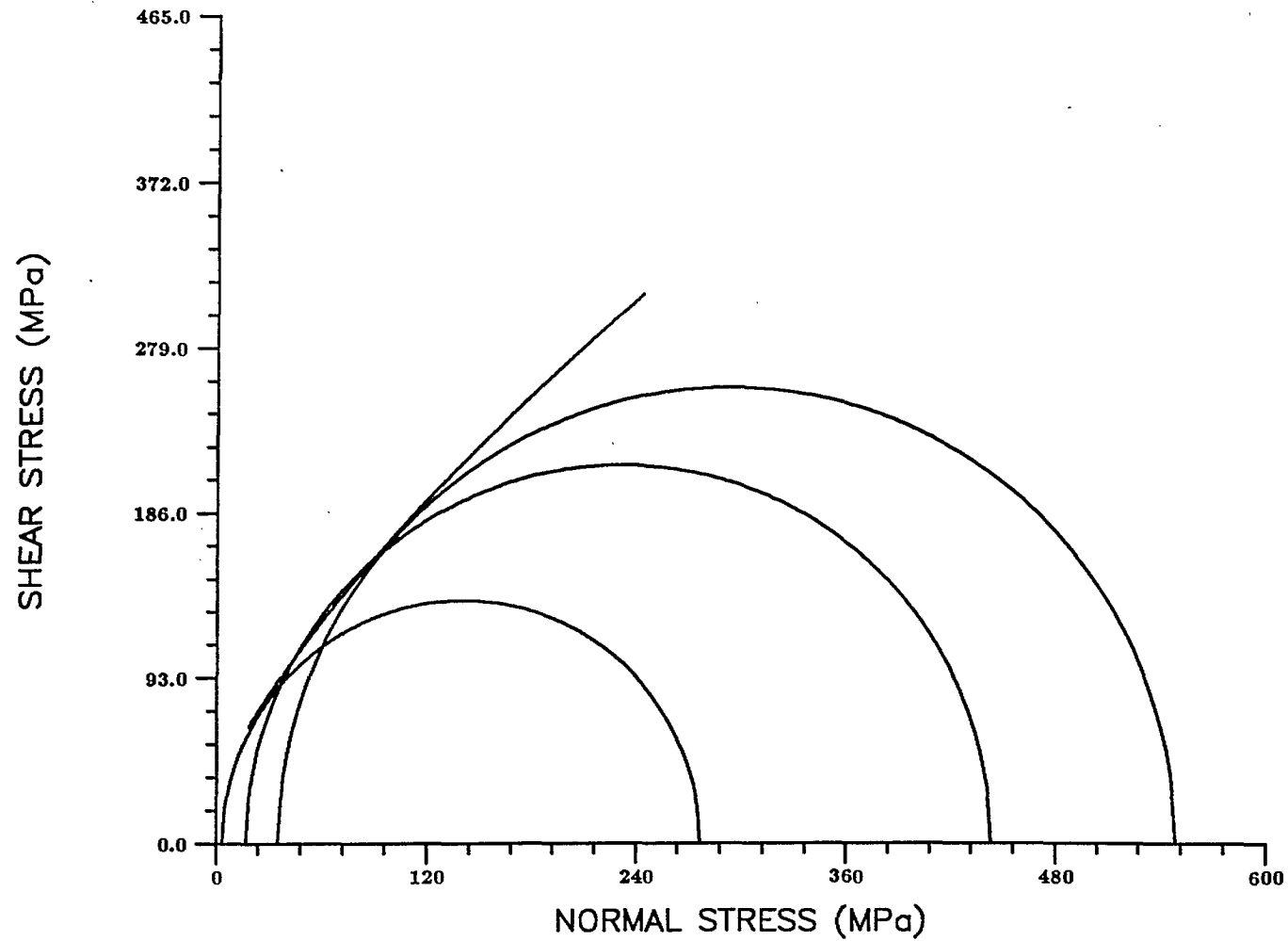


Figure 18. Mohr circles and failure envelope for the second series of tests carried out at the temperature of 23° C.

MOHR CIRCLES AND FAILURE ENVELOPE (SECOND SERIES, 100 DEG C.)

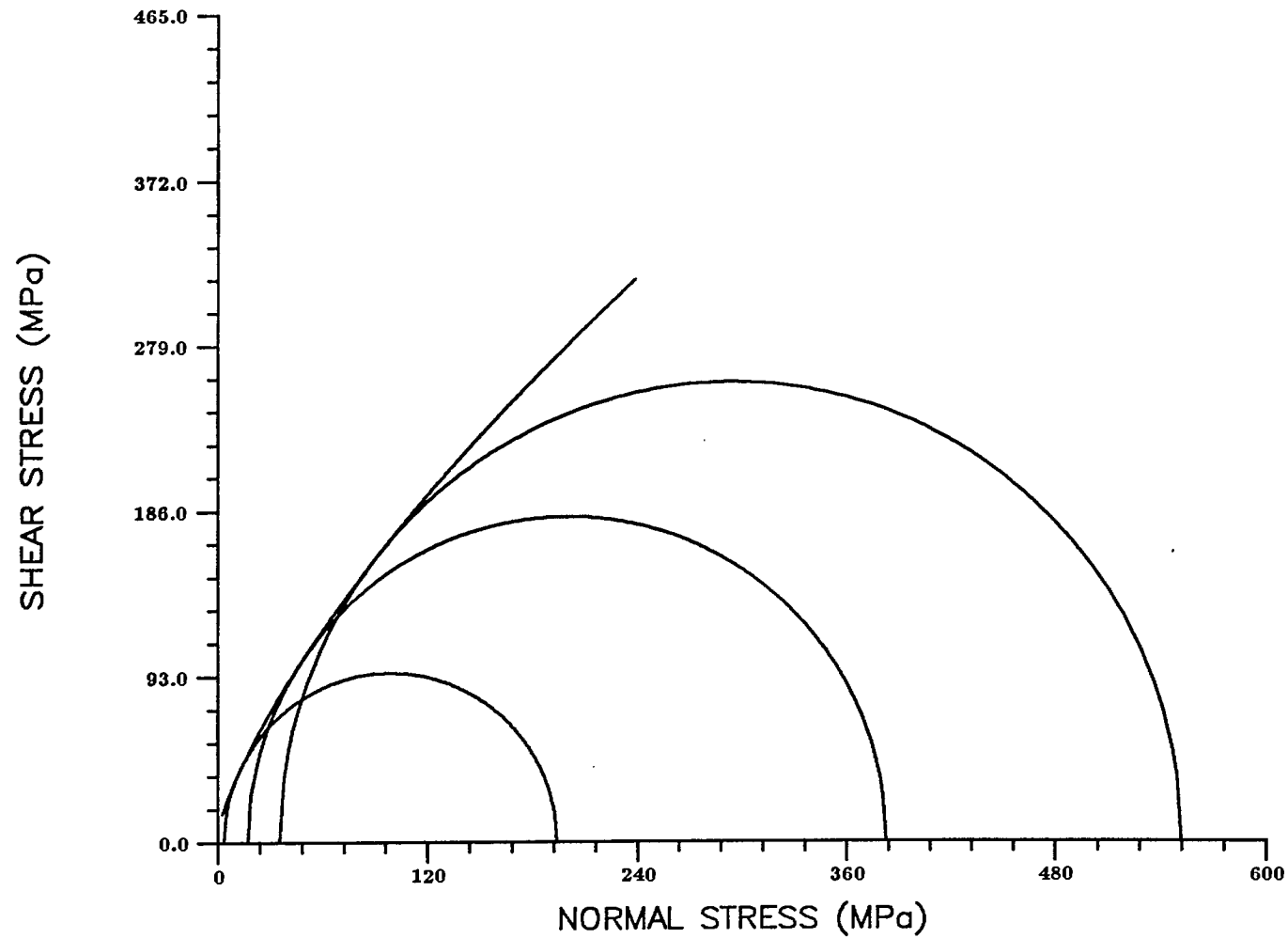


Figure 19. Mohr circles and failure envelope for the second series of tests carried out at the temperature of 100° C.

MOHR CIRCLES AND FAILURE ENVELOPE (SECOND SERIES, 200 DEG C.)

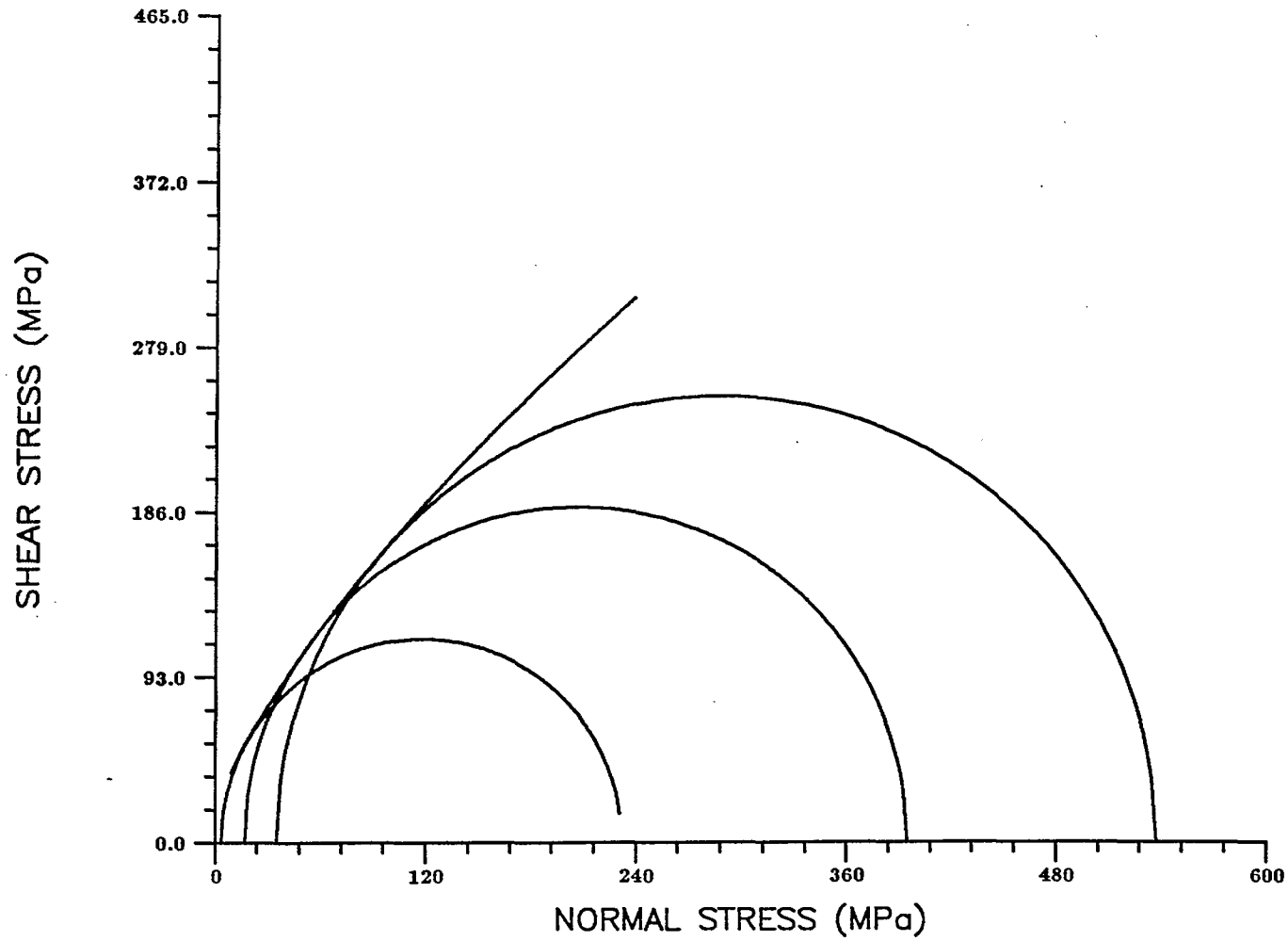


Figure 20. Mohr circles and failure envelope for the second series of tests carried out at the temperature of 200° C.

MOHR FAILURE ENVELOPES (FIRST SERIES)

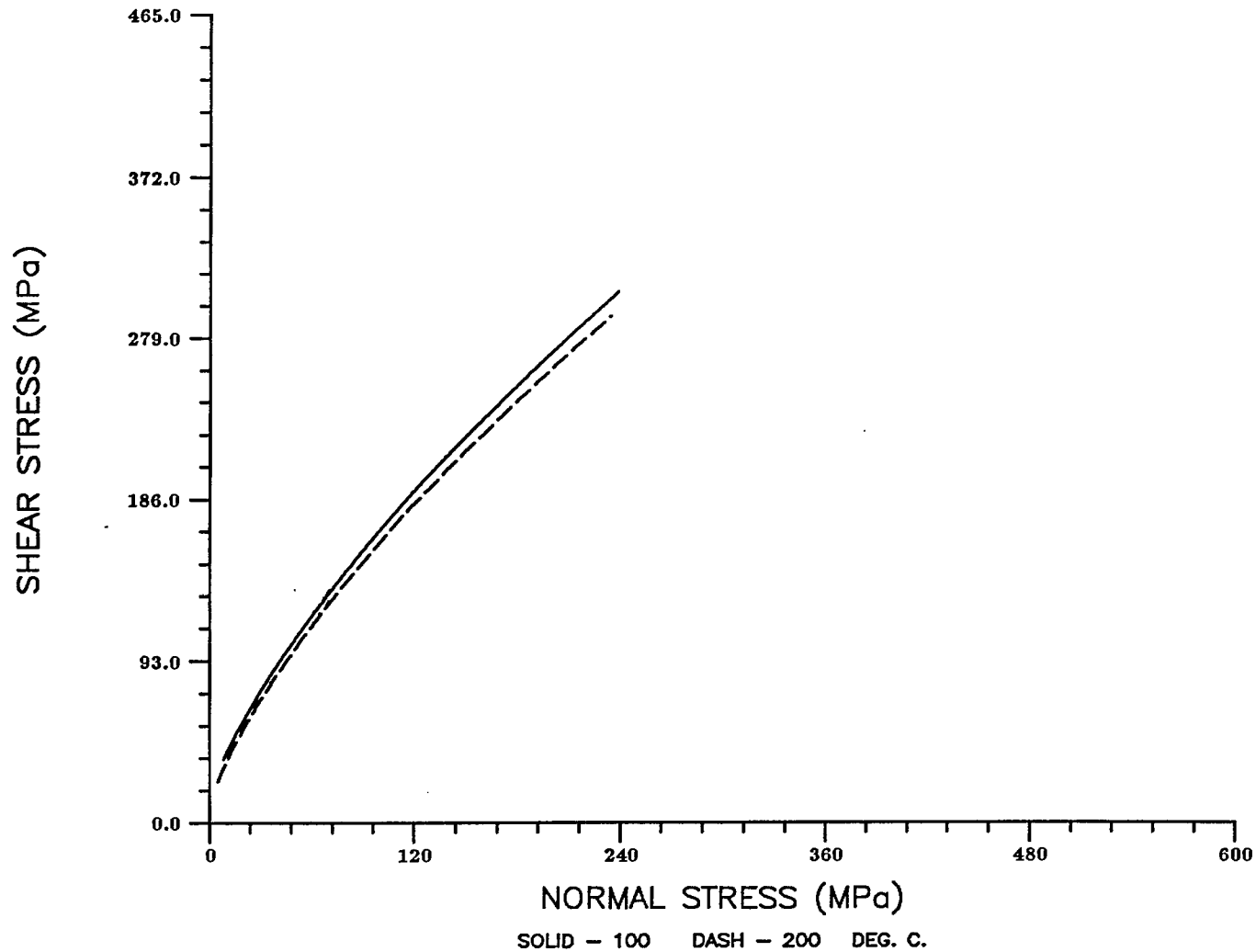


Figure 21. Mohr failure envelopes for the first series of tests.

MOHR FAILURE ENVELOPES (SECOND SERIES)

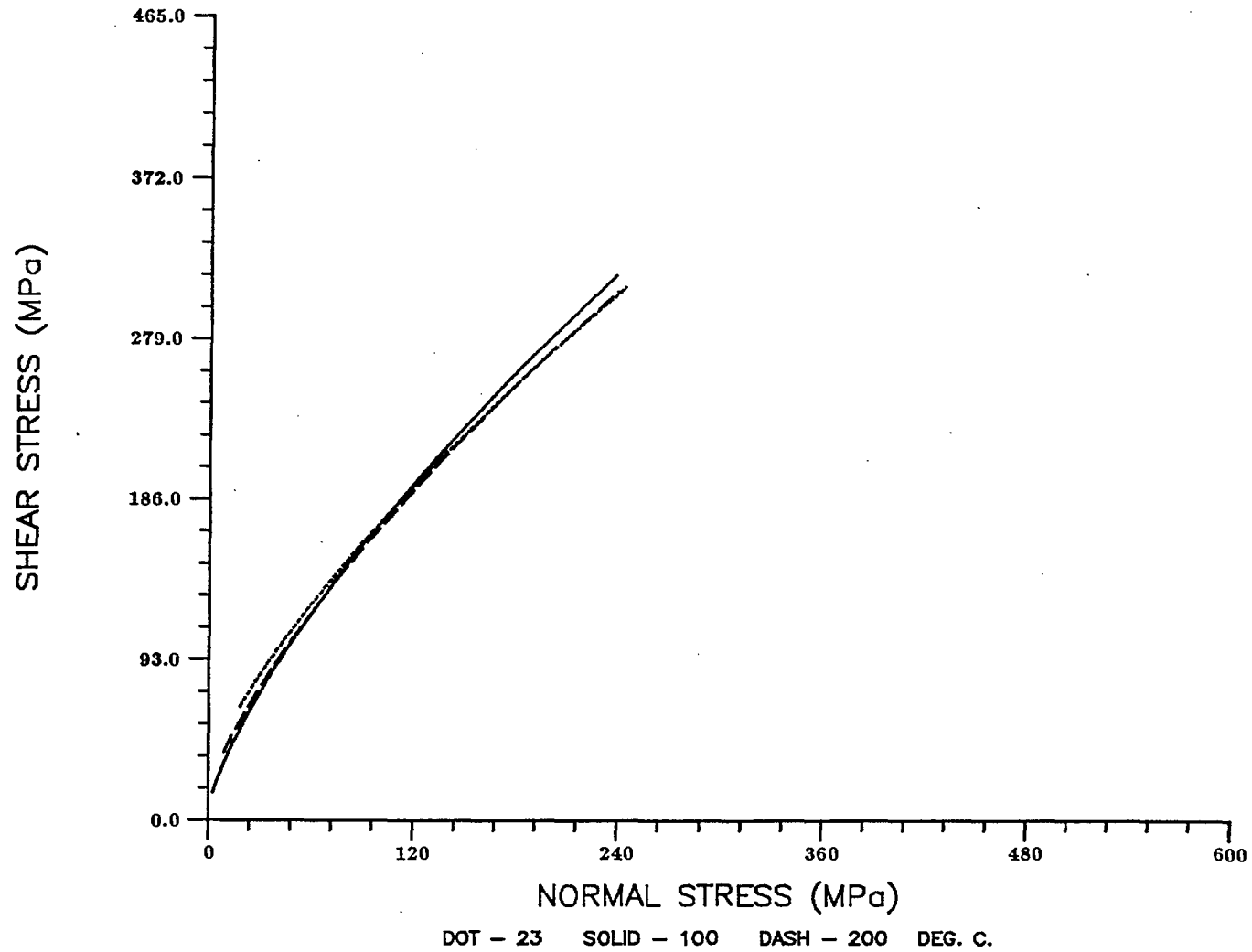


Figure 22. Mohr failure envelopes for the second series of tests.

Appendix A

Stress-strain curves

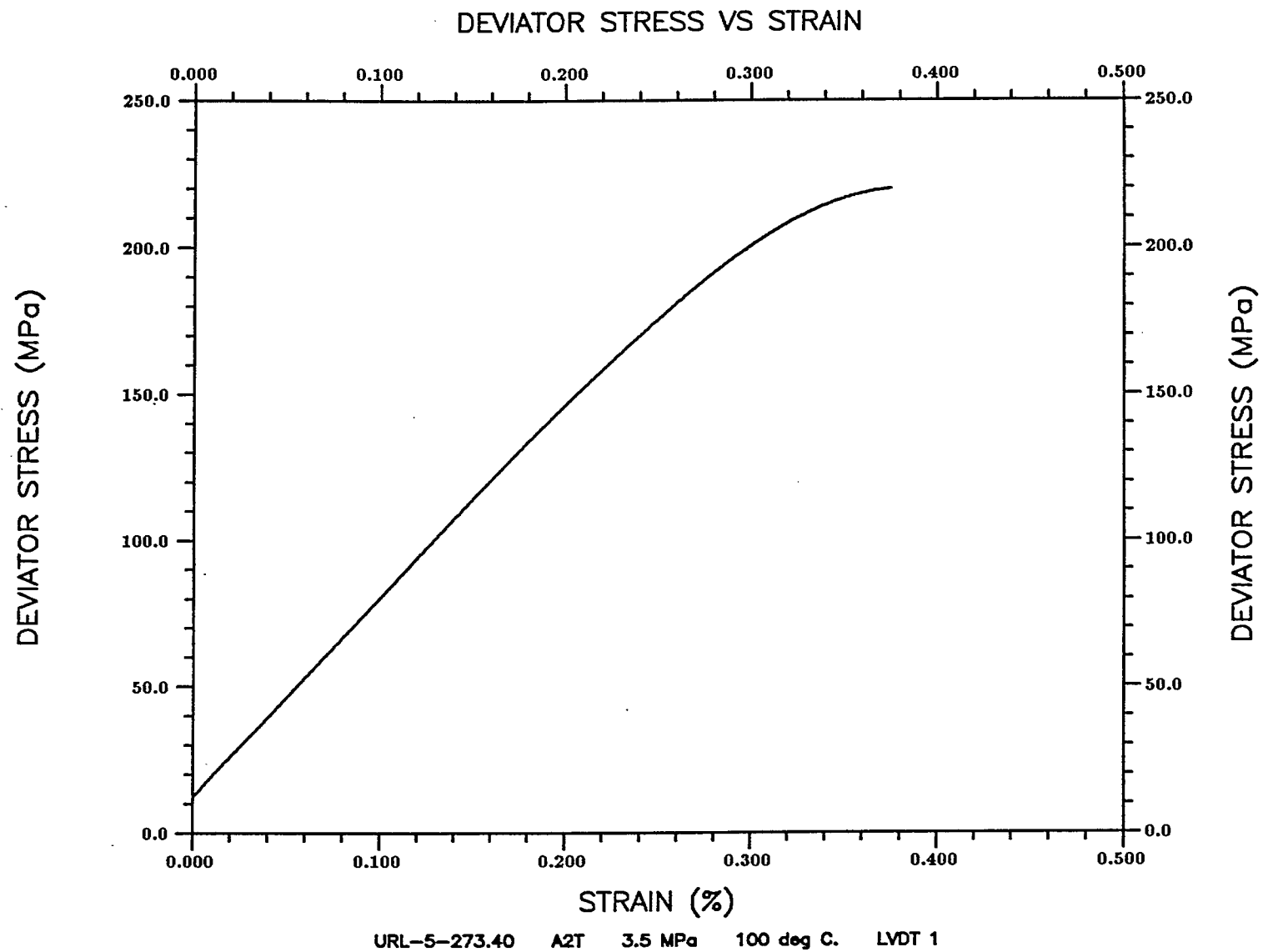


Figure A.1 Specimen A2T ($\sigma_3 = 3.5$ MPa, temperature = 100° C)

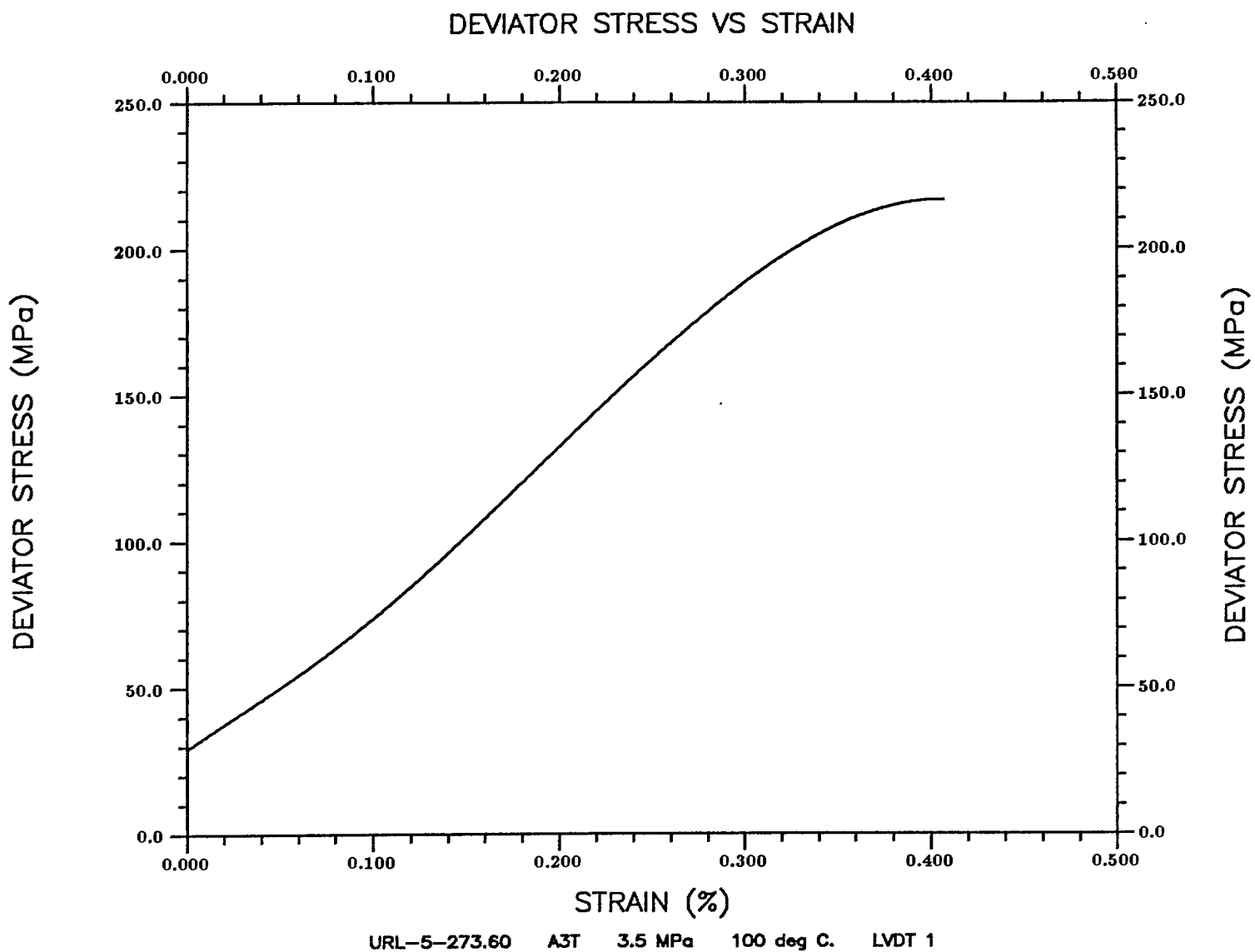


Figure A.2 Specimen A3T ($\sigma_3 = 3.5$ MPa, temperature = 100° C)

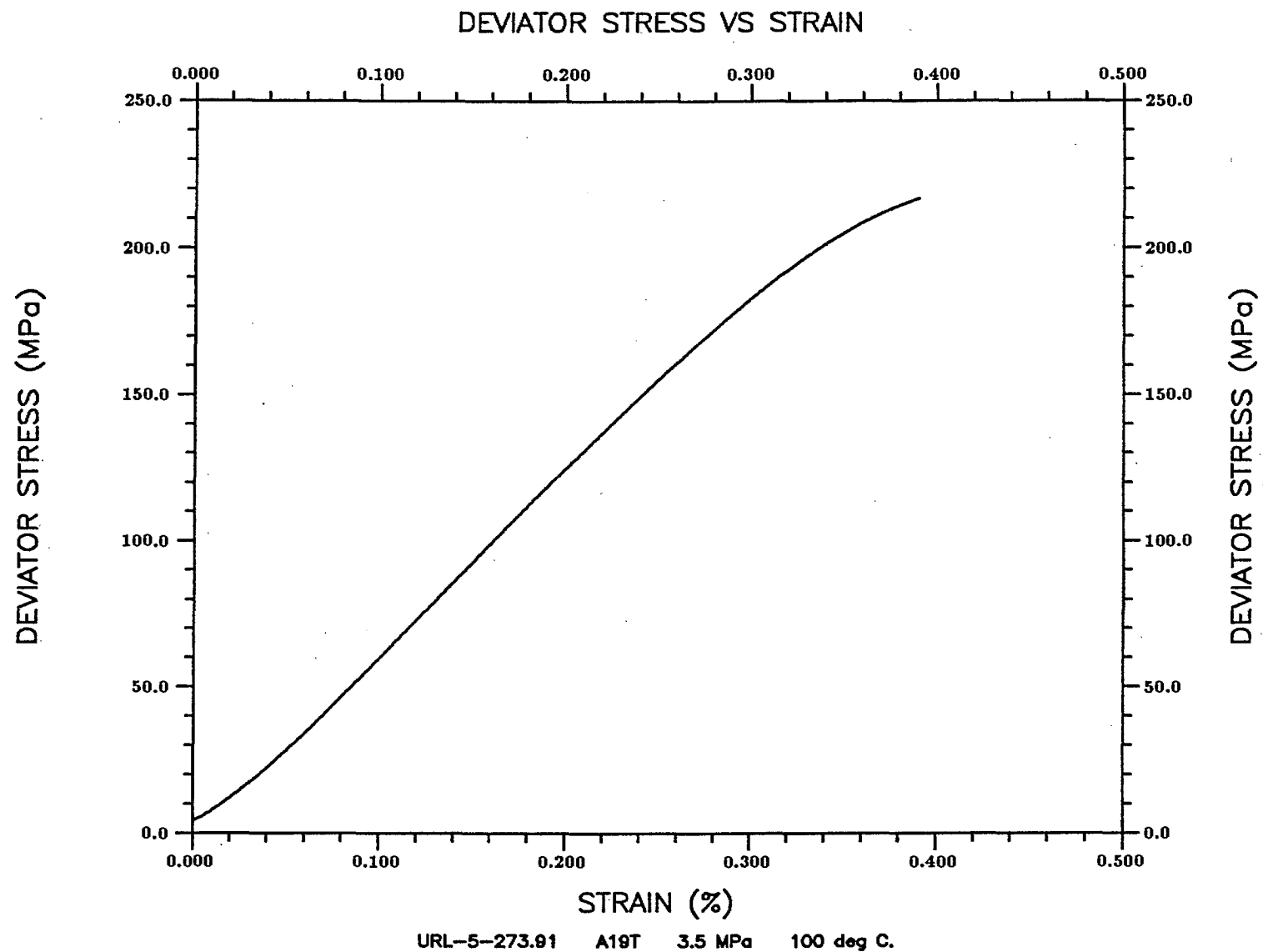


Figure A.3 Specimen A19T ($\sigma_3 = 3.5$ MPa, temperature = 100° C)

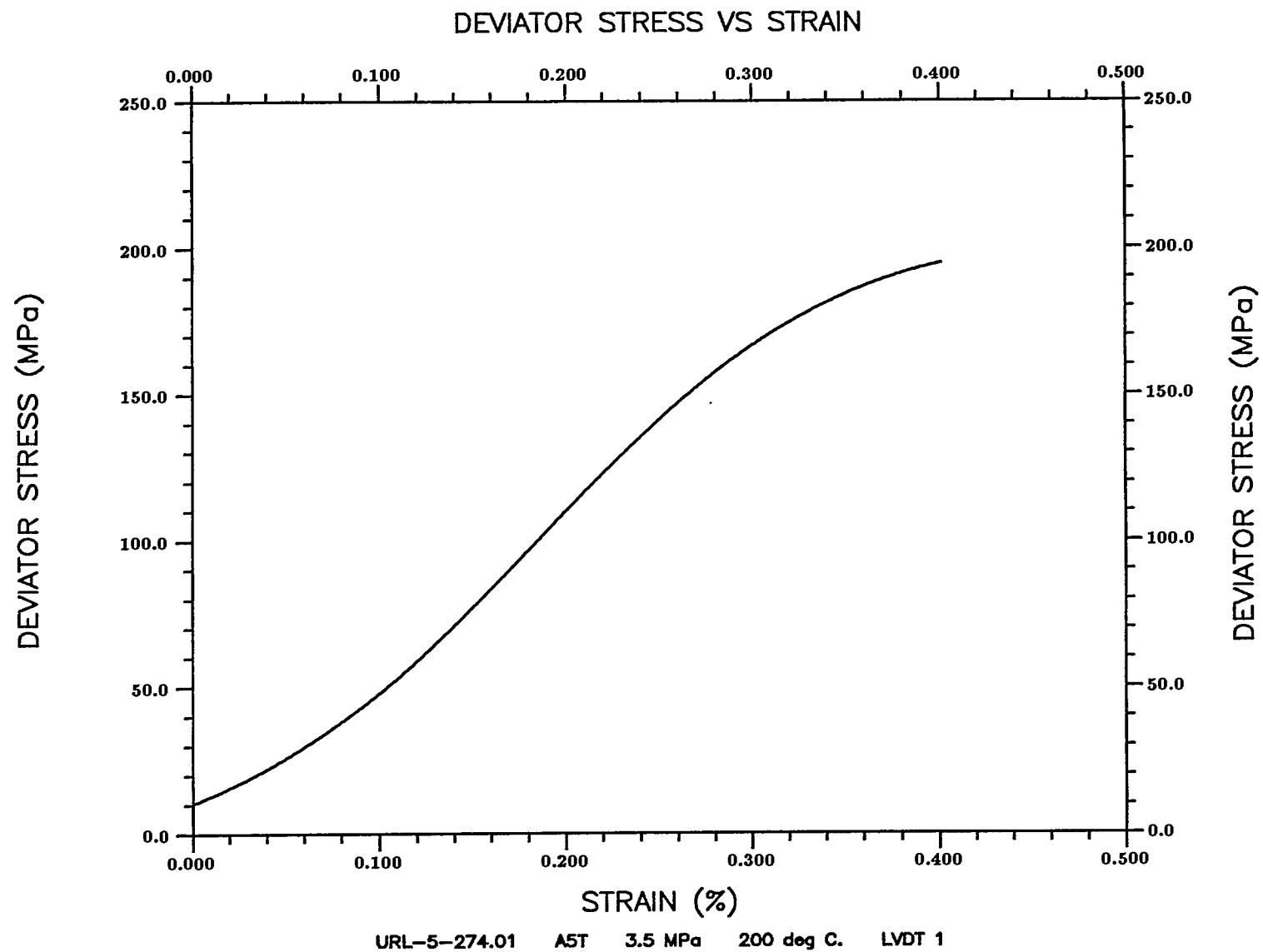


Figure A.4 Specimen A5T ($\sigma_3 = 3.5$ MPa, temperature = 200° C)

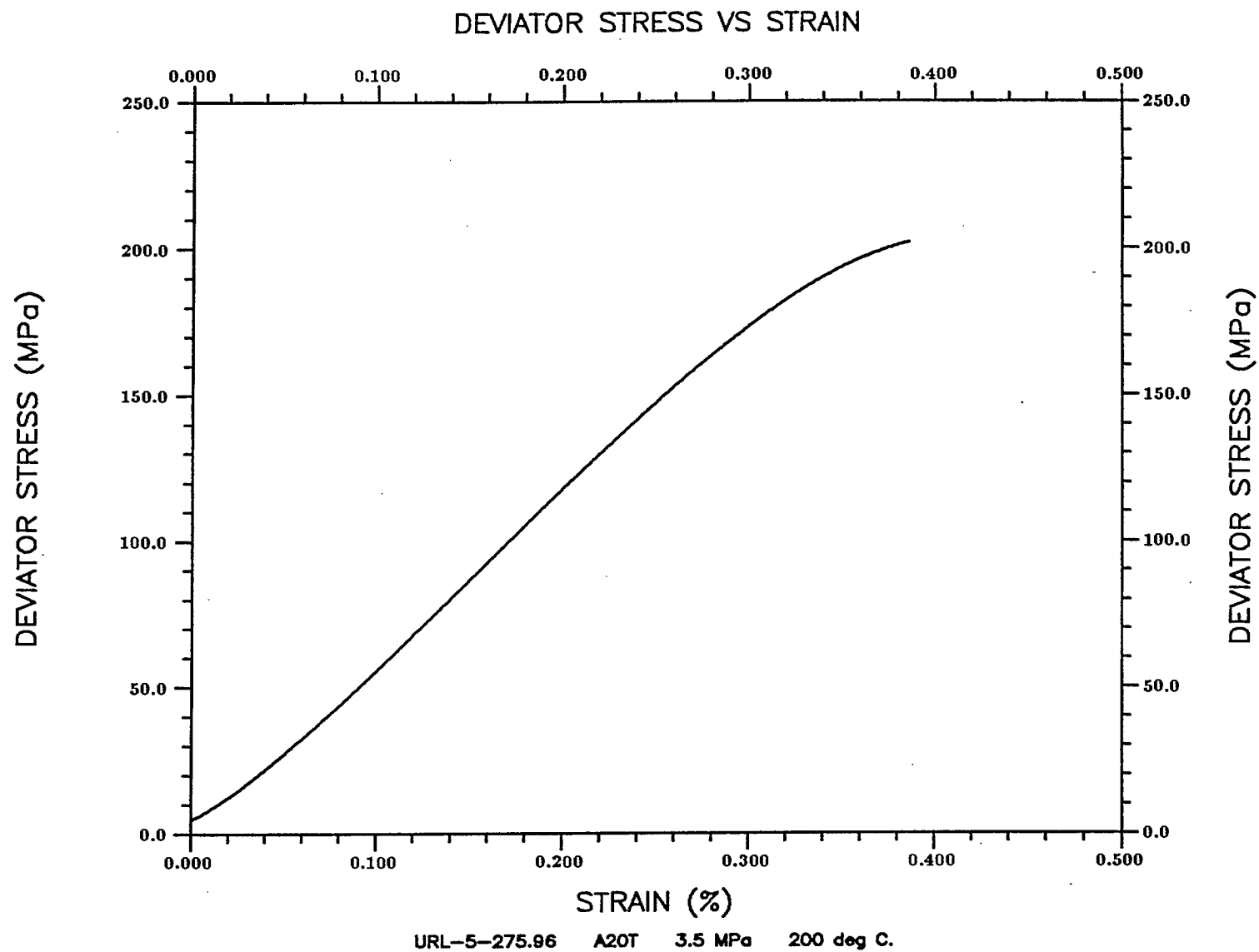


Figure A.5 Specimen A20T ($\sigma_3 = 3.5$ MPa, temperature = 200° C)

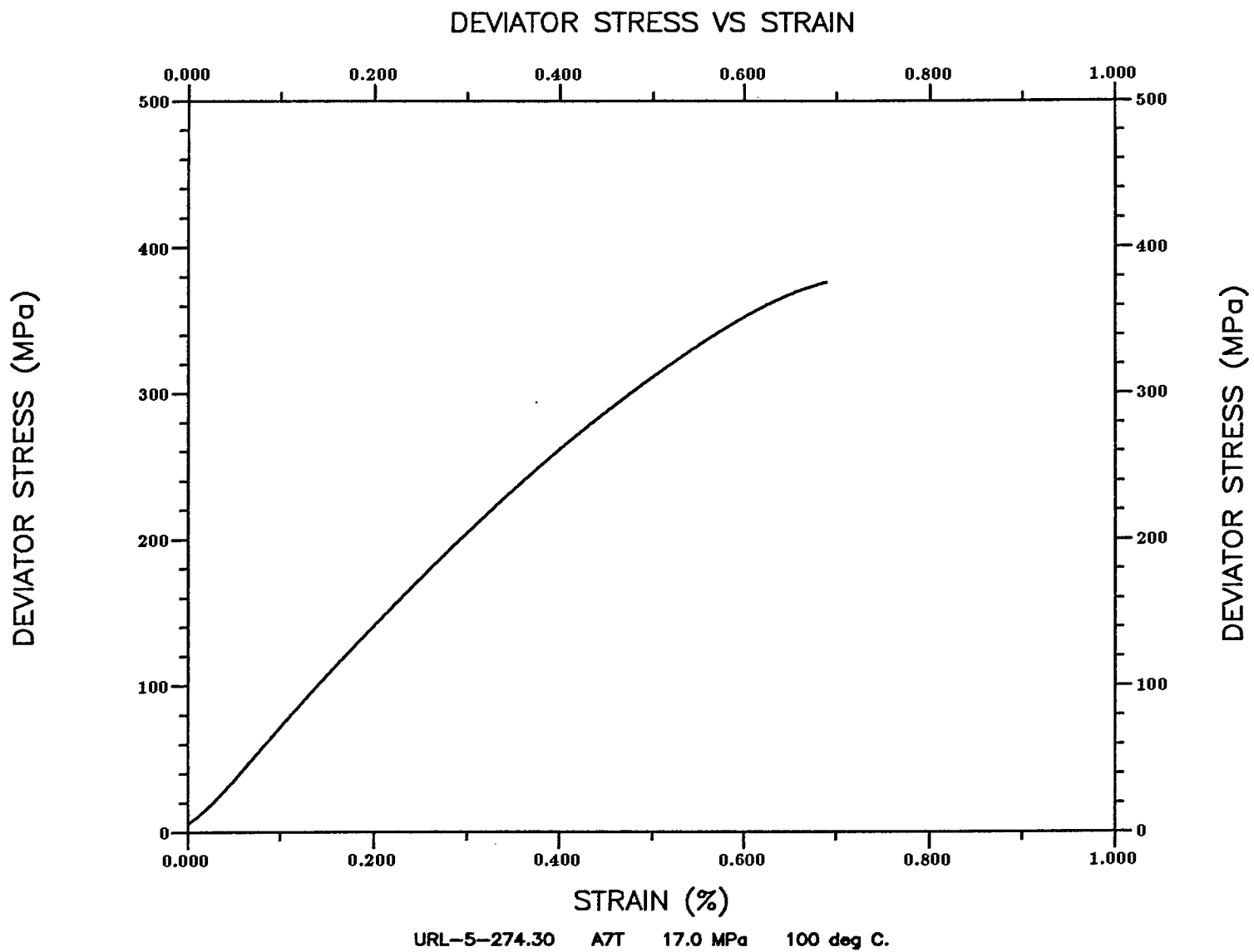


Figure A.6 Specimen A7T ($\sigma_3 = 17.0$ MPa, temperature = 100° C)

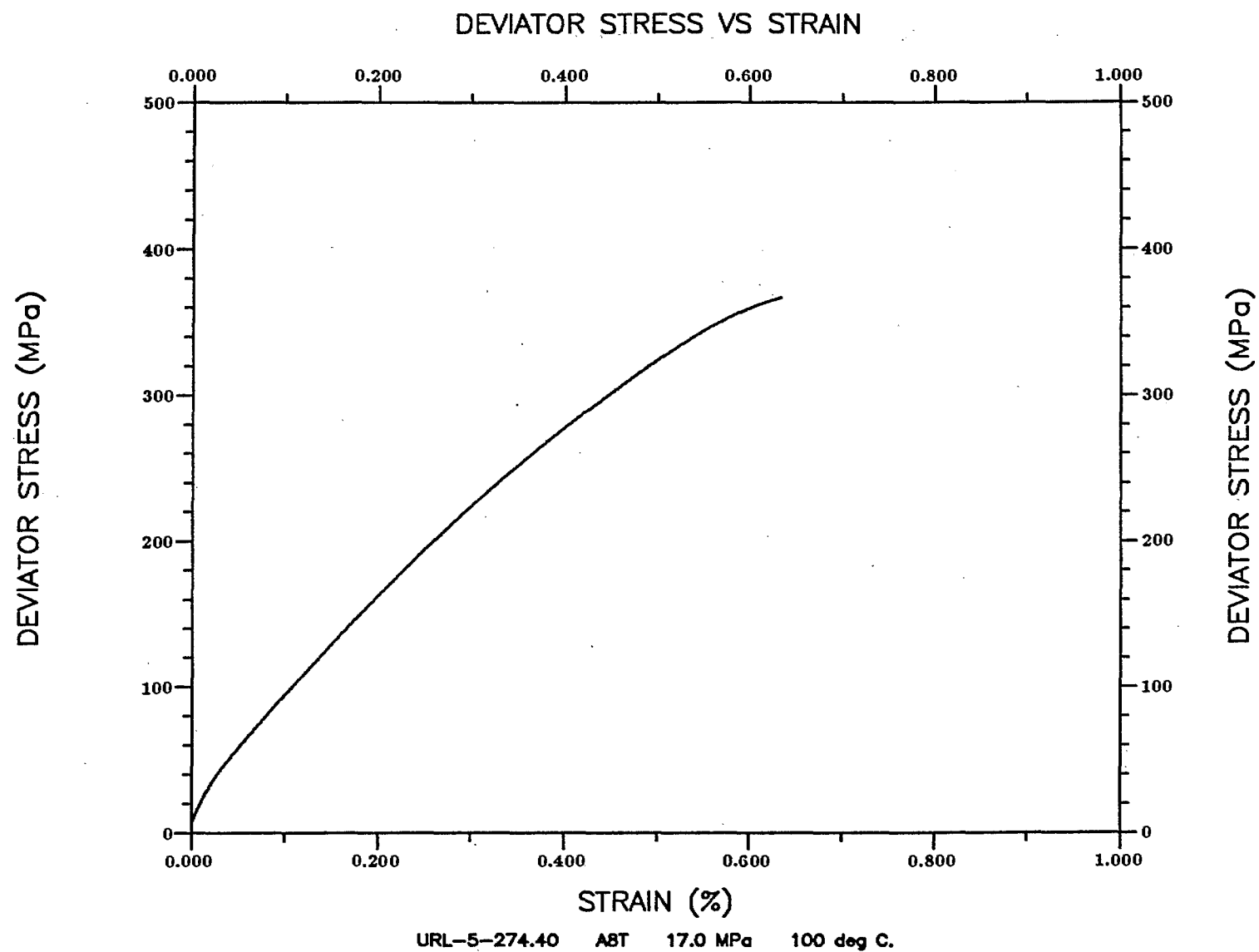


Figure A.7 Specimen A8T ($\sigma_3 = 17.0$ MPa, temperature = 100° C)

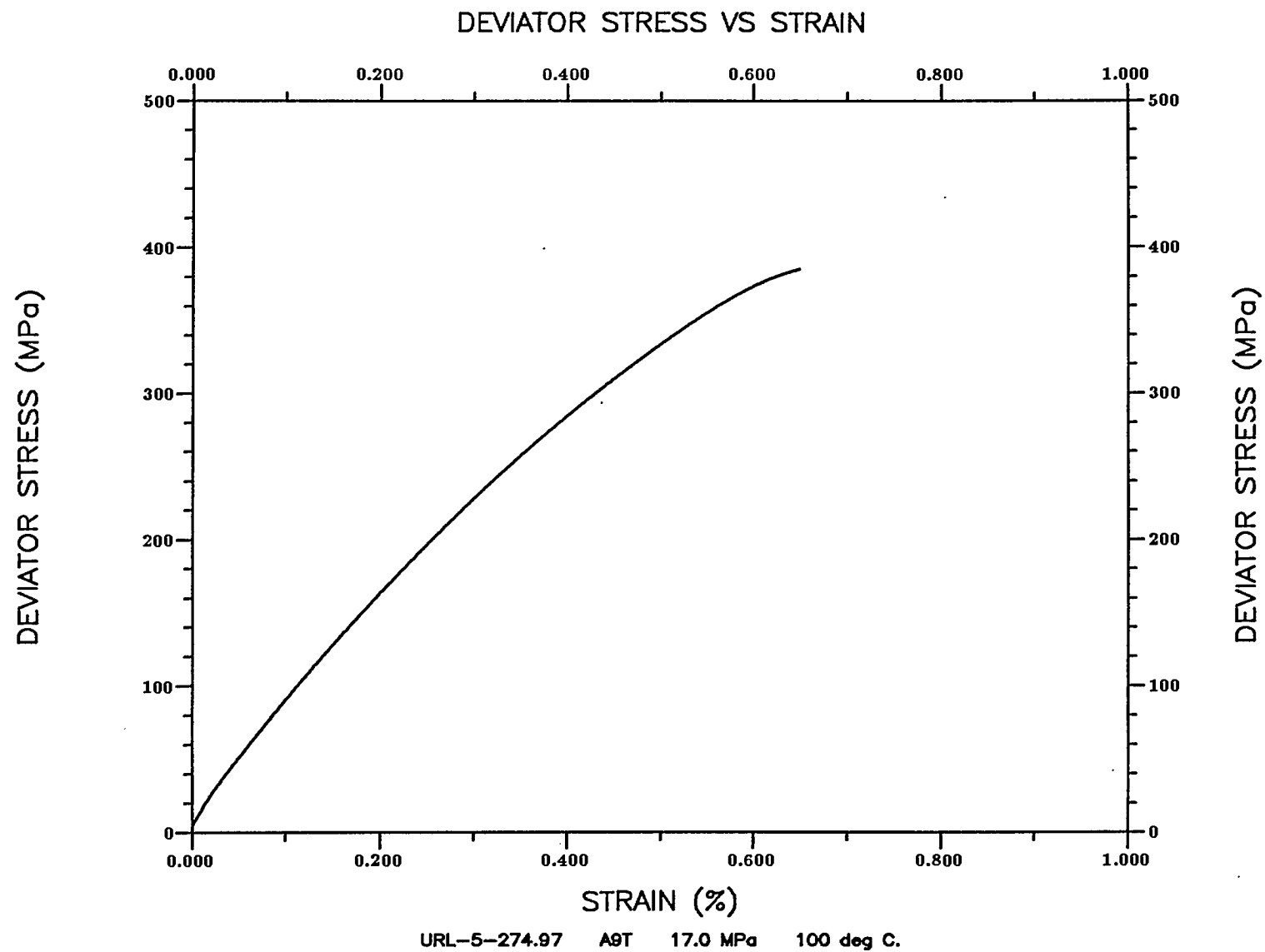


Figure A.8 Specimen A9T ($\sigma_3 = 17.0$ MPa, temperature = 100° C)

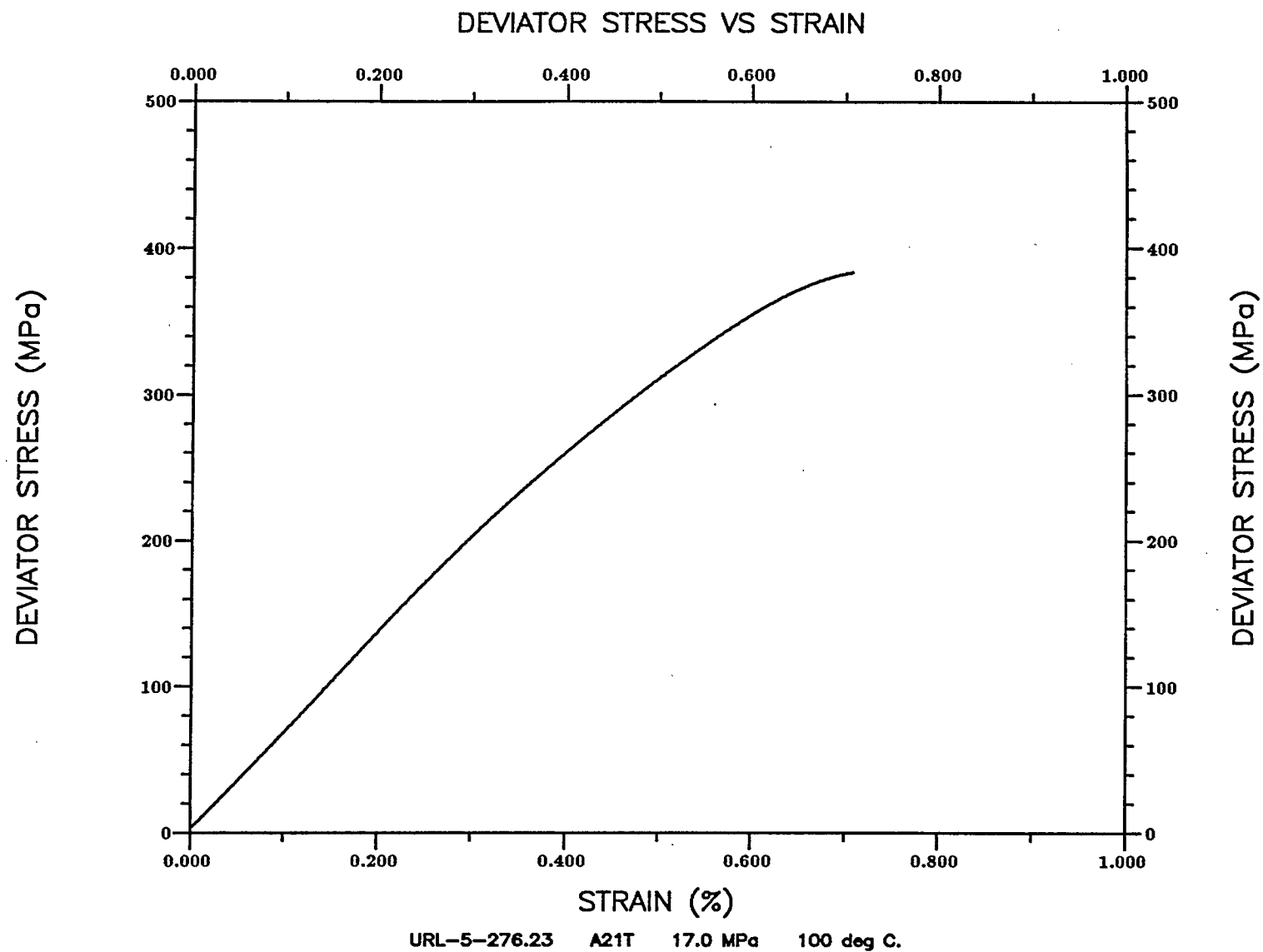


Figure A.9 Specimen A21T ($\sigma_3 = 17.0$ MPa, temperature = 100° C)

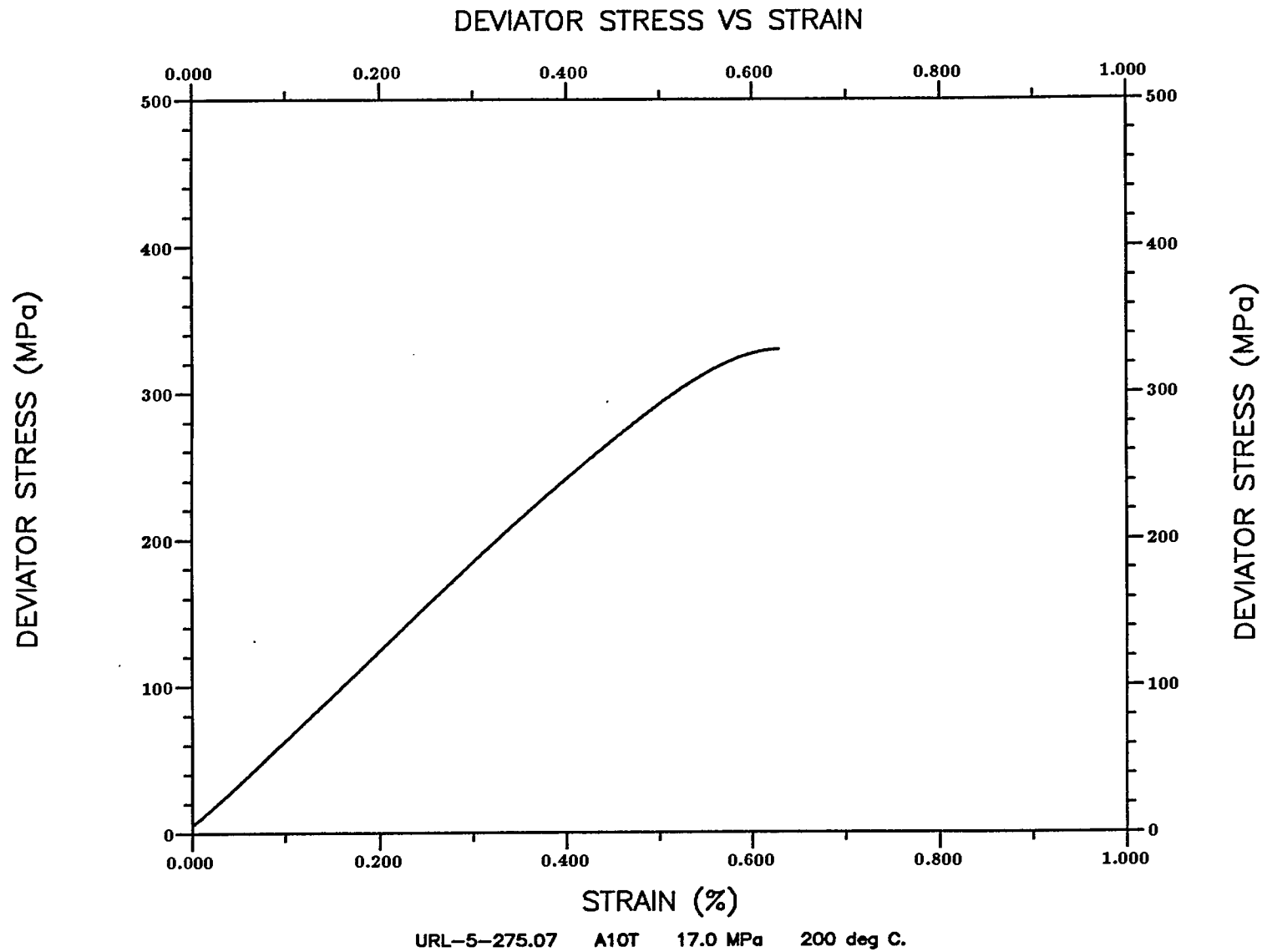


Figure A.10 Specimen A10T ($\sigma_3 = 17.0$ MPa, temperature = 200° C)

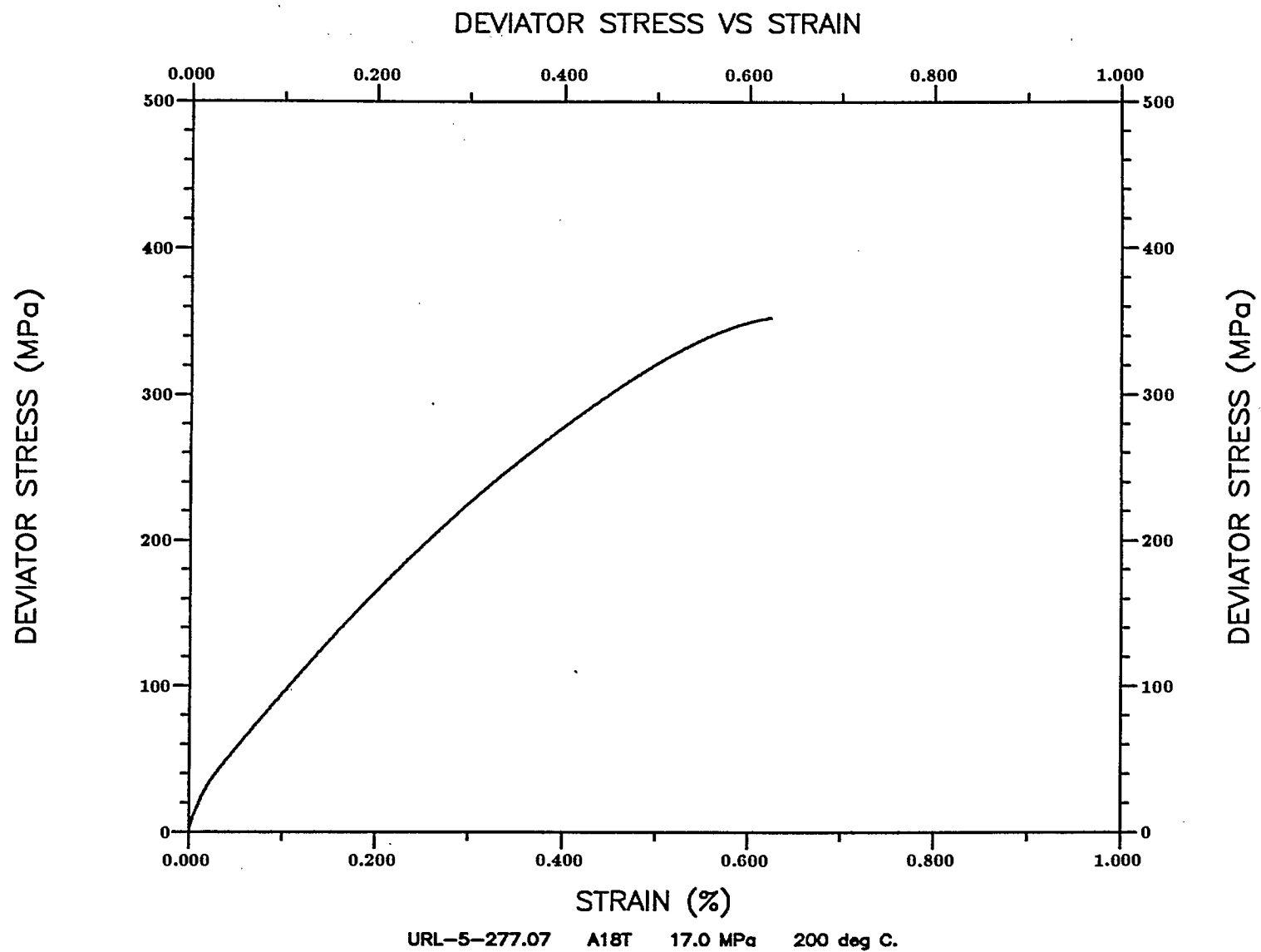


Figure A.11 Specimen A18T ($\sigma_3 = 17.0$ MPa, temperature = 200° C)

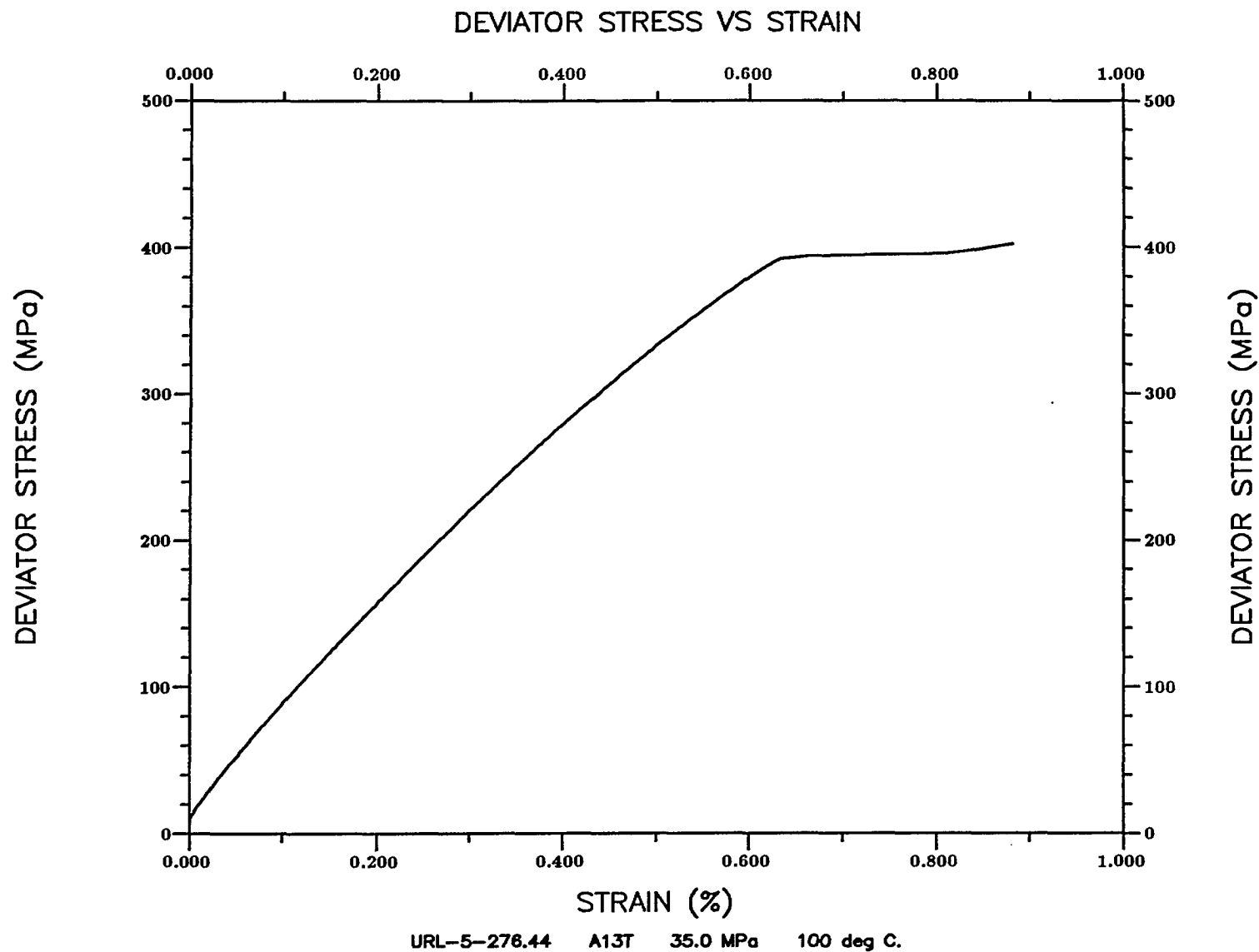


Figure A.12 Specimen A13T ($\sigma_3 = 35.0$ MPa, temperature = 100° C)

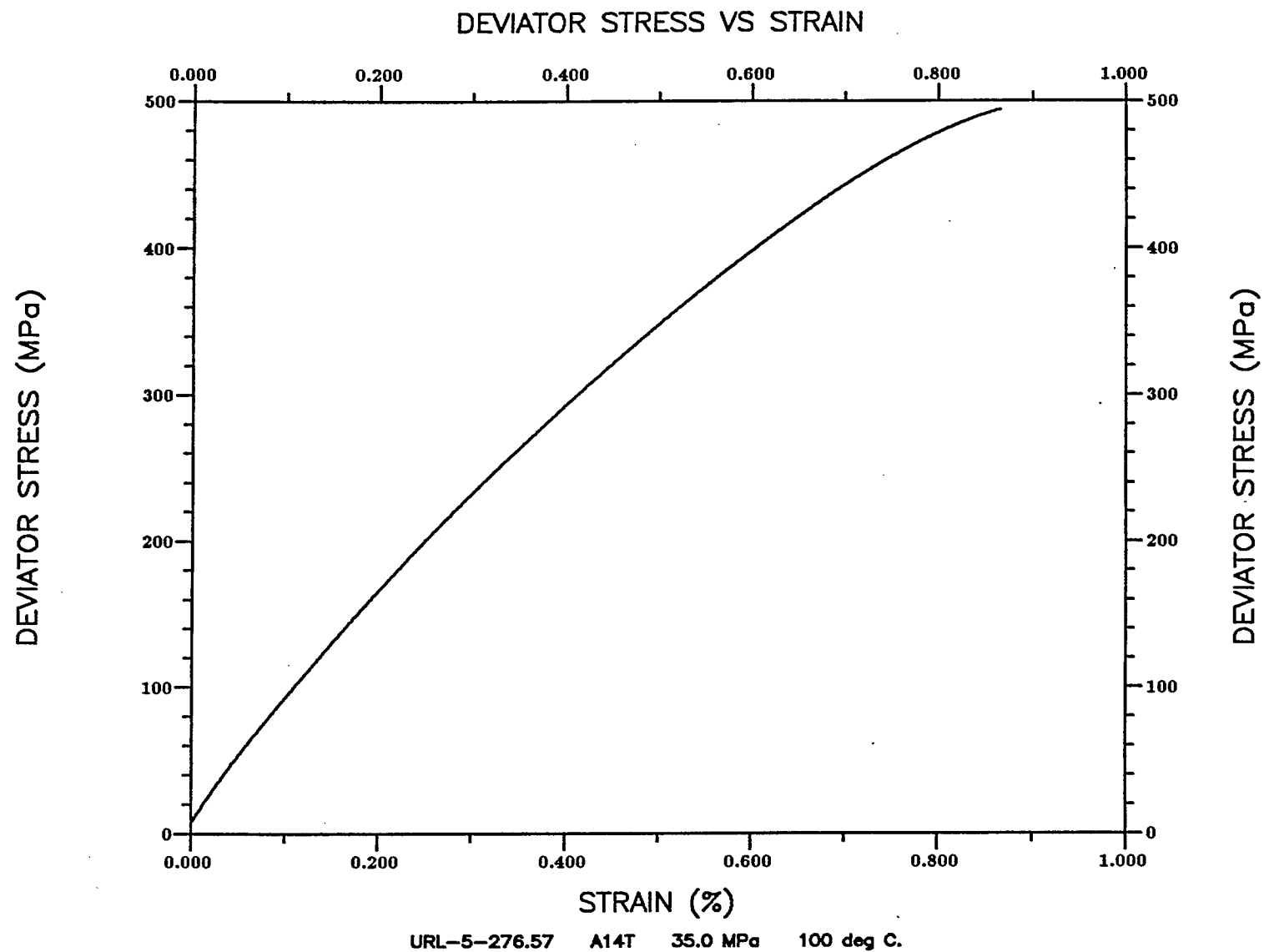


Figure A.13 Specimen A14T ($\sigma_3 = 35.0$ MPa, temperature = 100° C)

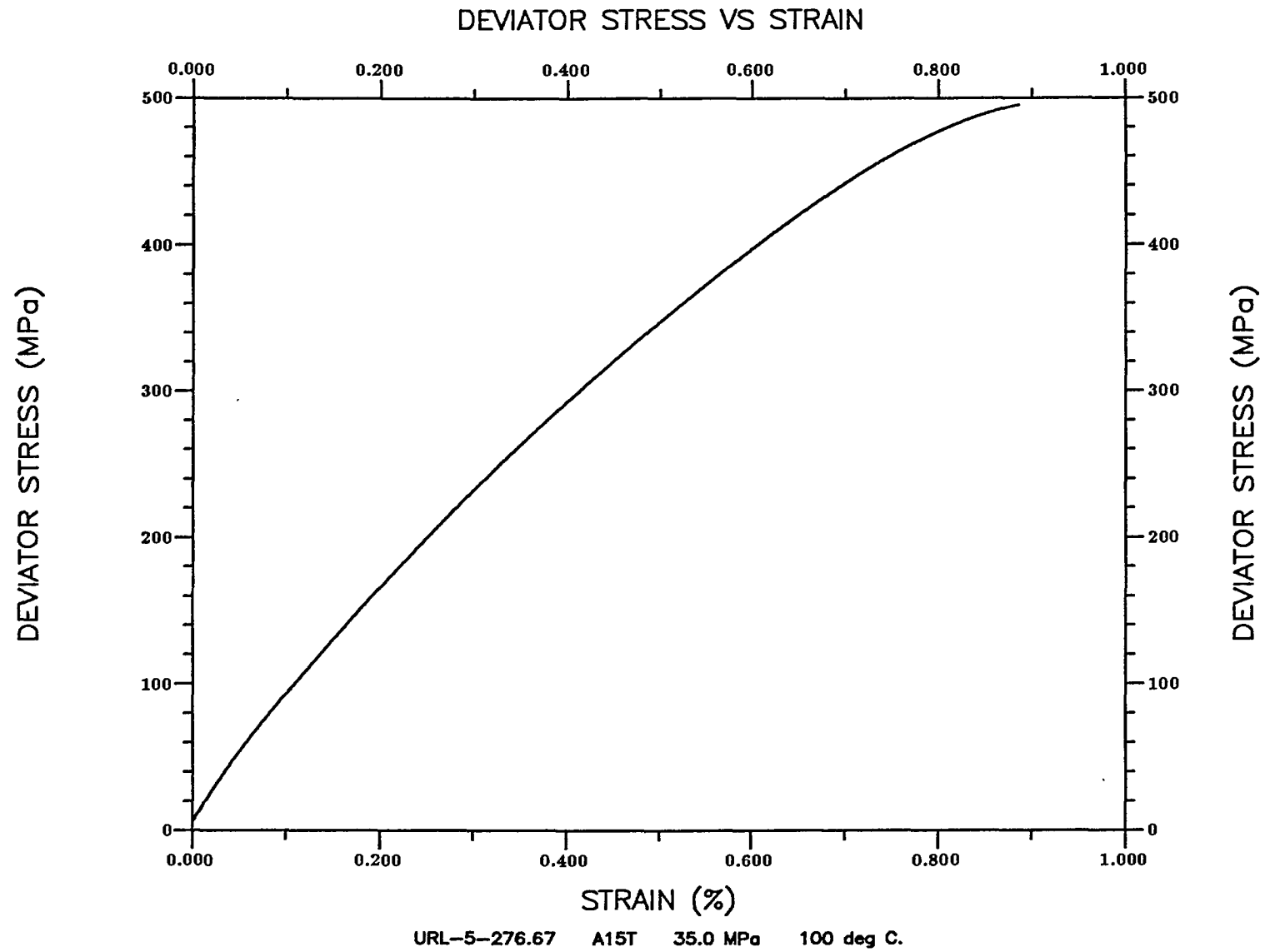


Figure A.14 Specimen A15T ($\sigma_3 = 35.0$ MPa, temperature = 100° C)

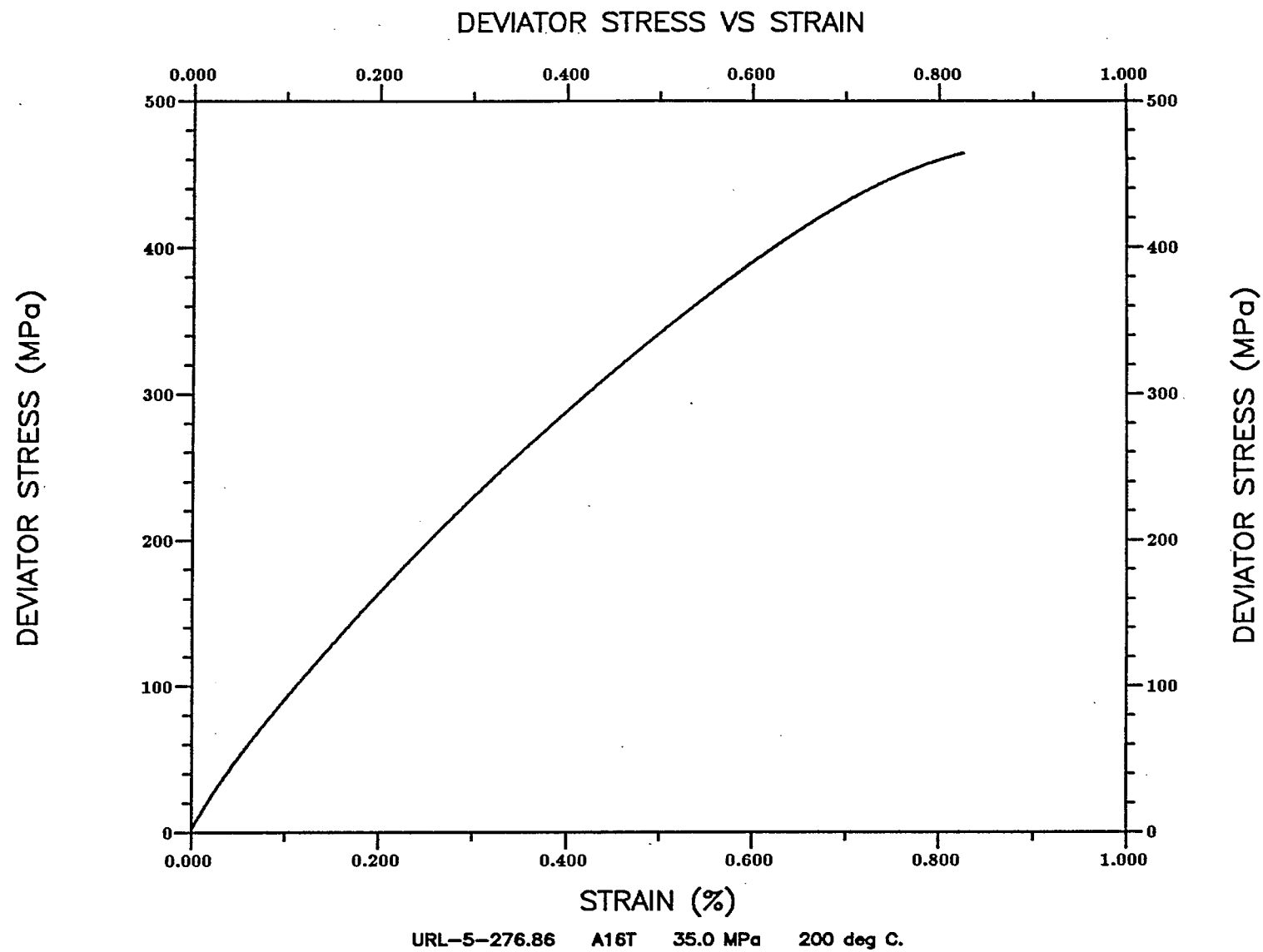


Figure A.15 Specimen A16T ($\sigma_3 = 35.0$ MPa, temperature = 200° C)

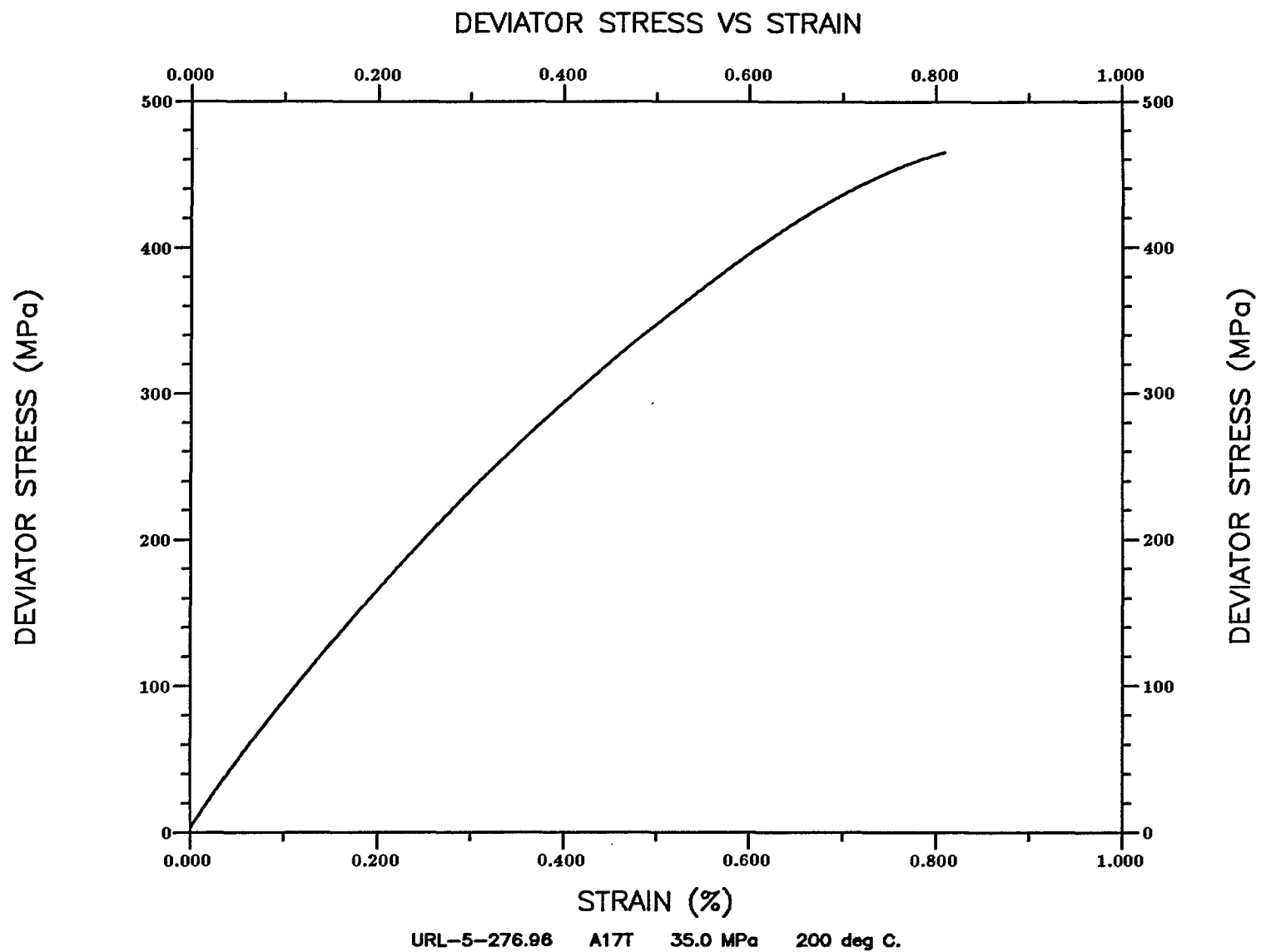


Figure A.16 Specimen A17T ($\sigma_3 = 35.0$ MPa, temperature = 200° C)

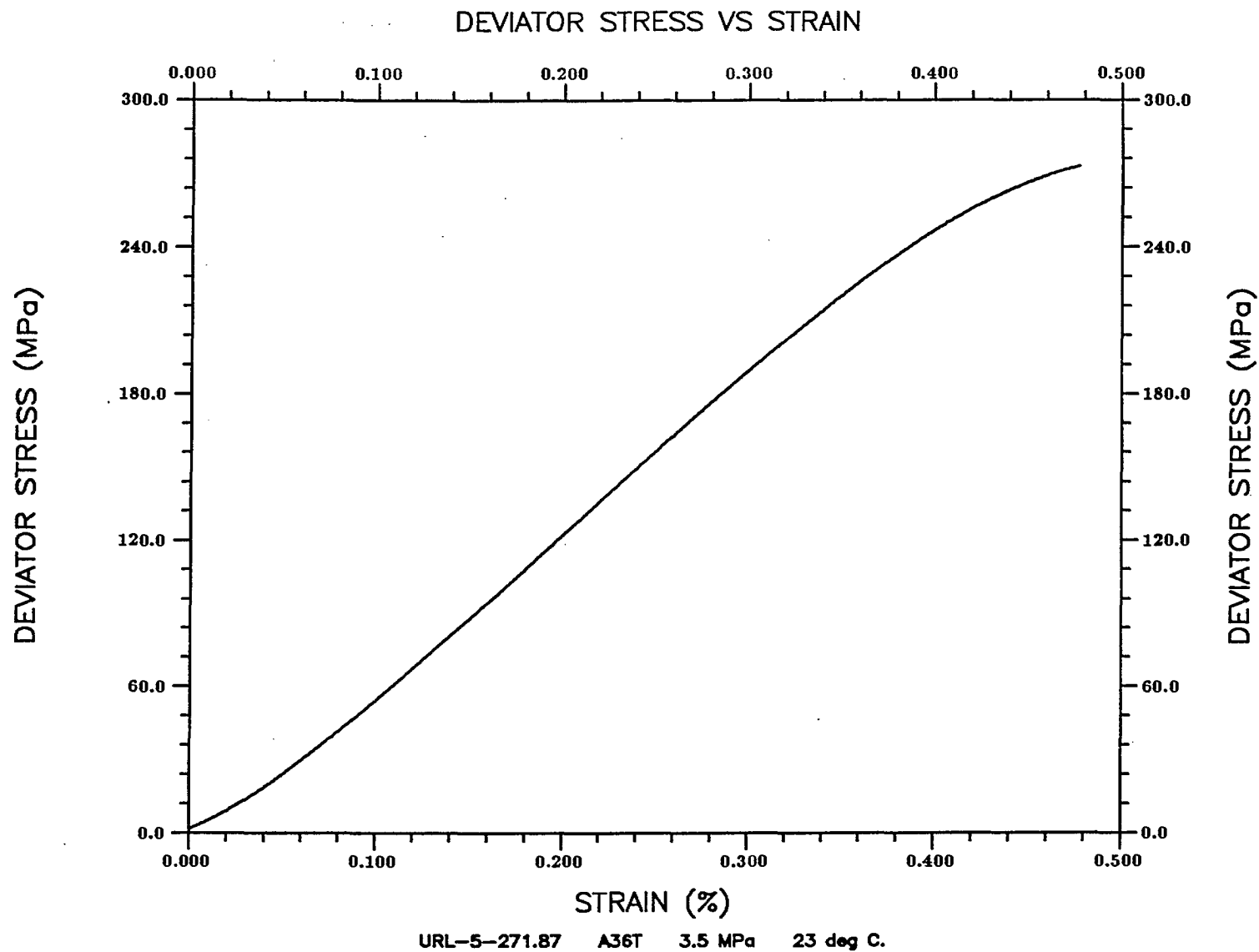


Figure A.17 Specimen A36T ($\sigma_3 = 3.5$ MPa, temperature = 23° C)

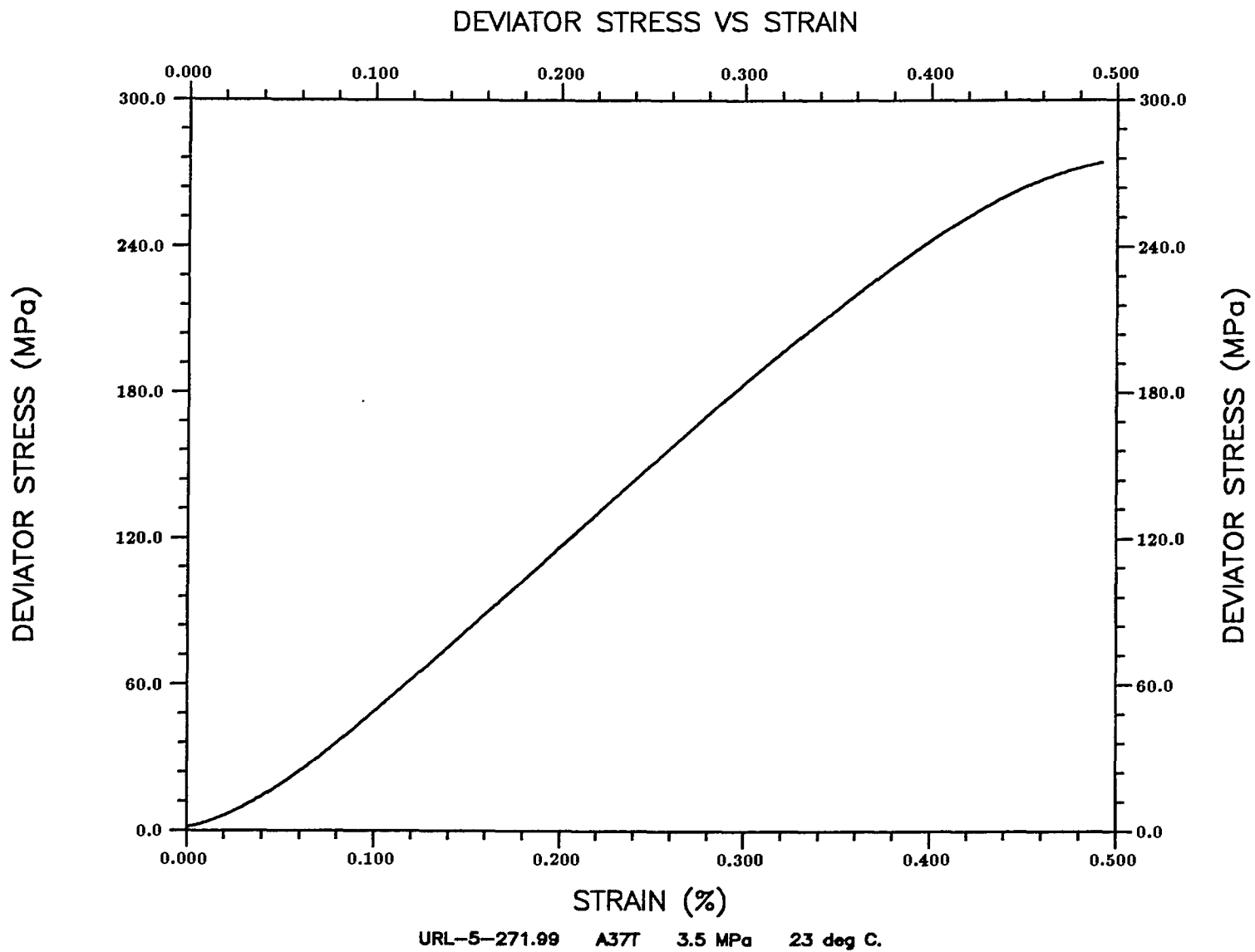


Figure A.18 Specimen A37T ($\sigma_3 = 3.5$ MPa, temperature = 23° C)

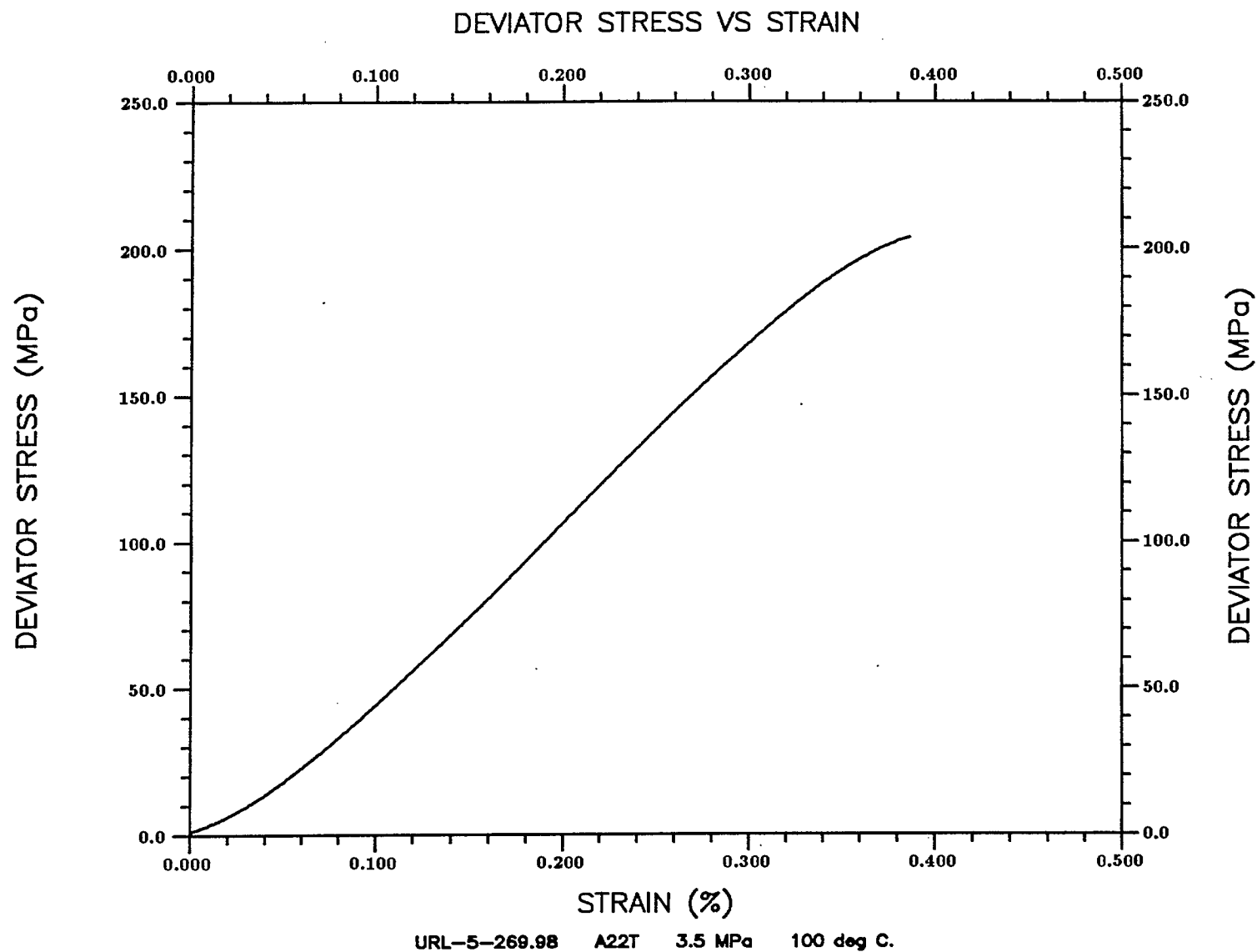


Figure A.19 Specimen A22T ($\sigma_3 = 3.5$ MPa, temperature = 100° C)

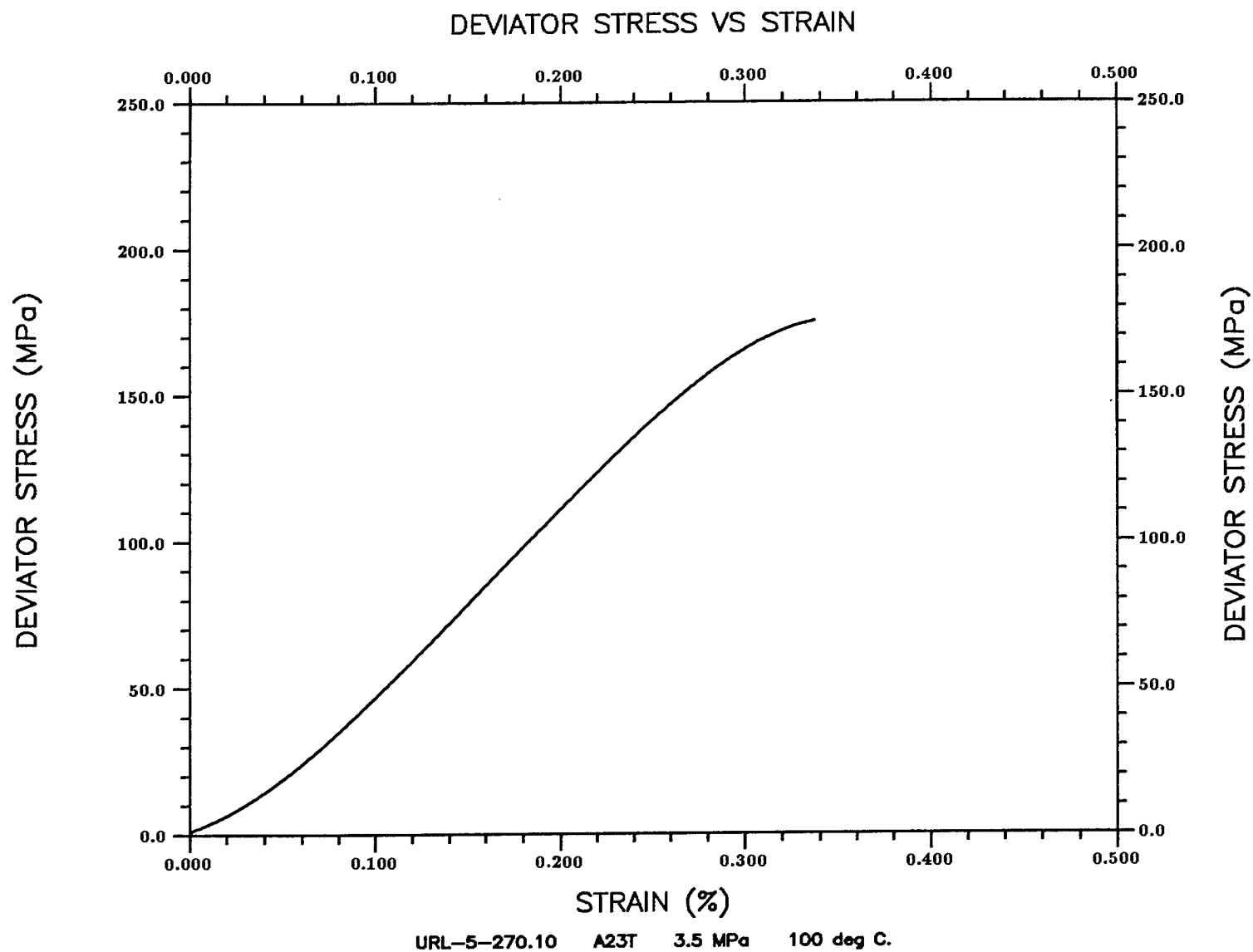


Figure A.20 Specimen A23T ($\sigma_3 = 3.5$ MPa, temperature = 100° C)

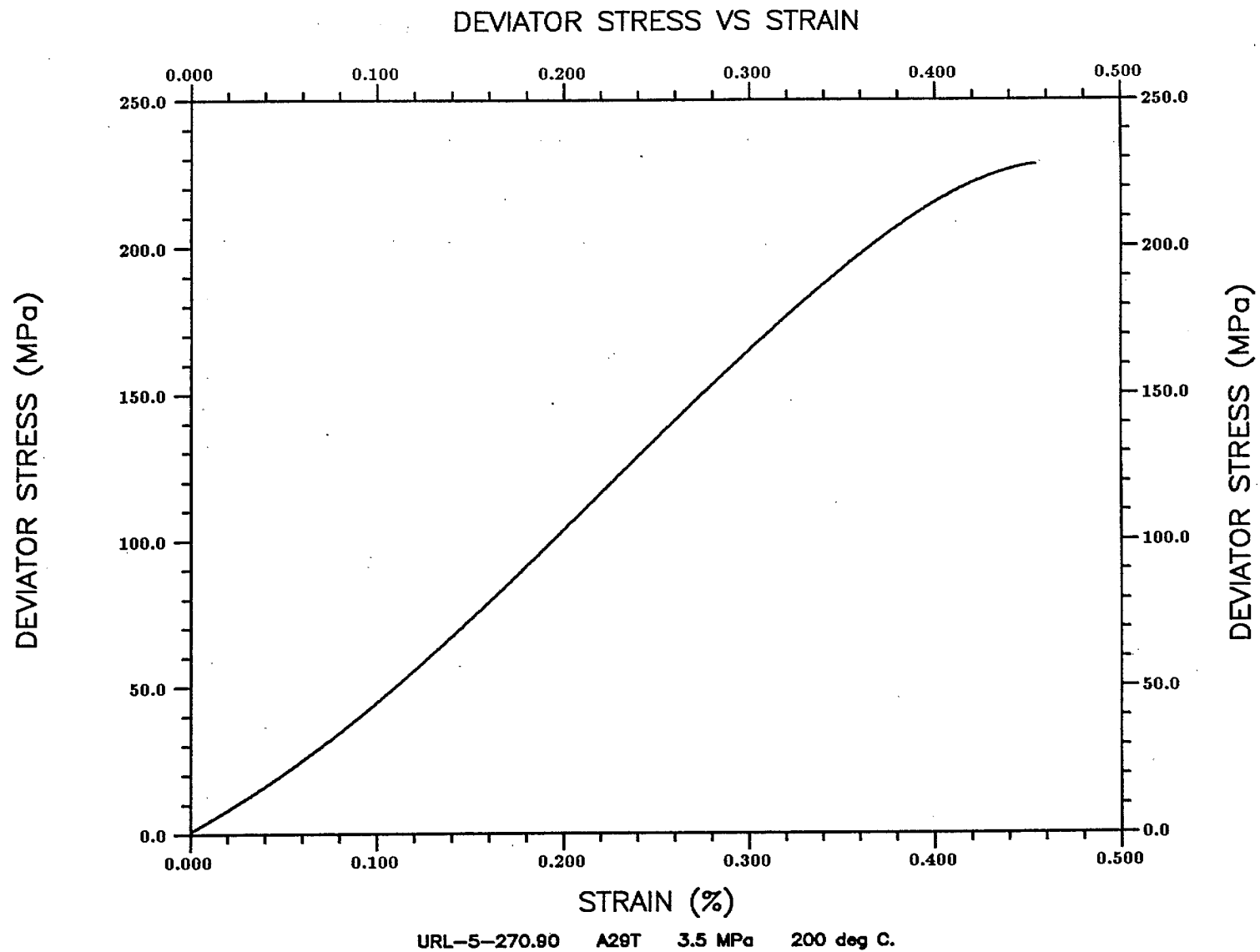


Figure A.21 Specimen A29T ($\sigma_3 = 3.5$ MPa, temperature = 200° C)

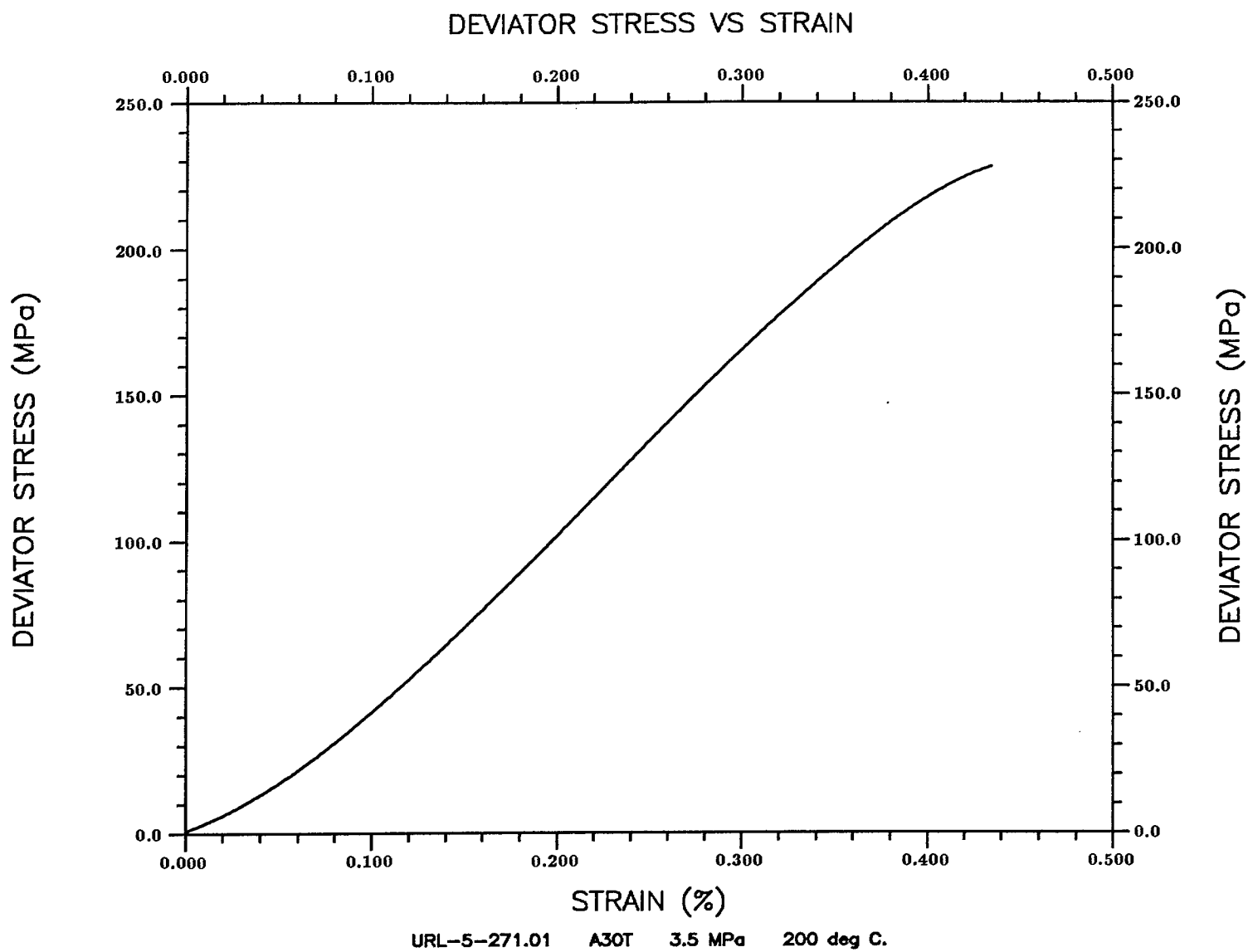


Figure A.22 Specimen A30T ($\sigma_3 = 3.5$ MPa, temperature = 200° C)

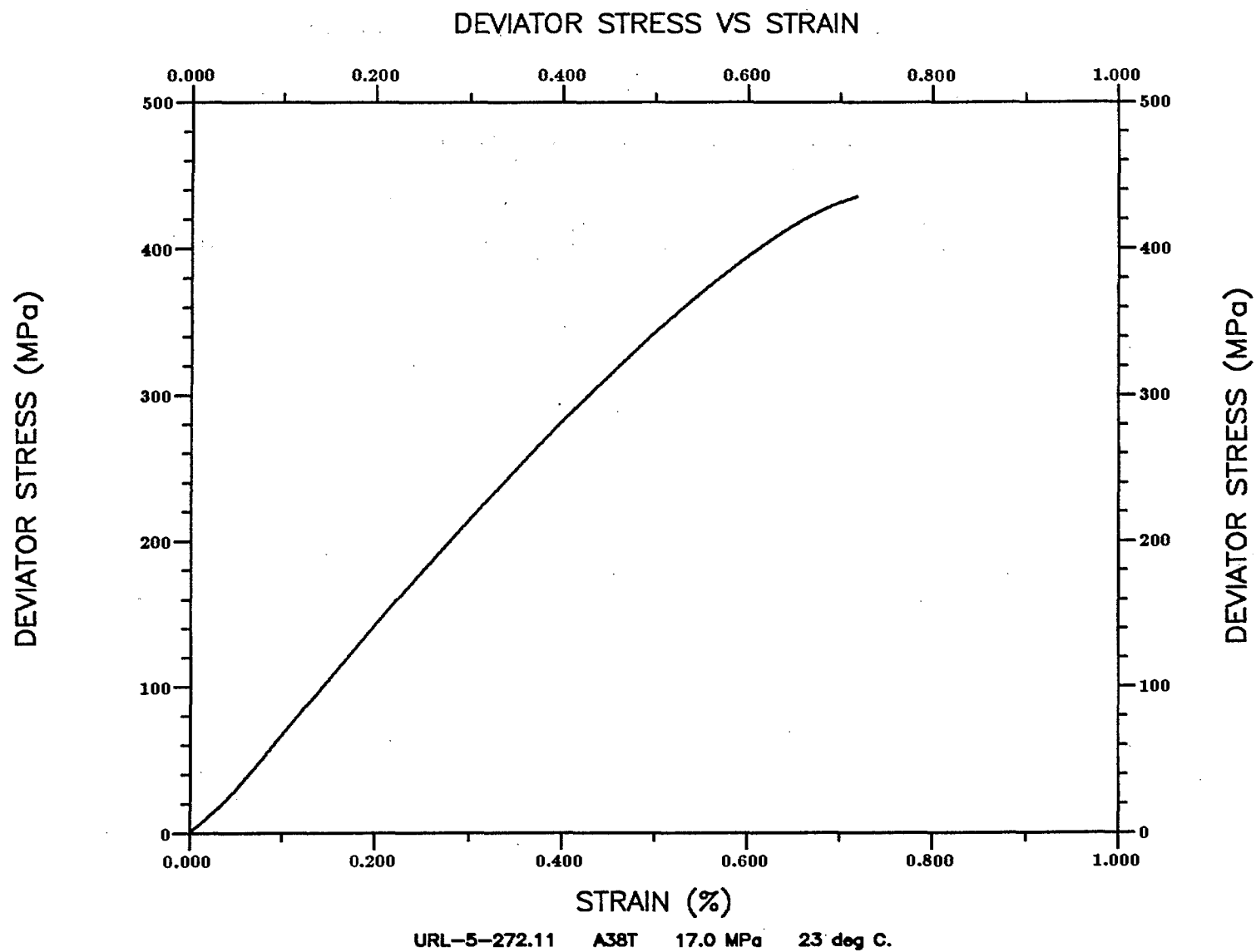


Figure A.23 Specimen A38T ($\sigma_3 = 17.0$ MPa, temperature = 23° C)

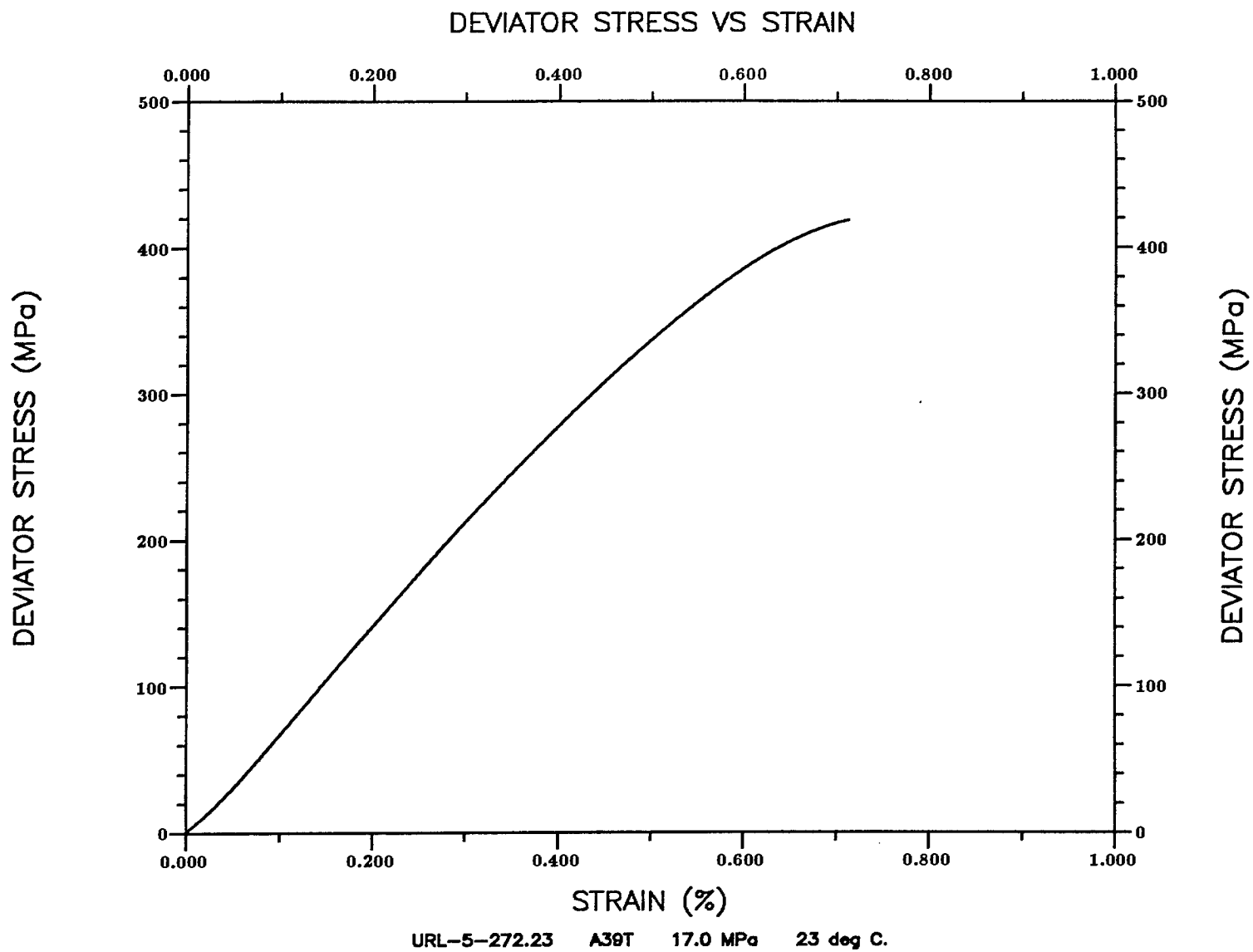


Figure A.24 Specimen A39T ($\sigma_3 = 17.0$ MPa, temperature = 23° C)

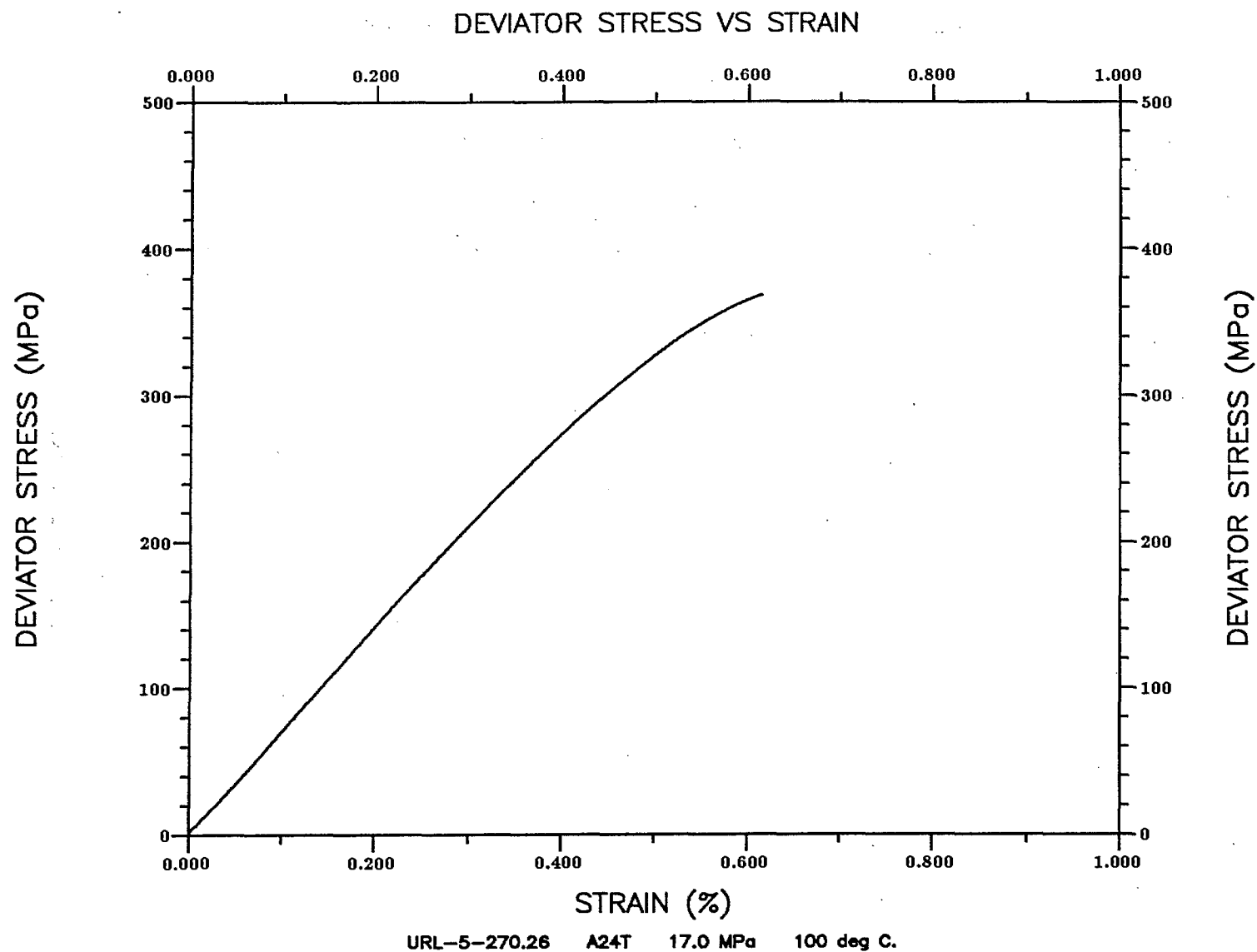


Figure A.25 Specimen A24T ($\sigma_3 = 17.0$ MPa, temperature = 100° C)

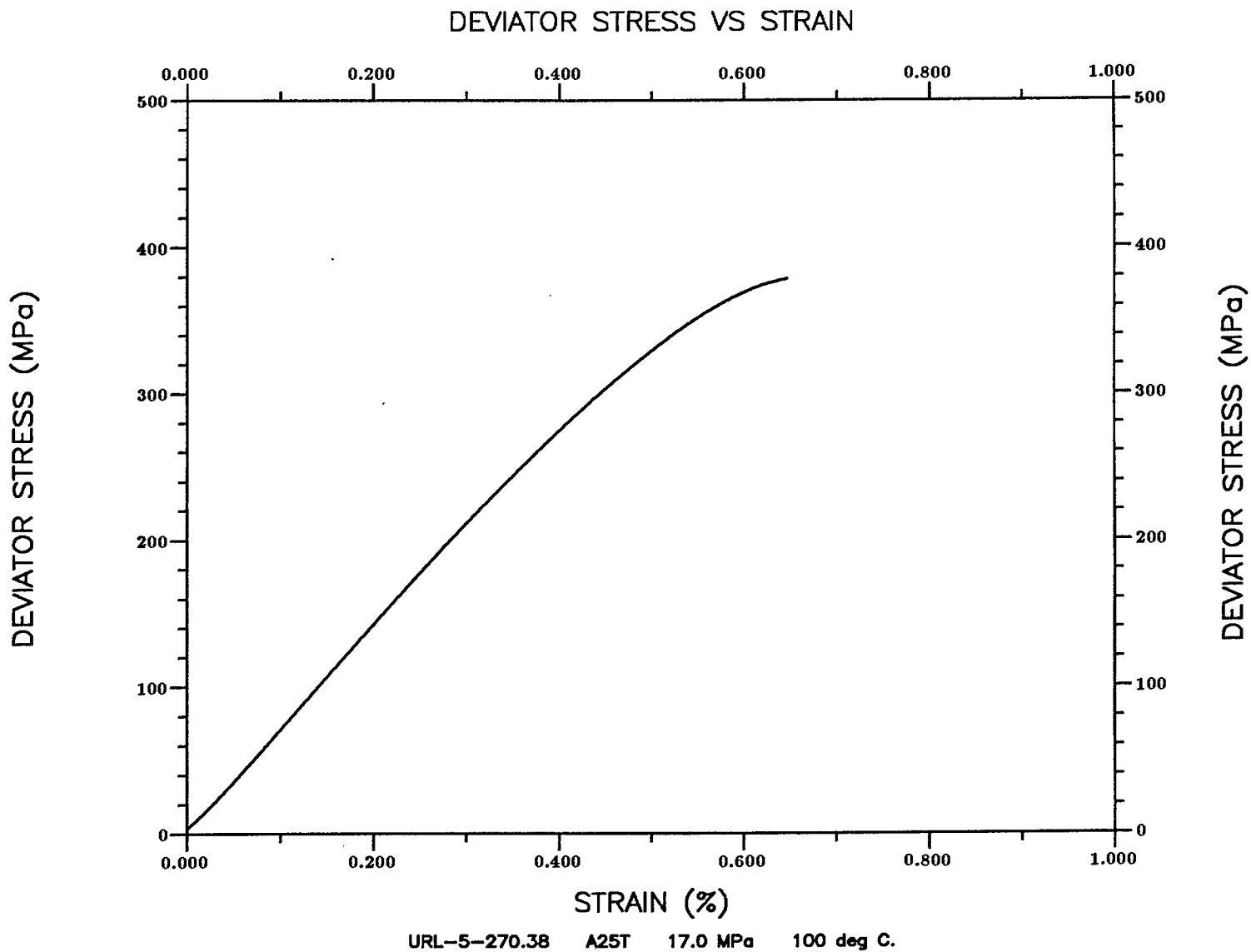


Figure A.26 Specimen A25T ($\sigma_3 = 17.0$ MPa, temperature = 100° C)

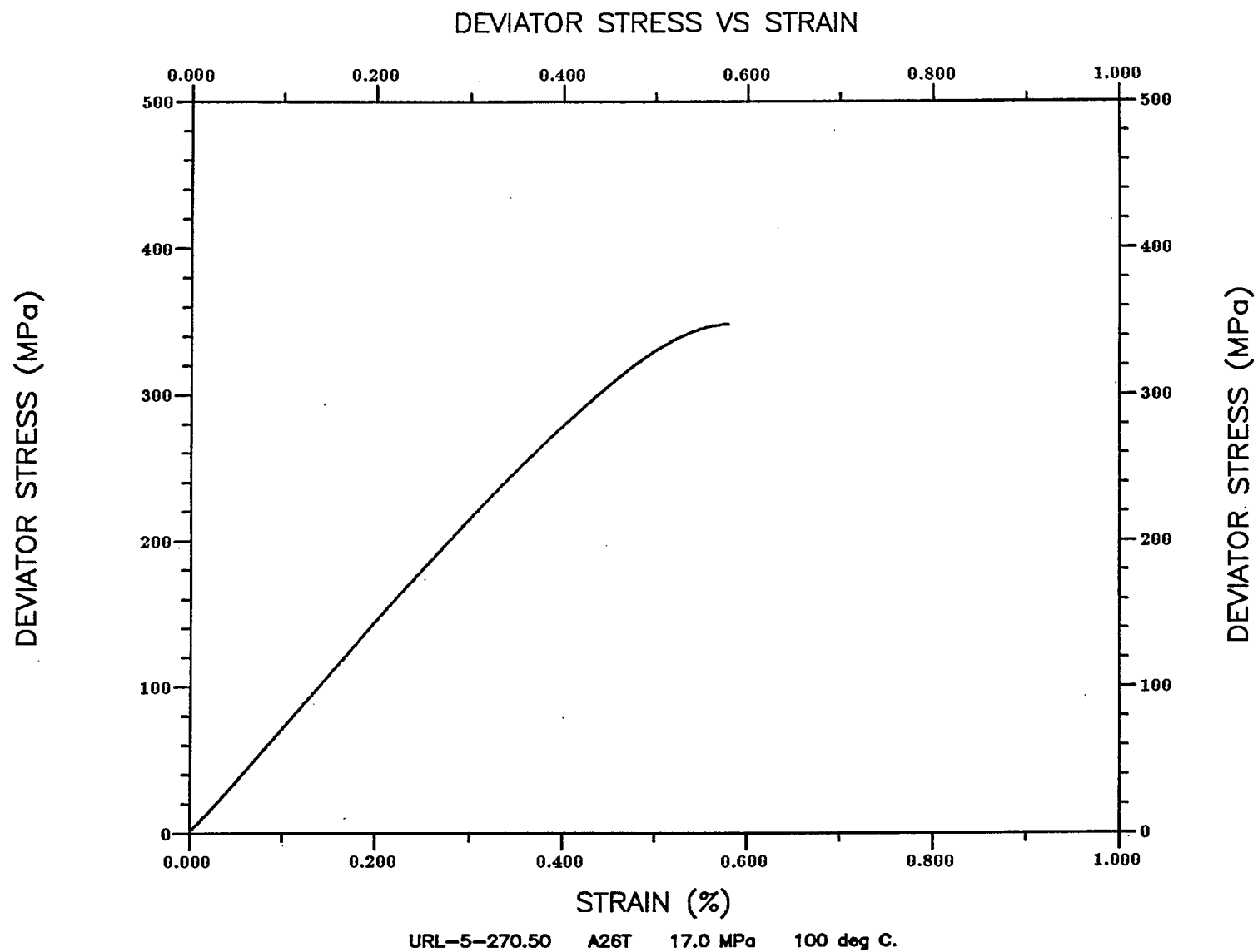


Figure A.27 Specimen A26T ($\sigma_3 = 17.0$ MPa, temperature = 100° C)

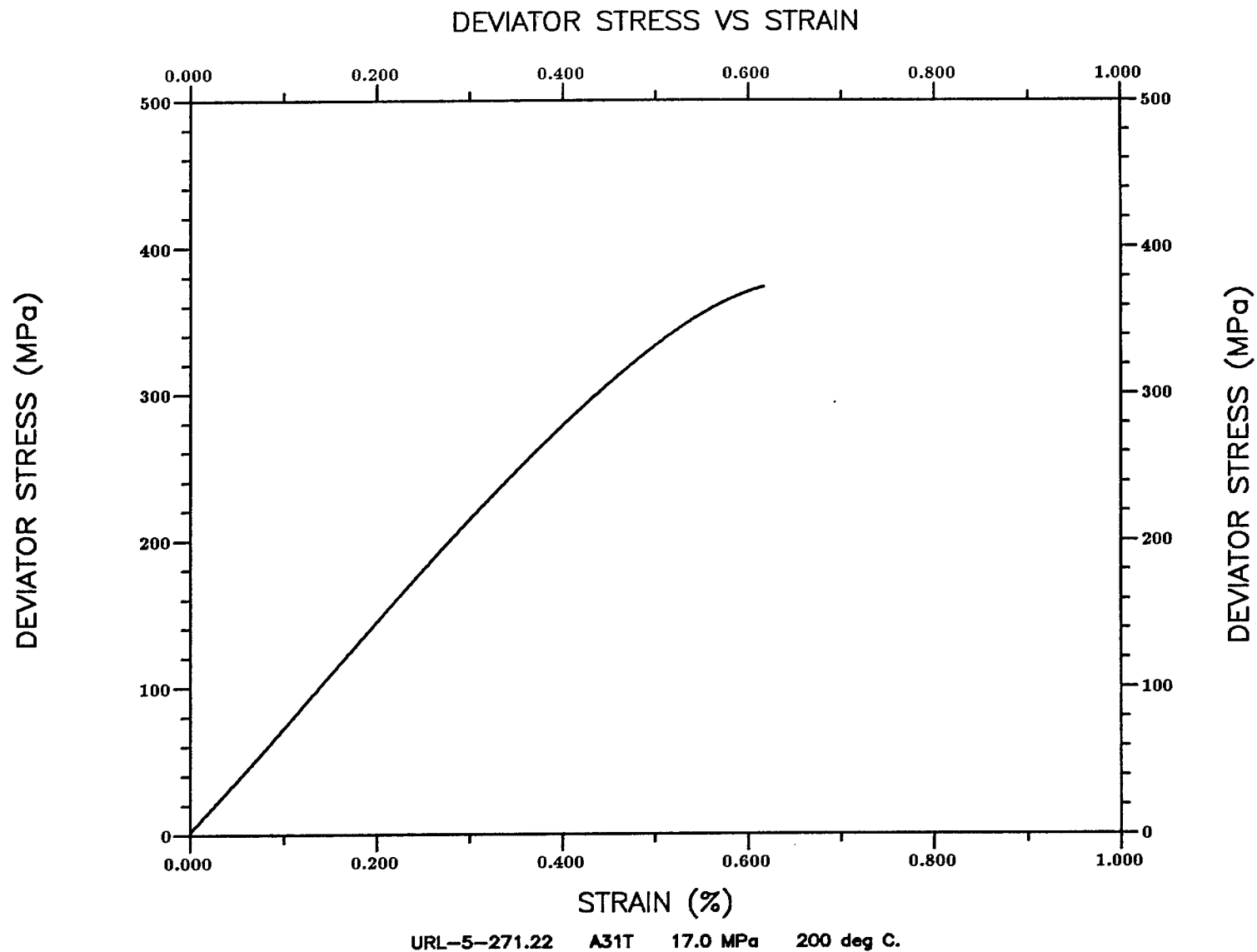


Figure A.28 Specimen A31T ($\sigma_3 = 17.0$ MPa, temperature = 200° C)

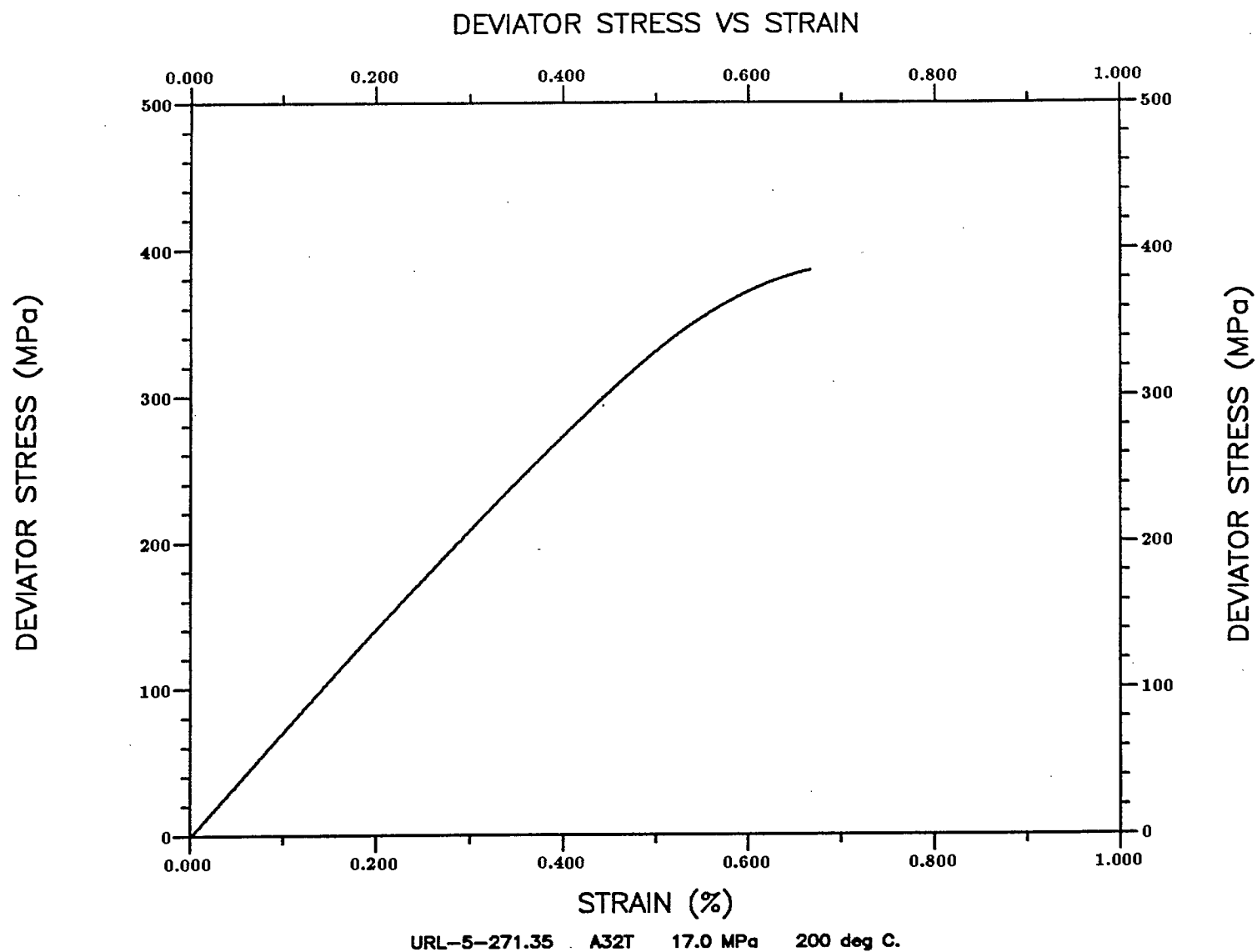


Figure A.29 Specimen A32T ($\sigma_3 = 17.0$ MPa, temperature = 200° C)

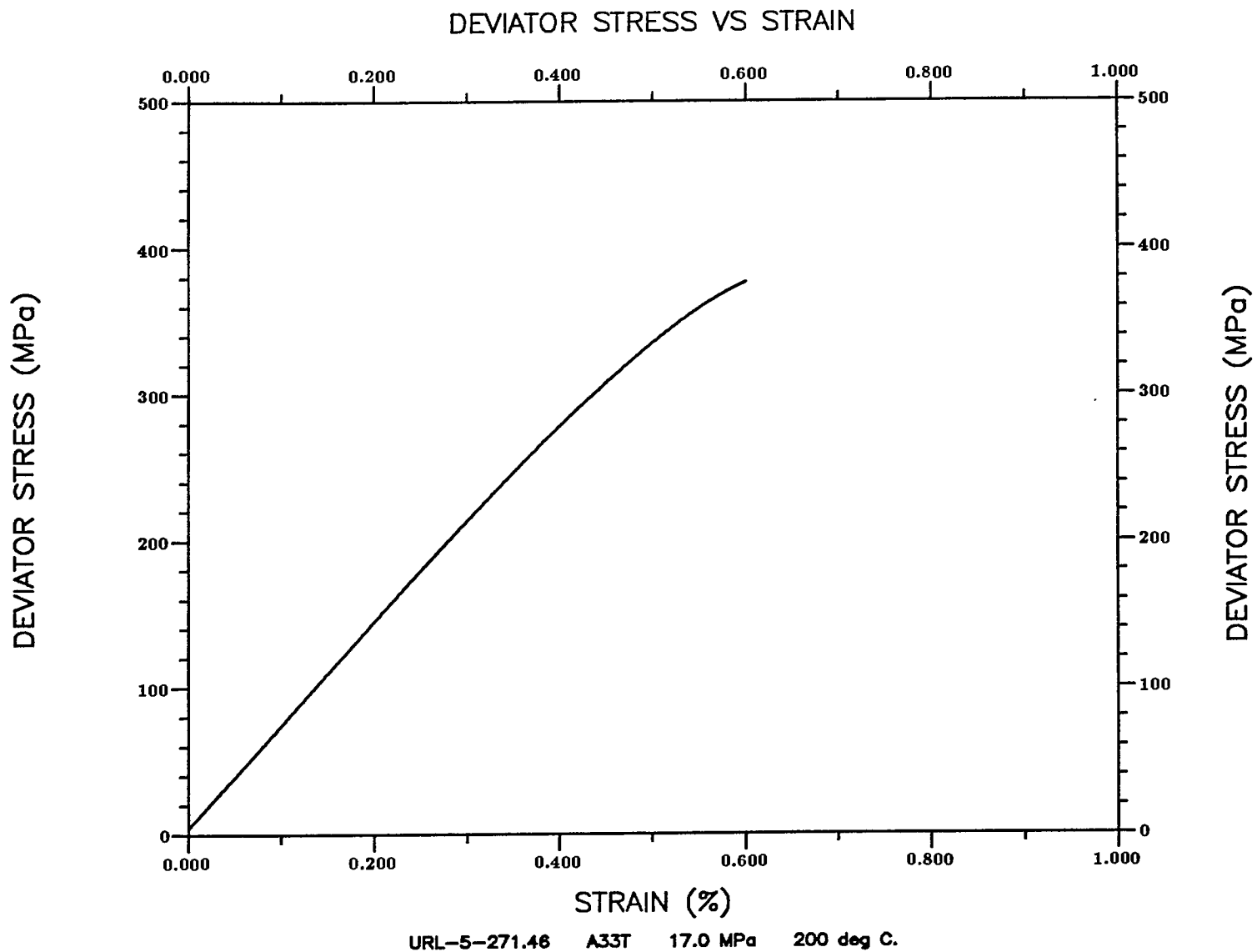


Figure A.30 Specimen A33T ($\sigma_3 = 17.0$ MPa, temperature = 200° C)

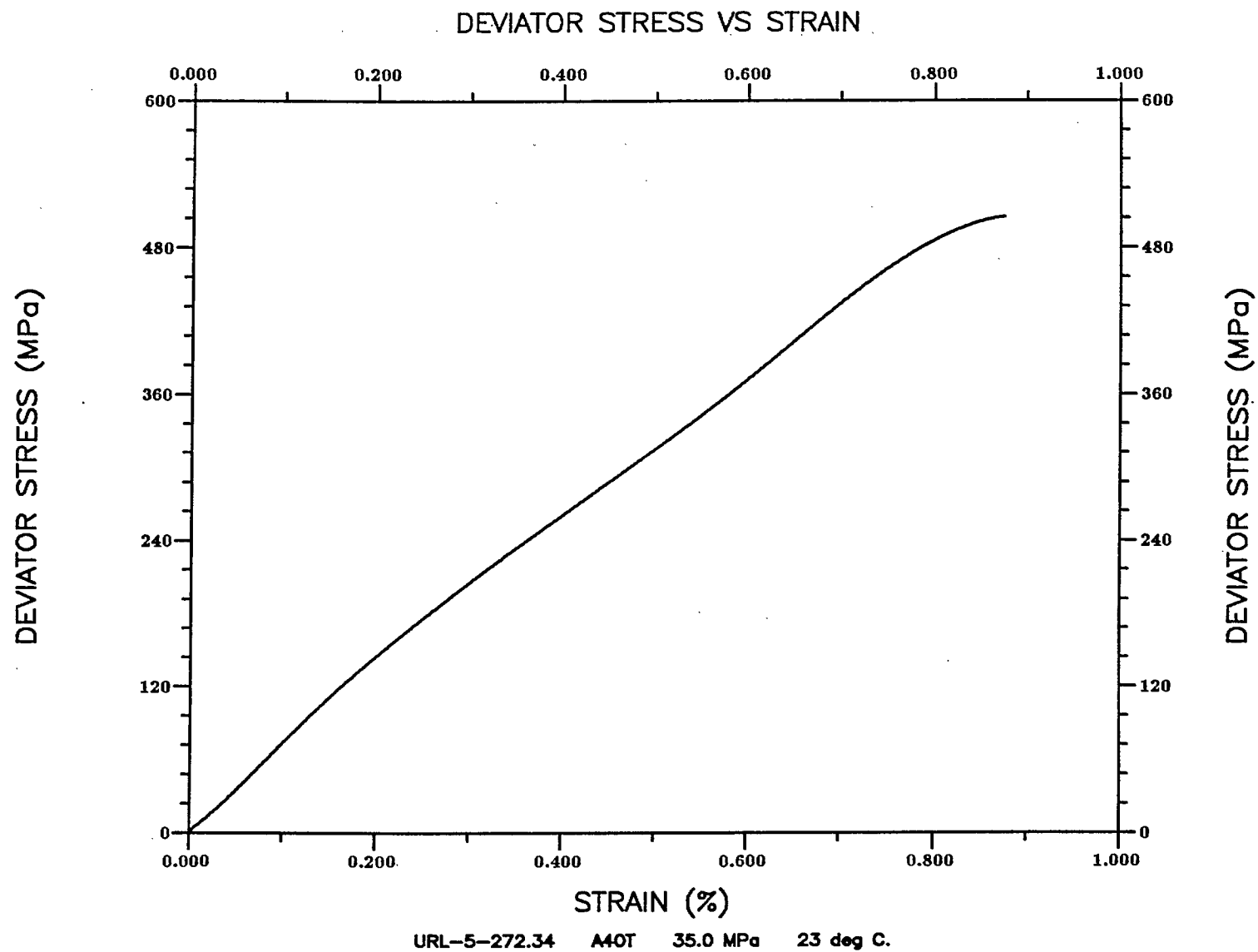


Figure A.31 Specimen A40T ($\sigma_3 = 35.0$ MPa, temperature = 23° C)

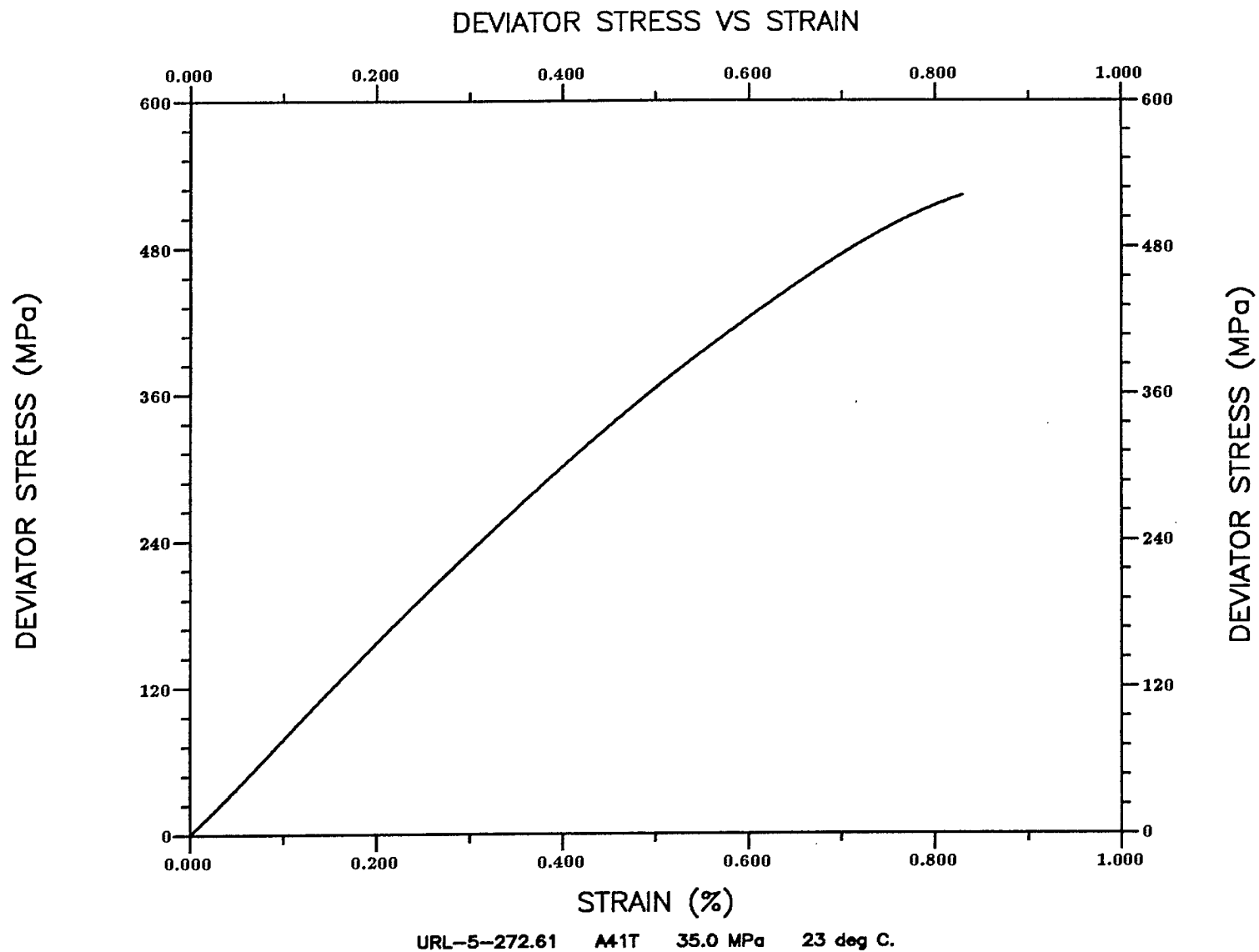


Figure A.32 Specimen A41T ($\sigma_3 = 35.0$ MPa, temperature = 23° C)

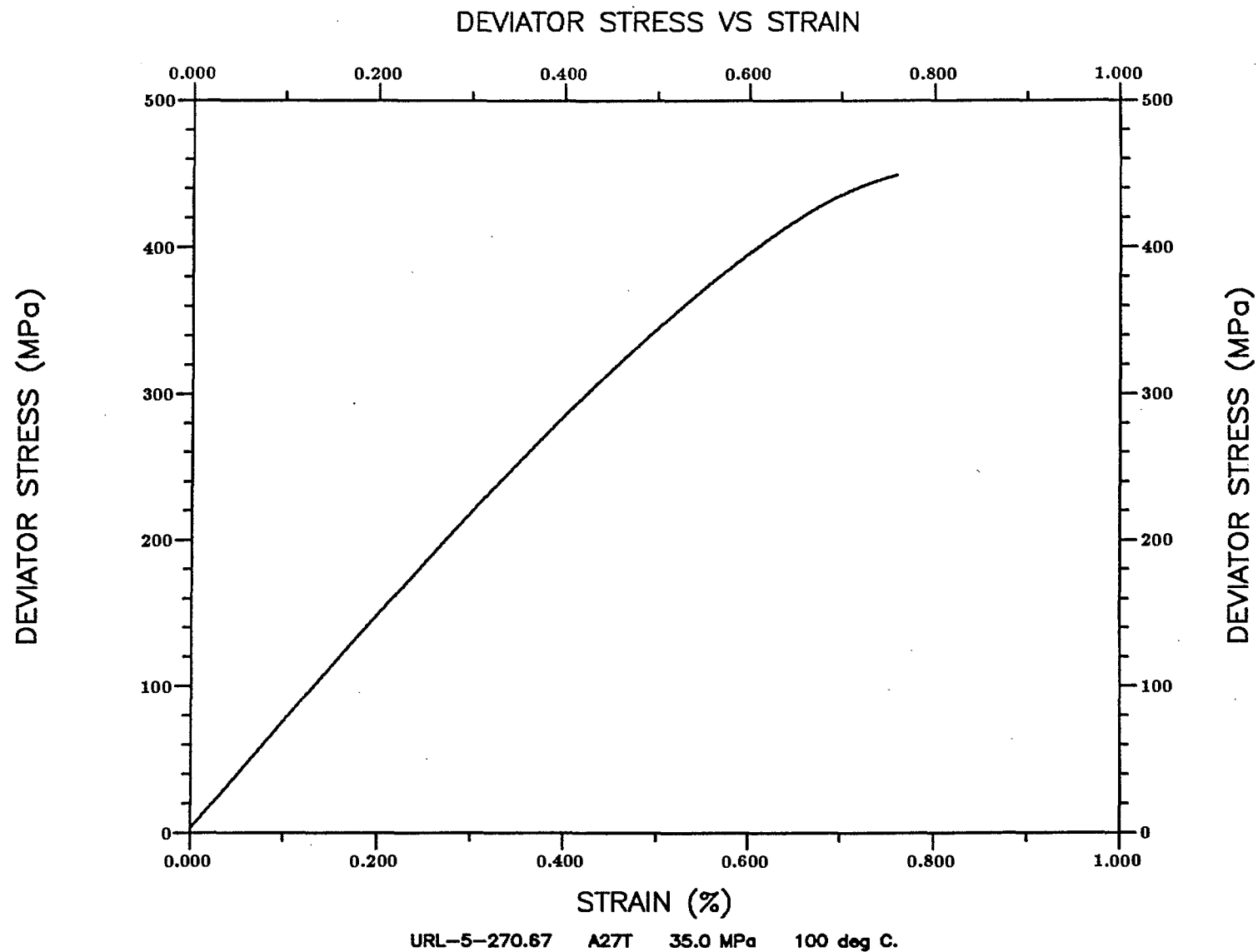


Figure A.33 Specimen A27T ($\sigma_3 = 35.0$ MPa, temperature = 100° C)

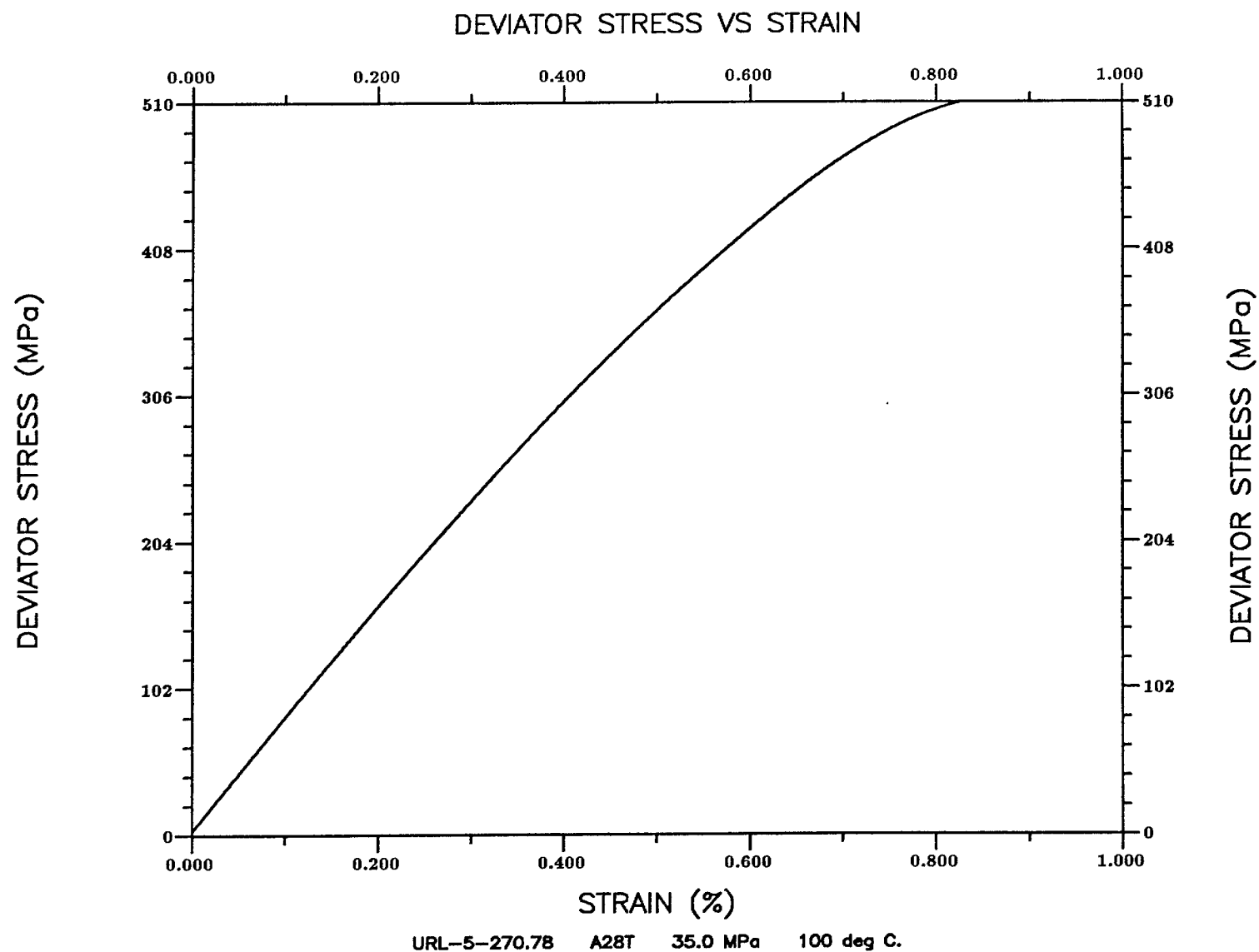


Figure A.34 Specimen A28T ($\sigma_3 = 35.0$ MPa, temperature = 100° C)

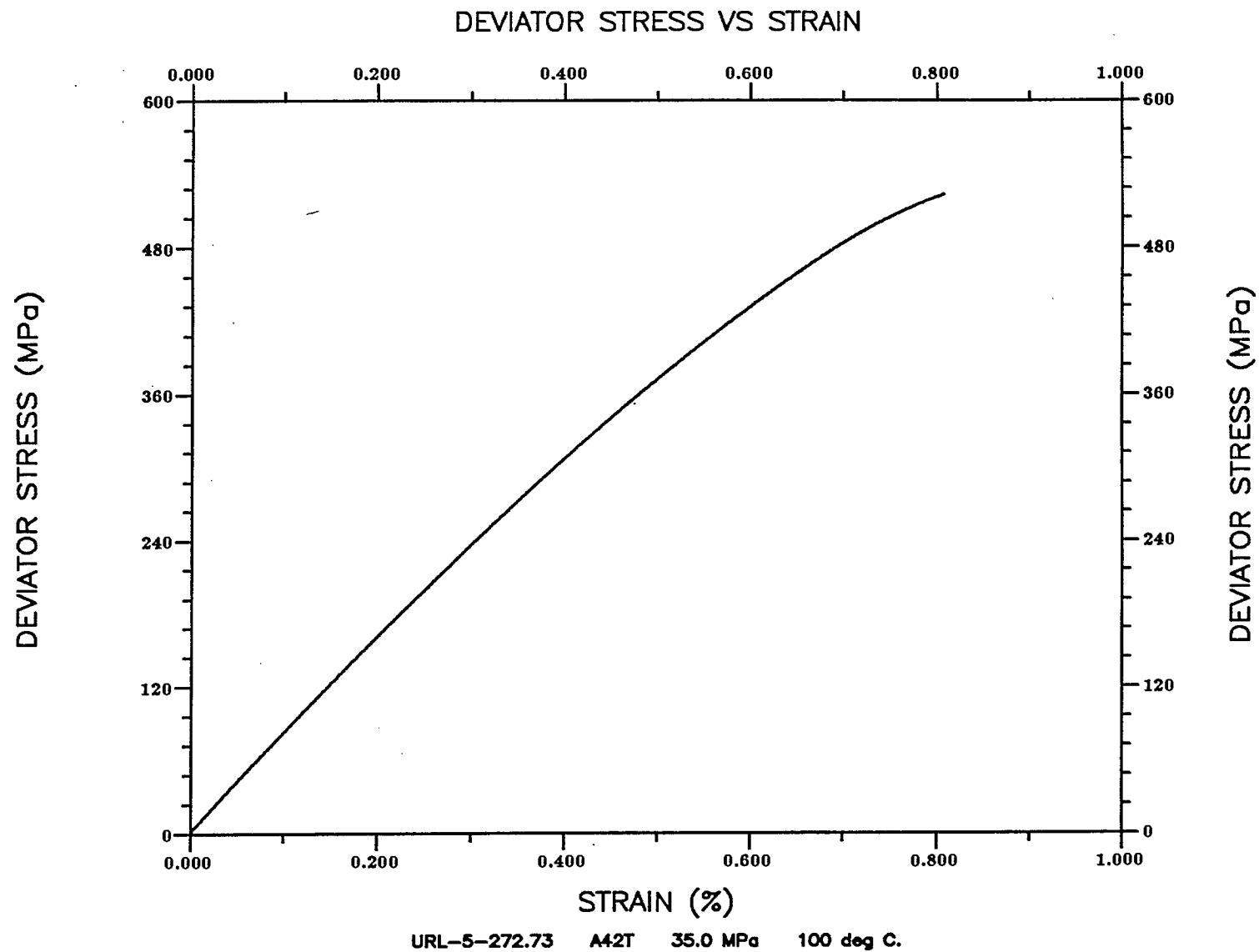


Figure A.35 Specimen A42T ($\sigma_3 = 35.0$ MPa, temperature = 100° C)

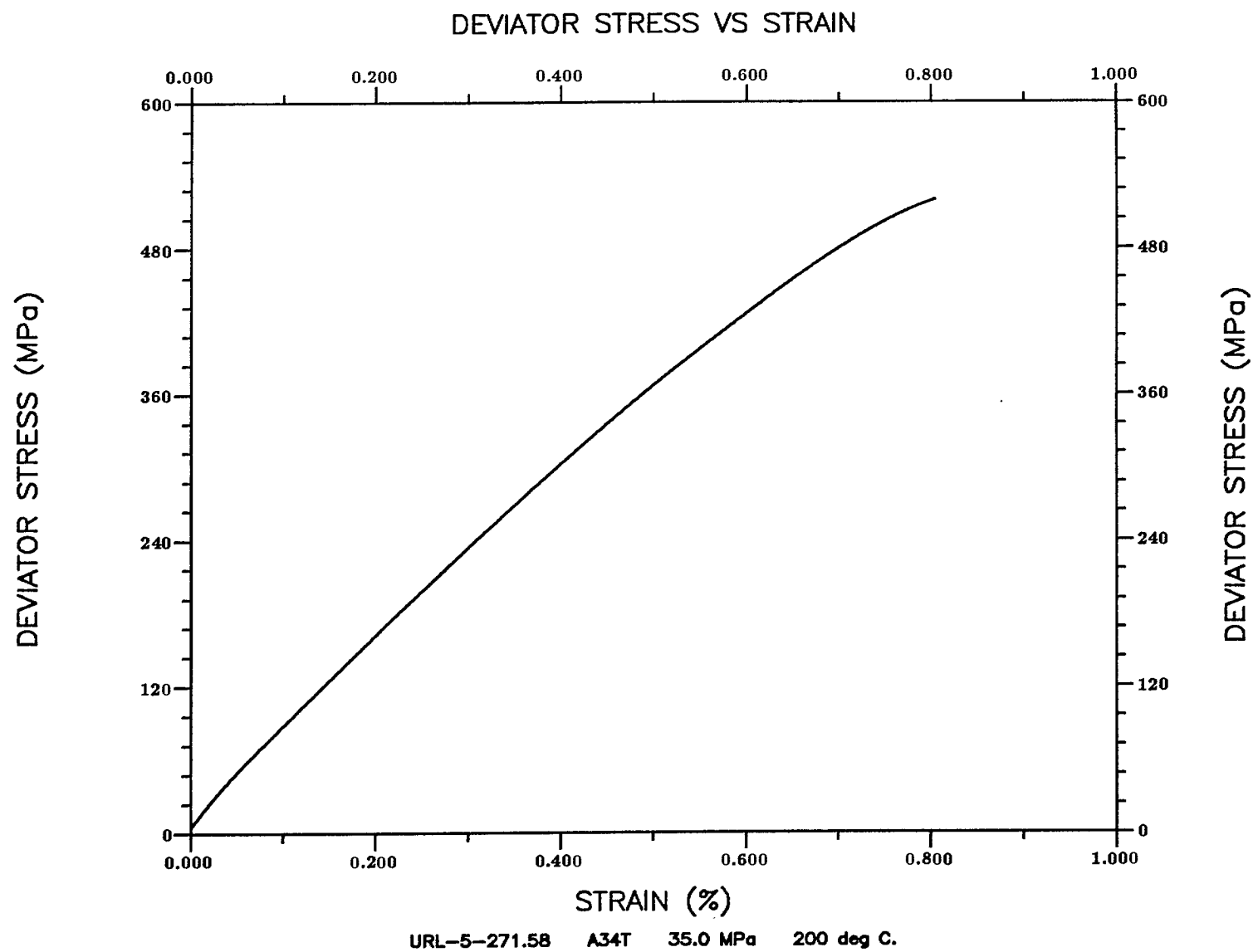


Figure A.36 Specimen A34T ($\sigma_3 = 35.0$ MPa, temperature = 200° C)

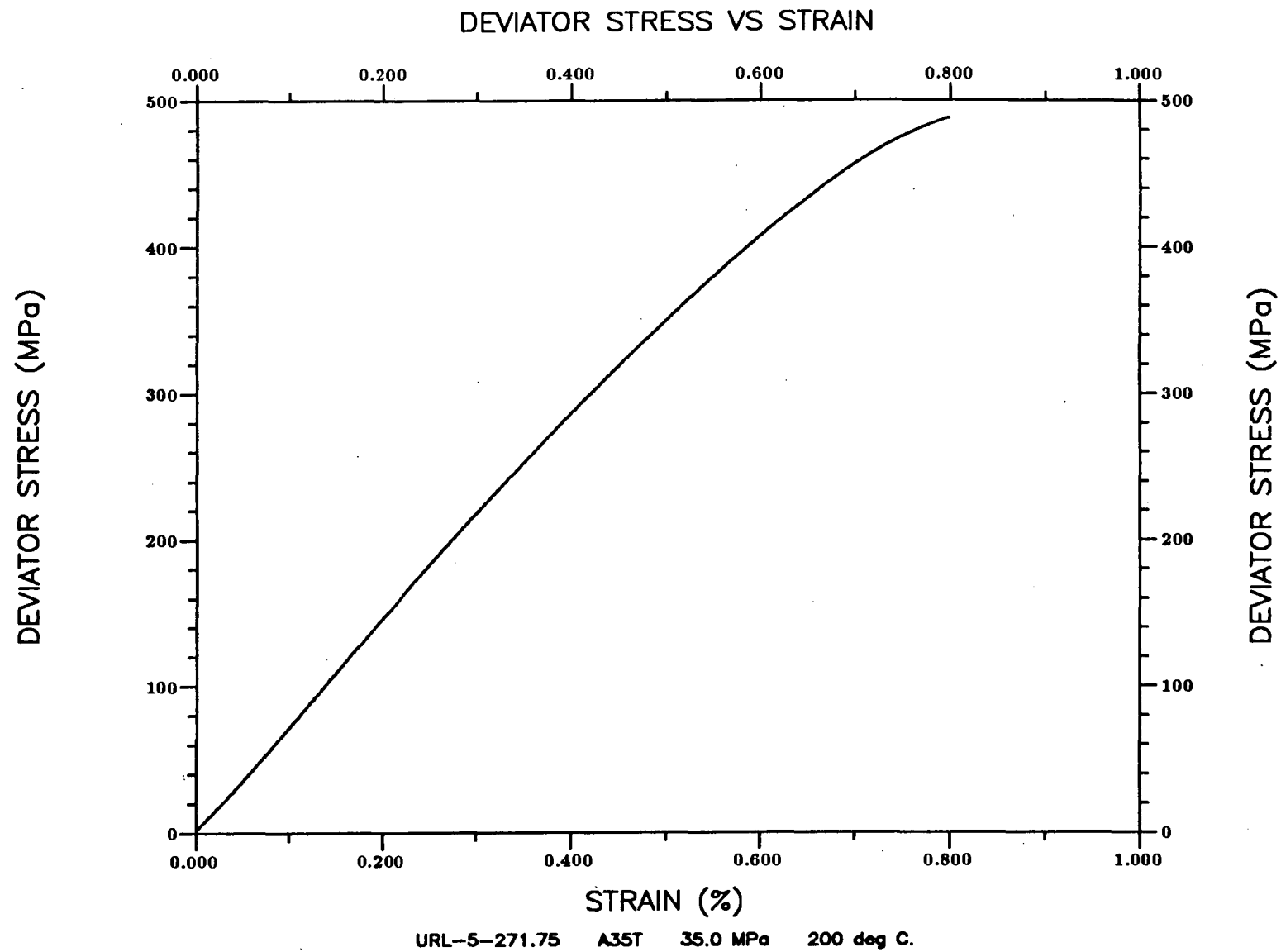


Figure A.37 Specimen A35T ($\sigma_3 = 35.0$ MPa, temperature = 200° C)

